Furtherance of modeling frameworks for multivariate directional statistics

PRIYANKA NAGAR

Furtherance of modeling frameworks for multivariate directional statistics

By

Priyanka Nagar

Submitted in fulfillment of the requirements for the degree

Doctor of Philosophy

in the

Faculty of Natural and Agricultural Sciences

at the

UNIVERSITY OF PRETORIA

Supervisors: Professor Andriëtte Bekker and Professor Mohammad Arashi

8 November 2022

Abstract

In this thesis, we propose multivariate directional models that serve to fill the gaps in literature and aim to develop innovative theoretical modeling frameworks for contemporary applications where either certain manifolds have been neglected or the use of directional statistics has been neglected. This thesis focuses on three different manifolds; the hyper-sphere, the disc and the poly-cylinder. For the multivariate circular observations we propose a family of distributions on the unit hyper-sphere obtained by considering normal mean mixture distributions from a transformation viewpoint. The resulting family of distributions, termed Mean Direction Mixture models, can account for symmetry, asymmetry, unimodality and bimodality. In addition to the multivariate circular domain, we consider the circular-linear domain. For the joint modeling of circular and linear observations we explore the disc manifold for the bivariate modeling of these observations and then delve into the multivariate domain of circular-linear observations by means of the poly-cylinder. A new class of bivariate distributions is proposed which has support on the unit disc in two dimensions that includes, as a special case, the existing Möbius distribution on the disc. Applications of the proposed model for the use in wind description and wind energy analysis is presented. Furthermore, we propose a multivariate dependent modeling framework applicable to the 6D joint distribution of circular-linear data based on vine copulas. This framework is motivated by the analysis of the mechanical behavior of external fixators in the biomechanical domain. The work proposed in this thesis aims to play a part in addressing the larger need for multivariate models in directional statistics due to the increased amount of complex data containing angular observations.

Keywords*:* Directional statistics; disc manifold; fracture displacement; hyper-sphere; multivariate models; poly-cylinder; wind energy.

Declaration

I, Priyanka Nagar, declare that this thesis, which I hereby submit for the degree PhD at the University of Pretoria, is my own work and has not previously been submitted by me for a degree at this or any other tertiary institution.

Signed:

_____

Date:

_____

Acknowledgements

"Research: the distance between an idea and its realization" - David Sarnoff

I wish to express my gratitude to the following people and organizations who made this thesis possible:

- First and foremost none of this could have happened without my family. My late maternal grandmother, Divali Tiekam, my mum, Joshna, and my sister, Jyotika, who are my three pillars of strength, courage, patience, wisdom, unconditional support and love. Thank you for your unwavering faith in my abilities which have allowed me to dream big and achieve my goals. To my dad, Prakash, for all your support and encouragement.
- My supervisors Professor Andriëtte Bekker and Professor Mohammad Arashi, thank you for your brilliant guidance, invaluable advice, continuous support and patience during my PhD study. To Professor Andriëtte Bekker, your passion for research and excellence has made this an inspiring experience for me. Your commitment to quality academic research and constant feedback has been admirable. I appreciate your attention to detail and quest for perfection. You have been a tremendous mentor for me both professionally and personally. I am in awe of your greatness! To Professor Mohammad Arashi, I am extremely grateful for your assistance and dedicated involvement in every step throughout this journey. I have had the privilege of experiencing your extensive knowledge and innovative ideas within the statistical domain. You truly embody the saying that "There are no problems—only opportunities to be creative". To both my supervisors, thank you for sharing your passion, enthusiasm, knowledge and experience with me.
- To my friends, thank you for being my sounding board and keeping me grounded throughout this journey.

- The following research collaborators:
  - Hannes Rautenbach (Faculty of Natural Sciences, Akademia, and School of Health Systems and Public Health, University of Pretoria, Pretoria, South Africa) and Elsa de Jager (National Climate Center, South African Weather Service) for assisting with obtaining, understanding and explaining the data from Marion Island, Humansdorp and Noupoort.
  - Adrian Bejan (Department of Mechanical Engineering and Materials Science, Duke University, Durham, USA), Sylvie Lorente (Dépt. de Génie Civil, INSA, University of Toulouse, Toulouse, France), Josua Meyer (Department of Mechanical and Aeronautical Engineering, University of Pretoria, South Africa), and Attahiru Alfa (Department of Electrical and Computer Engineering, University of Manitoba, Canada) for their time and valuable comments which led to improvements in the understanding of the technical aspects of wind energy generation.
  - Cor-Jacques Kat (Department of Mechanical and Aeronautical Engineering, University of Pretoria) and Annette-Christi Barnard (Walk-A-Mile Centre for Advanced Orthopaedics, Centurion) for allowing me to be a part of their research project which inspired the idea for the biomechanical study. I am grateful to them for allowing me to use their data and for their insightful comments and guidance with regards to the technical aspects within the biomechanical domain.
- The following funding bodies:
  - Universities Capacity Development Programme (UCDP) national collaborative project - strengthening academic staff development in mathematical and statistical sciences in South Africa.
  - National Graduate Academy for Mathematical and Statistical Sciences - Mathematical Sciences Early Career Fellowship.
  - South Africa SARChI Research Chair (UID: 71199) in Computational and Methodological Statistics, University of Pretoria.

  - STATOMET (Department of Statistics, University of Pretoria).

- Department of Statistics, University of Pretoria, South Africa.

- Faculty of Natural and Agricultural Sciences Ethics committee, University of Pretoria, South Africa, for ethical approval of this research project (Reference number: NAS062/2019).

- In reference to IEEE copyrighted material which is used with permission in this thesis, the IEEE does not endorse any of the University of Pretoria's products or services. Internal or personal use of this material is permitted. If interested in reprinting/republishing IEEE copyrighted material for advertising or promotional purposes or for creating new collective works for resale or redistribution, please go to http://www.ieee.org/publications_standards/publications/rights/rights_link.html to learn how to obtain a License from RightsLink. If applicable, University Microfilms and/or ProQuest Library, or the Archives of Canada may supply single copies of the dissertation.

Publications and Presentations

The following publications form the core of the research presented in this thesis:

- Bekker, A., Nagar, P., Arashi, M. and Rautenbach, H., 2019. From Symmetry to Asymmetry on the Disc Manifold: Modeling of Marion Island Data. Symmetry, 11(8), p.1030. [13]
- Arashi, M., Nagar, P. and Bekker, A., 2020. Joint Probabilistic Modeling of Wind Speed and Wind Direction for Wind Energy Analysis: A Case Study in Humansdorp and Noupoort. Sustainability, 12(11), p.4371. [7]
- Nagar, P., Bekker, A. and Arashi, M., 2021, September. Mean Mixtures in Directional Statistics. In 2021 IEEE International Conference on Multisensor Fusion and Integration for Intelligent Systems (MFI) (pp. 1-6). IEEE. [83]
- Nagar, P., Bekker, A., Arashi, M., Kat, C.J. and Barnard, A.C., Modelling of multivariate biomechanical data of the Ilizarov ring fixator through a dependent circular-linear model. Under review.

Presentations arising from research in this thesis

- South African Statistical Association (SASA) 2019 conference, Port Elizabeth – presented work titled “New contributions to Möbius transformation-induced distributions on the disc”.
- 12th International Conference of the ERCIM WG on Computational and Methodological Statistics (CMStatistics) 2019, London – presented work titled “Circular mean mixture models”.
- 2021 IEEE International Conference on Multisensor Fusion and Integration (MFI) 2021, Karlsruhe, Germany – presented paper titled “Mean Mixtures in Directional Statistics”.

- International Workshop Advances in Directional Statistics (ADISTA22) 2022, Spain - presented work titled “Biomechanical Data Modeling through a Multivariate Circular-Linear Model based on Vine Copulas”.
- 15th International Conference of the ERCIM WG on Computational and Methodological Statistics (CMStatistics) 2022, London – presented work titled “Modeling multivariate circular-linear data in a biomechanical study”.

Preface

The aim of this thesis is to play a part in addressing the larger need for multivariate models in directional statistics due to the increased amount of complex data containing angular observations. Directional statistics is a branch of statistics dealing with observations that are directions (cyclic in nature). In most cases, these observations lie on the circumference of the unit circle of $\mathbb{R}^2$ (one then speaks of circular statistics) or on the surface of the unit hyper-sphere of $\mathbb{R}^p$ for $p \geq 3$ (implying the terminology of spherical statistics which includes toroidal and cylindrical manifolds). Standard statistical methods for analyzing directional data cannot be used as they do not account for the structure of the sample space or cyclicity of the observations. Data of this type typically arise among others in meteorology, astronomy, earth sciences, biology, image analysis, medicine, cardiology, physics, automotive industry and psychology. Directional statistics has gained popularity in the last two decades due to massive amounts of data and the demands for adapted statistical techniques. By accounting for the angular nature of the observations in this type of data we can better understand the behavior and characteristics at play within various application domains. Professor Kanti V. Mardia ("father of directional statistics") pointed out, in 2022, that one of our resolves should be to make directional statistics more a mainstream statistical topic that is more prevalent in the wider statistical and scientific community.

This thesis comprises of journal articles under review and published. We looked at three different manifolds (sample spaces), namely the hyper-sphere (in Chapter 2), the disc (in Chapter 3) and the poly-cylinder (in Chapter 4). For each manifold, we proposed a new modeling framework that serves to fill the gaps in literature and considered contemporary applications where either these manifolds have been neglected or the use of directional statistics has been overlooked. The thesis will significantly contribute not only within the statistical knowledge domain but also within the engineering, ecological, meteorological, biomechanical and orthopaedic domains.

The societal impact of this thesis can be divided into two main areas, namely renewable energy and health care. Exploitation of wind has long been recognized as one of the key aspects among renewable energy sources for reducing carbon emissions and securing a sustainable energy supply. The analytic knowledge and modeling of wind climate in a candidate area is a critical issue in wind energy assessment in order to optimize the layout of a wind farm, improve system efficiency, estimate accurately wind energy potential and reduce costs. In South Africa, there is an increasing transition towards an environmentally sustainable, climate-change resilient and low-carbon economy. The models proposed in Chapter 3 have the possibility of bringing about change not only in wind energy avenues but also with the detection of climate change and climate patterns.

Chapter 4 is motivated by the biomechanical domain with focus on external fixators. The primary goal within the biomechanical domain are injury prevention and/or rehabilitation and performance enhancement. Patients are generally inoperative during the time in which a fracture heals, which impacts their functionality and quality of life. Some may even be impacted in the long term, due to long lasting damage caused by the fracture. Fracture healing is inevitably influenced by the complex interplay of biology and biomechanics - i.e. inter-fragmentary motion and biomechanics. The construct of an external fixator is determined by the configuration of the hardware. The construct's configuration may lead to different inter-fragmentary motions and it is therefore important to accurately model and understand the motions in play to obtain the most appropriate construct for optimal healing. The modeling framework proposed in this thesis provides a more accurate view for fracture displacements thus leading to improved evaluations and design of these devices.

Our intent with this thesis is not to provide an extensive and comprehensive account of the history of directional statistics nor all the available tools and techniques in the field. For this we refer the reader to the books of Mardia and Jupp [74], Jammalamadaka and SenGupta [45], Pewsey et al. [89], Ley and Verdebout [68] and Pewsey and García-Portugués [88]. Rather, we give the necessary background within

each chapter to guide the reader through relevant developments in each area to provide the appropriate context for understanding the pertinence of the research in this thesis.

"Incredible things can be done simply if we are committed to making them happen" - Sadhguru

Contents

List of Figures xiii

List of Tables xvi

Nomenclature xx

1 Introduction 1

2 Multivariate Circular Models 6

2.1 Introduction 6

2.2 Methodology 8

2.2.1 General model 9

2.2.2 Distribution on the circle 12

2.3 Numerical illustrations 13

2.3.1 Identifiability 13

2.3.2 Parameter estimation 14

2.3.3 Ants data 16

2.3.4 New Caledonian laterites data 17

2.3.5 Simulation study 18

2.4 Conclusion 20

3 Circular-Linear Models **22**

3.1 Introduction . . . 23
3.2 Methodology . . . 25
3.2.1 Möbius transformation . . . 25
3.2.2 Cartesian coordinate configuration of the general class . . . 26
3.2.3 General Möbius distribution on the disc . . . 27
3.2.4 Maximum likelihood estimation . . . 28
3.3 Special cases . . . 29
3.3.1 Möbius distribution on the disc . . . 29
3.3.2 Kummer beta Möbius distribution on the disc . . . 32
3.3.3 Beta type III Möbius distribution on the disc . . . 36
3.4 Application . . . 39
3.4.1 Evaluation criteria . . . 40
3.4.2 Wind description - Marion Island . . . 41
3.4.3 Wind energy potential - Humansdorp and Noupoort . . . 49
3.5 Conclusion . . . 63

4 Multivariate Circular-Linear Models **65**

4.1 Data and motivation . . . 66
4.2 Background . . . 73
4.3 Methodology . . . 75
4.3.1 Linear and circular distributions . . . 75
4.3.2 Copulas . . . 76
4.3.3 Proposed model . . . 77
4.4 Application . . . 79
4.5 Conclusion . . . 81

5 Summary and future work **82**

A Definitions **86**

A.1 Mathematical expressions 86

A.2 Linear-circular correlation 87

A.3 Circular-circular correlation 87

A.4 Goodness-of-fit measures 87

A.5 Code 88

B Circular-Linear Models **89**

B.1 Derivation: Transformation 89

B.2 Maximum likelihood estimators 92

B.2.1 Möbius distribution on the disc 92

B.2.2 Kummer beta Möbius distribution 92

B.2.3 Beta type III Möbius distribution 93

Bibliography **95**

List of Figures

1.1 Angular observations on the unit circle. 2

2.2 Histogram of the ants data with the five best fitted PDFs. The four-parameter model (dashed line), wrapped Cauchy (dotted line), proposed model with weight function wrapped Cauchy (solid line), proposed model with weight function von Mises (dot-dashed line) and proposed model with weight function sine-skewed von Mises (circle line) © 2021 IEEE. . 17

2.3 Estimated PDF plot for the model of best fit (proposed model with weight function von Mises) with the New Caledonian laterites data © 2021 IEEE. 18

2.4 Estimated PDF plots of best fit models for the simulated data. The wrapped Cauchy (dotted line), proposed model with weight function von Mises (solid line), proposed model with weight function wrapped Cauchy (dashed line) and proposed model with weight function sine-skewed von Mises (dot-dashed line) © 2021 IEEE. 20

3.1 The PDF and contour plot of the bivariate Pearson Type II distribution in (3.8) for $\gamma = 5$. 30

3.2 The marginal PDF of the bivariate Pearson Type II distribution in (3.8) for $\gamma = 0.5, 1, 3$ from left to right. 30

3.3 PDF and contour plots of the Möbius distribution on the disc, (3.10), for varying parameter values. 31

3.4 The PDF and contour plot of the bivariate Kummer beta distribution in (3.12) for $\gamma = 3, \beta = 2$ and $\lambda = 0.5$. 33
3.5 The marginal PDF plot of the bivariate Kummer beta distribution in (3.12) for $\gamma = 2, 2, 2, \beta = 3, 1, 3$ and $\lambda = 1, 1, 4$ from left to right. 33
3.6 PDF and contour plots of the Kummer beta Möbius distribution, (3.16), for varying parameter values. 34
3.6 PDF and contour plots of the Kummer beta Möbius distribution, (3.16), for varying parameter values. (cont.) 35
3.7 The PDF and contour plot of the bivariate beta type III distribution in (3.17) for $\gamma = 3$ and $\beta = 2$. 37
3.8 The marginal PDF plot of the bivariate beta type III distribution in (3.17) for $\gamma = 2, 0.5, 2$ and $\beta = 3, 3, 1$. from left to right. 37
3.9 PDF plot and contour plots of beta type III Möbius distribution, (3.20), for varying parameter values. (cont.) 39
3.10 Images of the location and weather station of Marion Island. (**a**) An image of the location of Marion Island. (**b**) An image of the Marion Island weather station. 42
3.11 A rose diagram of the wind direction (**left**); and histogram of the wind speed (**right**) from the data observed at Marion Island for 2017. 43
3.12 A scatter plot of the wind speed and wind direction data from Marion Island for 2017. 43
3.13 The normalized deviation for the model of best fit for each year. 48
3.14 The PDF plot and contour plot of the Möbius distribution on the disc for the estimated parameter values $\hat{a} = 0.22$, $\hat{\mu} = 1.59$ and $\hat{\gamma} = 12.14$. 49
3.15 The normalized deviation for the parametric models for 2017. 49
3.16 Locations of the two stations in South Africa. 51
3.17 Data plots for the Humansdorp location. 55
3.17 Data plots for the Humansdorp location (cont.). 56
3.18 Data plots for the Noupoort location. 56

3.18 Data plots for the Noupoort location (cont.). 57
3.19 The normalized deviations for the parametric models for the Humansdorp location (**a**–**d**) . The normalized deviations for the parametric models for the Noupoort location (**e**–**h**). 60
3.19 The normalized deviations for the parametric models for the Humansdorp location (**a**–**d**) . The normalized deviations for the parametric models for the Noupoort location (**e**–**h**) (Cont.). 61
3.20 Plots and contour plots of the estimated wind power density (3.23) for each location with the parametric model of best fit as the base joint model of wind speed and wind direction. 62
3.21 Estimated intensity plots of wind power density (3.23) values of the general Möbius distribution for various values of r and θ. 63

4.1 Model of fracture with extraction of points of interest after displacement. 67
4.2 Histograms of the translational (left) and rotational (right) variables for configuration 1. 69
4.3 Histograms of the translational (left) and rotational (right) variables for configuration 2. 70
4.4 Correlation plot for configuration 1. 71
4.5 Correlation plot for configuration 2. 71
4.6 A schematic diagram of the canonical vine structure considered for the proposed model. 78

List of Tables

2.1 Probability density functions used as weight functions. The PDFs considered are: the von Mises (vM) as defined in [74], Sine-skewed von Mises (ssvM) proposed by [4] and the wrapped Cauchy (wC) as defined in [74] © 2021 IEEE. 12

2.2 Maximized log-likelihood (MLL), Akaike information criterion (AIC) and Bayesian information criterion (BIC) values for the von Mises (vM), sine-skewed von Mises, wrapped Cauchy (wC), four-parameter distribution, our proposed model with weight functions von Mises (**MDM-vM**), sine-skewed von Mises (**MDM-ssvM**) and wrapped Cauchy (**MDM-wC**) distributions fitted to the ants data © 2021 IEEE. 16

2.3 Performance measures from fitting the proposed distributions to the New Caledonian laterites data. The maximized log-likelihood (MLL), Akaike information criterion (AIC) and Bayesian information criterion (BIC) values for the the von Mises-Fisher (vMF), Watson, Kent, isotropic angular Gaussian (IAG) and our proposed model with weight functions von Mises (**MDM-vM**) and sine-skewed von Mises (**MDM-ssvM**) © 2021 IEEE. . . 18

2.4 Maximum likelihood estimates for the parameters of the proposed model (2.7) with weight functions von Mises (MDM-vM), sine-skewed von Mises (MDM-ssvM) and wrapped Cauchy (MDM-wC) for the simulated data © 2021 IEEE. 19

2.5 Performance measures from fitting the proposed distributions to the simulated data. The maximized log-likelihood (MLL), Akaike information criterion (AIC) and Bayesian information criterion (BIC) values for von Mises (vM), sine-skewed von Mises (ssvM), wrapped Cauchy (wC), our proposed model with weight functions von Mises (MDM-vM), sine-skewed von Mises (MDM-ssvM) and wrapped Cauchy (MDM-wC) distributions © 2021 IEEE. 19

3.1 Circular statistics for the wind direction at Marion Island for nine years. . 44
3.2 Results from fitting the proposed distributions to the Marion Island data. . 45
3.3 Normalized deviation ranges for model of best fit for each year. 47
3.4 Normalized deviation ranges for the parametric models for 2017. 48
3.5 Geographical details of the two stations. 51
3.6 Information of the wind data for the two locations. 52
3.7 Descriptive statistics of the wind speed data. 52
3.8 Descriptive circular statistics for the wind direction data. 52
3.9 Correlation coefficient for the wind speed and wind direction. 54
3.10 Parameter estimates from fitting the proposed distributions to the two locations at 20 and 60 m height. 59
3.11 Normalized deviations for parametric models for each location. 61

4.1 Descriptive statistics of the translational variables for each configuration. . 67
4.2 Descriptive statistics of the rotational variables for each configuration. . . 68
4.3 Paired variables for configuration 1 with correlation coefficients significant at a 5% significance level. 72
4.4 Paired variables for configuration 2 with correlation coefficients significant at a 5% significance level. 72
4.5 Cases denoting the combination of marginal and copula functions considered for each configuration. 79

4.6 The number of parameters (p), Maximized log-likelihood (MLL), Akaike information criterion (AIC) and Bayesian information criterion (BIC) values for the different combinations of marginal and copula functions. . . . 80

A.1 Evaluated goodness-of-fit metrics. 88

Nomenclature

Abbreviations

AIC	Akaike information criteria
BIC	Bayesian information criteria
CDF	Cumulative distribution function
C-C	Circular-circular
C-L	Circular-linear
EM	Expectation Maximization
FGM	Farlie-Gumbel-Morgenstern
GA	Genetic Algorithm
GM	General Möbius distribution model
HCQ	Hannan-Quinn information criteria
JCDF	Joint cumulative distribution function
JPDF	Joint probability density function
IAG	Isotropic angular Gaussian distribution
IQR	Interquartile range
JW	Johnson-Wehrly
KDE	Kernel density estimation
L-L	Linear-linear

LRT	Likelihood ratio test
MDM	Mean Direction Mixture model
ML	Maximum likelihood
MLE	Maximum likelihood estimation
MLL	Maximum log-likelihood
MN	Mixture of normal distributions
MwC	Mixture of wrapped Cauchy distributions
N	Normal distribution
NMM	Normal mean mixture
PDF	Probability density function
PSO	Particle swarm optimization
sd	Standard deviation
ssvM	Sine-skewed von Mises distribution
vM	von Mises distribution
vMF	von Mises-Fisher distribution
wC	Wrapped Cauchy distribution

Notation

$cor_{x,\theta}$	Correlation coefficient of circular-linear variable pair
d_{ij}	Normalized deviation
$E_U[\cdot]$	Expected value with respect to the random variable U
$e(\boldsymbol{\Theta})$	Direction cosine of $\boldsymbol{\Theta}$
${}_1F_1(\cdot)$	Confluent hypergeometric function of the first kind
${}_1F_1^{(\cdot)}(\cdot)$	Derivative of the confluent hypergeometric function
$f_X(x)$	Probability density function of the random variable X
$F_X(x)$	Cumulative distribution function of the random variable X
$G(u)$	Weight function

$I_z(\cdot)$	Modified Bessel function of the first kind and order z
$log(L)$	Log-likelihood function

Symbols

a, λ	Skewness parameters
$\alpha, \beta, \gamma, \kappa, \rho$	Concentration parameters
C	Normalizing constant
$\mathcal{C}$	Copula
$\tilde{\mathbb{C}}$	Extended complex plane
$\bar{c}$	Complex conjugate
d	Dimension
δ	Circular dispersion
η	Circular random variable for copula
i	unit imaginary number
k	Circular kurtosis
$\hat{L}$	Maximum value of the likelihood function
m	Number of mixture components
μ	Mean direction parameter
n	Total number of observations
ν_Θ	Circular standard deviation
ω	Mixing proportion
$\bar{\omega}$	Mean resultant length
p	Number of parameters
$\Psi(\cdot)$	Digamma function
q	Copula parameter
R	Random variable for distance
$\mathbb{R}^d$	Euclidean space of dimension d

ρ_A	Air density (kg/m^3)
s	Circular skewness
$\mathbb{S}^{d-1}$	Hyper-sphere in $\mathbb{R}^d$
τ	Direction parameter
$\bar{\theta}$	Mean direction
V_Θ	Circular variance

Chapter 1

Introduction

In this thesis, we propose multivariate directional models that serve to fill the gaps in literature and consider contemporary applications where either certain manifolds have been neglected or the use of directional statistics has been neglected. Due to the increase in the amount of complex data containing angular observations, there is a larger need for multivariate models in directional statistics.

There are a large number of applications which require the analysis of data not realized in the Euclidean space, but rather on some manifold. For example, a complete description of the wind at a given point in time requires that both the direction and the speed be known. As a result, the manifold on which the data are realized is a disc or cylinder. Similarly, there are a number of applications for which data are realized on circles, spheres, hyper-spheres, torus etc. Various distributions have already been defined and studied on these spaces; however, the number of distributions available pale in comparison to the number of distributions available in Euclidean spaces.

Directional statistics is a branch of statistics dealing with angular observations. The key difficulty when dealing with directional data is the curvature of the sample space as the circle or circular manifold is a non-linear manifold. Ley and Verdebout [68] pointed out that directional statistics has gained popularity in the last two decades due to abundance of data and the demands for adapted statistical techniques. A summary of the

existing directional models is given in [74; 68; 88]. Questions that emerge when one thinks of the need for directional statistics is "Why does the curvature of the sample space require an adapted technique? Why can standard linear statistical techniques not suffice?" The rationale behind the need for directional statistics can be illustrated by the following example:

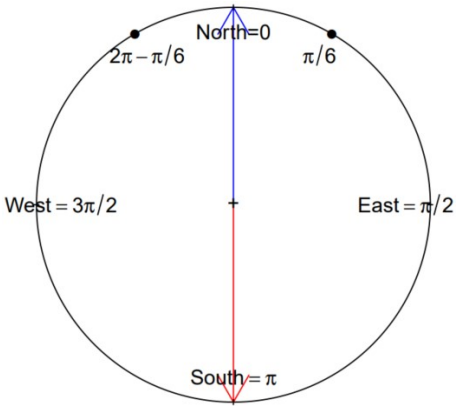

Figure 1.1: Angular observations on the unit circle.

Consider the two directional observations, $\left(2\pi - \frac{\pi}{6}, \frac{\pi}{6}\right)$ on the unit circle as illustrated in Figure 1.1. If we apply the techniques as defined in linear statistics, the arithmetic mean of the two observations would equate to $\frac{\sum_j^n \theta_j}{n} = \frac{2\pi - \frac{\pi}{6} + \frac{\pi}{6}}{2} = \pi$ (indicated in red in Figure 1.1). However, this mean is not a true indication of the mean direction of the observations. From Figure 1.1 we note that the two observations lie on the upper semicircle and thus we would expect the mean direction to fall within the upper semicircle range and lie between the two observations. Thus, it is necessary to redefine the arithmetic mean to account for the cyclicity of the observations. Using the circular mean direction [74], $\bar{\theta} = arg\left(\left(\frac{\sum_{j=1}^n cos\theta_j}{n}\right) + i\left(\frac{\sum_{j=1}^n sin\theta_j}{n}\right)\right)$, the mean of the two observations is 0 (indicated in blue in Figure 1.1). This value provides an accurate representation of the mean direction of the two observations whereas the arithmetic mean produces a misleading result. The principle illustrated by the mean example justifies the need for directional statistical techniques. Further details can be found in [74; 68].

This thesis comprises of five chapters and two appendices. Chapters 2 and 3 comprise of journal articles and Chapter 4 is based on an article under review. Chapters 2 - 4 focus

on three different manifolds, namely; a multivariate circular model defined on the hyper-sphere, a circular-linear model defined on the disc and a multivariate circular-linear model defined on the poly-cylinder. Appendix A provides some relevant definitions and formulae. Additional derivations and expressions for the disc models are given in Appendix B.

Chapter 1 provides the background to the research area and motivates the need for the research proposed in this thesis.

Chapter 2 based on the hyper-sphere manifold aims to fill a theoretical gap by applying the technique of mean mixtures in the directional world. This chapter was inspired by mean mixtures in the linear domain and the work of Shimizu and Iida [99] in the directional domain, where a modeling framework was developed by means of a normal scale mixture distribution via transformations. The question that hovered when working through the normal mixture models proposed by Jammalamadaka and Sengupta [44], which considered a wrapped approach to obtaining a normal mixture model, and by Shimizu and Iida [99], in which the scale mixture model via a spherical transformation was considered, is *Why not consider a mean mixture via a spherical transformation to obtain a multivariate model?*. On the real line various flexible distributions have been constructed by using a normal mixture approach as pointed out in [9] and [84]. Normal mean-variance mixture models have been studied in detail and applied in univariate and multivariate settings abundantly in [81; 97; 104; 8; 43]. The use of a mean mixture can result in an asymmetrical distribution as pointed out in [71]. The skew normal distribution in the linear domain is a well-known model that can be constructed by using a normal mean mixture as illustrated in [84]. Other applications of mean mixture models, among others, can be found in [72; 65; 62]. Besides the wrapped approach discussed by Jammalamadaka and Sengupta [44], no literature involving mean mixture models in directional statistics exists.

Chapter 3 concentrates on the disc manifold which comprises of a pair of circular-linear observations. The disc offers an alternative modeling manifold to the norm of a

cylindrical model for circular-linear observations. A comprehensive summary of circular-linear distributions on the cylindrical manifold can be found in [68]. However, there are very few distributions available with support on the unit disc. The only literature that investigates distributions on the hyper-disc are those by Jones [51; 52] and Uesu et al. [108]. The following question inspired a deeper look into models defined on the disc: *Why are there only three distributions on the disc manifold present in literature?*. The aim of this chapter is twofold, firstly from a theoretical aspect we consider the addition of models defined on the disc manifold by proposing a general family of distributions which can assume either a semi-parametric or parametric form and secondly from an application viewpoint the modeling of wind data for better understanding of wind characteristics as well as modeling potential wind energy for wind farm optimization. The joint modeling of wind speed and direction is important for climatology and a variety of ocean engineering and ecological applications. Modeling of short-term wind characteristics is essential for evaluating wind energy potential. Assessing the wind speed and wind direction play an equally important role in analyzing the wind energy potential [35].

Chapter 4 based on the poly-cylinder focuses on multivariate circular-linear observations. The work in this chapter serves as an applied study with focus on a multivariate dependent modeling framework for examining the mechanical behavior of external fixators. The biomechanical domain is rich with angular data, however, the use of directional statistics techniques is neglected. The inspiration for this chapter resulted from identifying a domain neglected by directional statistics and ripe with opportunity. *Could existing directional techniques be combined to account for dependency and cyclicity in the biomechanical domain?* The techniques utilized in this chapter are known and are not newly developed, however, they are fused together in a craftful manner to provide a elegant framework for the multivariate joint modeling of circular-linear data. The use of directional statistics in orthopedic studies is very limited. The few studies [91; 92; 86; 105]. that considered this domain focused on univariate or bivariate circular applications.

Chapter 5 provides some final remarks and alludes to future work based on the pro-

posed research in this thesis.

The work proposed in this thesis aims to play a part in addressing the larger need for multivariate models in directional statistics due to the increased amount of complex data containing angular observations. Each chapter in this thesis focuses on multivariate data and contributes to the directional statistics domain either through identifying a theoretical gap in the literature or by considering a novel application in an unexplored domain. The structure of this study illustrates the progression of the research contribution from developing theoretical frameworks by only considering the gap in literature to developing modeling frameworks for contemporary applications.

This thesis will significantly contribute not only to the statistical knowledge domain but also to the engineering, ecological, meteorological, biomechanical and orthopaedic domains.

Chapter 2

Multivariate Circular Models

In this chapter, we aim to fill a gap in the literature in the circular domain by considering normal mean mixture distributions from a transformation viewpoint. We construct a family of distributions on the unit hyper-sphere by conditioning a spherical normal mean mixture distribution with a general weight function. The resulting family of distributions accounts for symmetry, asymmetry, unimodality and bimodality depending on the choice of the weight function and parameter set. The problem of identifiability is partially addressed by re-parameterization. The circle and sphere are considered as special cases with various weight functions in a numerical illustration. A synopsis of the estimation procedure utilized in the numerical study is given. The fit of the proposed model to two real data sets as well as a simulated data set is evaluated and compared to well known circular models.

2.1 Introduction

A new family of flexible distributions on the unit hyper-sphere of arbitrary dimension, which we call the Mean Direction Mixture (**MDM**) family is proposed. This family is

This chapter is based on content that has been published in [83].

inspired by a variant of mixture modeling namely a mean mixture. Applying an adaptation of the mean mixture technique results in a weight function being associated with the mean direction parameter. The complexity of the data influences the choice of the weight function. The characteristics of flexibility that the proposed model can account for are skew-symmetric behavior, bimodal behavior and peakedness. A common problem that arises in mixture modeling is that of identifiability. For our proposed family, we address the problem of identifiability and suggest a remedy to partially addresses this matter. We propose re-parameterization to reduce the number of parameters in the model. To demonstrate our model's performance we consider the two cases of reduced dimension namely, distribution on the circle ($d = 2$) and the distribution on the sphere ($d = 3$), with various weight functions. Simulation from our proposed family is easily computable and involves a modification of a von Mises-Fisher random variable.

The need for flexible distributions is not limited to the circle but extends to other manifolds too, specifically the hyper-sphere. Various multivariate directional models have been proposed in literature. Most of these models are symmetric and extensions of distributions proposed on the circle such as [58]. A summary of the existing models is given in [68; 69; 74; 31; 88].

On the real line various flexible distributions have been constructed by using a normal mixture approach as pointed out in [9] and [84]. The use of a scale mixture to add to the flexibility of a model in terms of the shape is highlighted in [15], however, the resulting distribution is still symmetric. The use of a mean mixture can result in an asymmetrical distribution as pointed out in [71]. The skew normal distribution in the linear domain is a well-known model that can be constructed by using a normal mean mixture as illustrated in [84]. Other applications of mean mixture models, among others, can be found in [72; 65; 62]. Another variant of the normal mixture approach is that of mean-variance mixture models which combines the scale and mean mixture approach resulting in flexibility of skewness and tail behavior. Normal mean-variance mixture models have been studied in detail and applied in univariate and multivariate settings abundantly in [81; 97; 104; 8; 43].

The concept of a normal mixture is one that is not new to directional statistics but the application of this technique in the circular domain is limited. From a wrapping viewpoint the scale mixture of normal distributions has been explored in [44] and using the transformation approach scale mixture of normal distributions has been utilized in [99; 59; 100]. In [44] a general overview of the construction of location-scale mixtures on the circle is given for wrapped distributions, however, the scale mixture of normal distributions is studied in greater detail. Mean mixtures have not been investigated in the circular domain from a transformation perspective. This chapter aims to fill that gap by applying an adapted mean mixture in directional statistics to obtain more flexible models. Mixture distributions are appealing due to their elementary stochastic representation. They also allow us to model data with great flexibility accommodating for skewness, multi-modality and peakedness.

The remainder of this chapter follows as, Section 2.2 provides the details for the construction of the proposed family of distributions on the unit hyper-sphere of arbitrary dimension and considers the reduced dimension of the circle. Section 2.3 discusses the challenge of identifiability and provides a solution to address this challenge. The value of the proposed model is numerically illustrated using observed data as well as a simulated data set to emphasize the importance of this family in the directional domain. Section 2.4 concludes with some final remarks.

2.2 Methodology

In this section we present the construction of the proposed family of distributions on the unit hyper-sphere. An adaptation of the mean mixture technique in the linear domain is applied in the circular domain to fulfill the aim of obtaining a flexible family of distributions. Before we construct our proposed family of distributions a brief revisit of normal mean mixture (NMM) distributions in the linear domain is outlined.

A univariate random variable X is said to have a NMM if $X \overset{d}{=} \delta U + Z$, where $Z \sim N(0, w^2)$ independent of the random variable U, $w > 0$ and $X, \delta \in \mathbb{R}$. Hence, the

probability density function (PDF) of $X|(U=u) \sim N(\delta u, w^2)$ is given as

$$\phi(x;\delta u, w^2) = \frac{\exp\left[-\frac{[x-u\delta]^2}{2w^2}\right]}{(2\pi)^{\frac{1}{2}}w}.$$

Then the PDF of X is given by

$$f_X(x) = \int_{D_U} f_{X|U}(x|u)dG(u),$$

where D_U represents the domain of U and $G(u)$ the weight function.

2.2.1 General model

Drawing inspiration from the NMM in the linear domain, we propose a family of distributions in the directional domain using an adaptation of the mean mixture approach. The construction of this family of distributions does not follow a direct application of the NMM, instead the concept of using of a weight function associated with the respective parameter (mean direction in this case) is considered as the basis for the proposed models. We consider the Euclidean space, $\mathbb{R}^d$, and apply a spherical co-ordinate transformation from the random variable $\mathbf{X} = (X_1, X_2, ..., X_d)' \in \mathbb{R}^d$ to a vector $(R, \theta_1, \theta_2, ..., \theta_{d-1})'$ such that $\mathbf{X} = R \cdot e(\mathbf{\Theta})$, where $R = \|\mathbf{X}\|$ and $e(\mathbf{\Theta})$ denotes the direction cosine of $\mathbf{\Theta}$ and the domain of $\mathbf{\Theta}$ is

$$\omega = \left\{ (\boldsymbol{\theta} \mid \theta_1, \theta_2, ..., \theta_{d-2} \in \left[\frac{-\pi}{2}, \frac{\pi}{2}\right), \theta_{d-1} \in [-\pi, \pi) \right\}. \tag{2.1}$$

Following a similar approach to the construction of the von Mises-Fisher distribution, we construct the proposed mean direction mixture (MDM) distribution on the unit hyper-sphere. As our point of departure we consider the spherical multivariate normal distribution which is given as

$$f(r,\boldsymbol{\theta}) = \int_{D_U} \frac{C\exp\left[-\frac{r^2+\rho^2-2r\rho<e(\boldsymbol{\theta}),e(u\boldsymbol{\tau})>}{2w^2}\right]}{(2\pi)^{\frac{d}{2}}(w^d)} \times r^{d-1}\prod_{j=1}^{d-2}\cos^{d-j-1}\theta_j dG(u), \tag{2.2}$$

where $w>0$, $\rho=\|\boldsymbol{\delta}\|$, C is the normalizing constant, $G(u)$ the weight function, D_U represents the domain of U and $<e(\boldsymbol{\theta}),e(u\boldsymbol{\tau})>$ denotes the inner product of $e(\boldsymbol{\theta})$ and $e(u\boldsymbol{\tau})$ with

$$e(\boldsymbol{\Theta}) = \begin{bmatrix} \cos\theta_1\cos\theta_2\ldots\cos\theta_{d-2}\cos\theta_{d-1} \\ \cos\theta_1\cos\theta_2\ldots\cos\theta_{d-2}\sin\theta_{d-1} \\ \vdots \\ \cos\theta_1\sin\theta_2 \\ \sin\theta_1 \end{bmatrix}.$$

We consider the random variable, U, to be associated with the mean direction parameter $\boldsymbol{\tau}$. Similar to associating the random variable U with the mean parameter in the linear domain we adjust the approach slightly to consider the random variable U to be associated with the mean direction parameter. Thus, we can assume that the random variable U can take the form of a circular distribution. This construction differs from the direct application of the mean mixture approach in the linear domain. The construction of the proposed model does not consider the conditional normal $(X|(U=u)\sim N(\delta u,w^2))$ as the point of departure but rather the the spherical multivariate normal with a weight function integrated with the mean direction parameter.

Integrating (2.2) with respect to $\boldsymbol{\Theta}$, we have the marginal PDF of the distance R,

$(r > 0)$,

$$\begin{aligned} f(r) &= \int_{D_U} \left[\frac{Cr^{d-1}}{(2\pi)^{\frac{d}{2}} w^d} \exp\left(-\frac{r^2+\rho^2}{2w^2}\right) \right. \\ &\quad \left. \times \int_{\omega} \exp\left(\frac{r\rho < e(\boldsymbol{\theta}), e(u\boldsymbol{\tau}) >}{w^2}\right) \prod_{j=1}^{d-2} \cos^{d-j-1}\theta_j d\boldsymbol{\theta} \right] dG(u) \\ &= \int_{D_U} \left(\frac{Cr^{\frac{d}{2}}}{w^2 \rho^{\frac{d}{2}-1}}\right) \exp\left(-\frac{r^2+\rho^2}{2w^2}\right) I_{\frac{d}{2}-1}\left(\frac{r\rho}{w^2}\right) G(u) \\ &= \left(\frac{Cr^{\frac{d}{2}}}{w^2 \rho^{\frac{d}{2}-1}}\right) \exp\left(-\frac{r^2+\rho^2}{2w^2}\right) I_{\frac{d}{2}-1}\left(\frac{r\rho}{w^2}\right), \end{aligned} \tag{2.3}$$

where ω is the domain of $\boldsymbol{\Theta}$ as defined in (2.1) and $I_z(\cdot)$ is the modified Bessel function of the first kind with order z defined in Appendix A.1.

Thus, the conditional PDF of the direction given the distance $f(\boldsymbol{\theta}|r) = \frac{f(r,\boldsymbol{\theta})}{f(r)}$, produces a family of PDFs on the unit hyper-sphere. Using (2.2) and (2.3), we can obtain the MDM distribution on the unit hyper-sphere $(d \geq 2)$ as

$$\begin{aligned} f(\boldsymbol{\theta}|r) &= \frac{Cr^{\frac{d}{2}-1}\rho^{\frac{d}{2}-1} E_U\left[\exp\left(\frac{r\rho < e(\boldsymbol{\theta}), e(U\boldsymbol{\tau})>}{w^2}\right)\right]}{(2\pi)^{\frac{d}{2}} w^{d-2} I_{\frac{d}{2}-1}\left(\frac{r\rho}{w^2}\right)} \\ &\quad \times \left(\prod_{j=1}^{d-2} \cos^{d-j-1}\theta_j\right), \end{aligned} \tag{2.4}$$

where $E_U[\cdot]$ represents the expected value with respect to U.

2.2.2 Distribution on the circle

If we let $d = 2$, then the unit hyper-sphere reduces to an unit circle. Thus, the joint PDF in (2.2) simplifies to the distribution on the circle

$$\begin{aligned} f(r,\theta) &= \int_{D_U} \frac{Cr}{2\pi w^2} \exp\left[-\frac{r^2+\rho^2-2r\rho\cos(\theta-u\tau)}{2w^2}\right] dG(u) \\ &= \frac{Cr}{2\pi w^2} \exp\left[-\frac{r^2+\rho^2}{2w^2}\right] E_U\left[\exp\left(\frac{r\rho\cos(\theta-u\tau)}{w^2}\right)\right]. \end{aligned}$$

Subsequently the mean direction mixture distribution on the circle can be obtained from (2.4) as

$$f(\theta|r) = \frac{CE_U\left[\exp\left(\frac{r\rho\cos(\theta-U\tau)}{w^2}\right)\right]}{2\pi I_0\left(\frac{r\rho}{w^2}\right)}, \tag{2.5}$$

where $\tau \in [-\pi,\pi)$, $w,\rho > 0$ and $\theta \in [-\pi,\pi)$.

To illustrate the flexibility of the proposed model we consider the three PDFs defined in Table 2.1 as weight functions for U in (2.5). Substituting these weight functions for U, we obtain various families of distributions on the unit hyper-sphere. Due to the complex form of the proposed model (2.5), we evaluate the proposed family of distributions from a computational viewpoint.

Table 2.1: Probability density functions used as weight functions. The PDFs considered are: the von Mises (vM) as defined in [74], Sine-skewed von Mises (ssvM) proposed by [4] and the wrapped Cauchy (wC) as defined in [74] © 2021 IEEE.

Distribution	Function	Parameter Domain
vM	$\frac{\exp[\kappa\cos(u-\mu)]}{2\pi I_0(\kappa)}$	$\kappa > 0$, $\mu \in [-\pi,\pi)$
ssvM	$\frac{\exp[\kappa\cos(u-\mu)](1+\lambda\sin(u))}{2\pi I_0(\kappa)}$	$\kappa > 0$, $\mu \in [-\pi,\pi)$, $\lambda \in [-1,1]$
wC	$\frac{\sinh(\kappa)}{2\pi[\cosh(\kappa)-\cos(u-\mu)]}$	$\kappa > 0$, $\mu \in [-\pi,\pi)$

2.3 Numerical illustrations

In this section, interpretations of the parameters and identifiabilitly problems are discussed and addressed. A synopsis of the estimation procedure utilized is discussed. As well as a numerical examples of the models is provided.

2.3.1 Identifiability

A discussion on identifiability is fundamental when developing new distributions. The models proposed in this chapter encounter identifiability. Regarding skew families of distributions on the circle, the issue of identifiability is not new. This problem is shown to be a common occurrence in directional statistics by [79] and [42]. In order to partially address this concern, we consider a re-parameterization similar to the von Mises-Fisher distribution given in [73]. The parameters w and ρ in the model (2.4) are identified as concentration parameters. Since w and ρ are both concentration parameters and r is given, we propose the following re-parameterization, $\alpha = \frac{r\rho}{w^2}$, where $\alpha > 0$. Re-parameterizing the PDF in (2.4) we obtain,

$$\begin{aligned} f(\boldsymbol{\theta}|r) &= \frac{C\alpha^{\frac{d}{2}-1}E_U\left[\exp\left(\alpha < e(\boldsymbol{\theta}), e(U\boldsymbol{\tau}) >\right)\right]}{(2\pi)^{\frac{d}{2}} I_{\frac{d}{2}-1}(\alpha)} \\ &\quad \times \left(\prod_{j=1}^{d-2} \cos^{d-j-1}\theta_j\right). \end{aligned} \tag{2.6}$$

Similarly the re-parameterization of the distribution on the circle (2.5) results in

$$f(\theta) = \frac{CE_U\left[\exp\left(\alpha\cos\left(\theta - U\tau\right)\right)\right]}{2\pi I_0(\alpha)}. \tag{2.7}$$

Remark 1. *By re-parameterizing we do not fully solve the problem of identifiability of our model instead we partially relieve the problem by reducing the number of parameters.*

The PDF plots for the proposed model, (2.6) for various parameter values, with weight

functions defined in Table 2.1, are displayed in Figure 2.1. From Figure 2.1, it can be noted that the parameters α and κ control the concentration of the distribution. The PDF becomes more concentrated as α and/or κ increases. The parameter κ also controls the skewness of the distribution together with τ and μ. The parameters τ and μ together influence the modal points. For certain combinations of τ and μ the PDF displays bimodal behavior. The parameter λ influences the peakedness and skewness of the PDF.

2.3.2 Parameter estimation

For the parameter estimation we will focus on the distribution on the circle, however, the notion can be extended to the multivariate case. Our proposed model on the circle (2.7) has two general parameters, α and τ, and then depending on the choice of the weight function additional parameters will require estimation. We consider two approaches for parameter estimation for the proposed model namely the application of maximum likelihood estimation via numerical optimization and maximum likelihood estimation via the Expectation Maximization (EM) algorithm.

As a result of the complexity of the functional form of the density (2.7) there are no closed form expressions for the maximum likelihood estimates (MLEs) that maximize the log-likelihood function, thus, the function is optimized numerically. To obtain the parameter estimates for the numerical examples we used MATLAB's [77] optimization packages. While investigating the estimation process we observed that the log-likelihood surface contained multiple maxima. Another note was that the parameter estimates converged to different sets depending on the initial values (this ties in to the problem of identifiability discussed, see Remark 1). To help address these observations the **GlobalSearch** and **MultiStart** functions in MATLAB were utilized to assist with the search for a global maxima and also account for multiple initial values to obtain stable parameter estimates.

Another approach to estimating the parameters is via the EM algorithm. The construction of the proposed model lends itself well to the use of the EM algorithm for

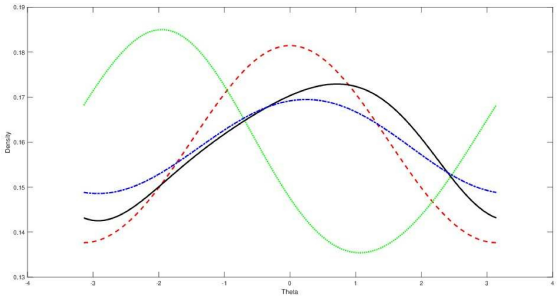

(a) Proposed model with von Mises weight function for: (a) $\alpha = 0.8$, $\tau = 0.9$, $\kappa = 0.1$ and $\mu = 1.5$ (solid line); (b) $\alpha = 0.8$, $\tau = 1.5$, $\kappa = 1$ and $\mu = 0$ (dashed line); (c) $\alpha = 0.4$, $\tau = 0.9$, $\kappa = 1$ and $\mu = -2.3$ (dotted line); (d) $\alpha = 0.8$, $\tau = 2.7$, $\kappa = 1.5$ and $\mu = 0.1$ (dot-dashed line)

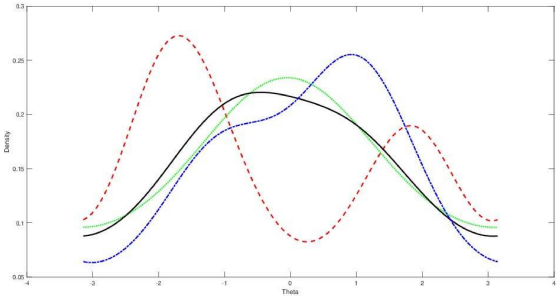

(b) Proposed model with sine-skewed von Mises weight function for: (a) $\alpha = 0.8$, $\tau = 0.4$, $\kappa = 1.3$, $\mu = 2.8$ and $\lambda = 0.7$ (solid line); (b) $\alpha = 2.1$, $\tau = 0.7$, $\kappa = 1.3$, $\mu = 2.9$ and $\lambda = 0.7$ (dashed line); (c) $\alpha = 0.5$, $\tau = 0.2$, $\kappa = 1$, $\mu = -2.5$ and $\lambda = -0.6$ (dotted line); (d) $\alpha = 1.2$, $\tau = 0.4$, $\kappa = 3.1$, $\mu = 2.9$ and $\lambda = 0.2$ (dot-dashed line)

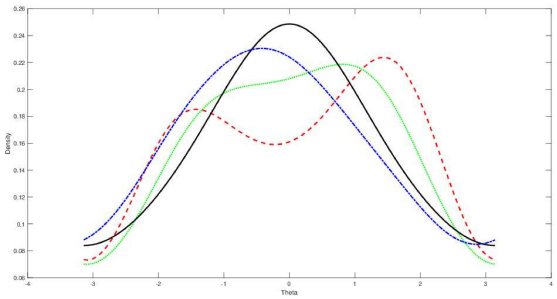

(c) Proposed model with wrapped Cauchy weight function for: (a) $\alpha = 1.4$, $\tau = 0.9$, $\kappa = 0.1$ and $\mu = 1.5$ (solid line); (b) $\alpha = 2.1$, $\tau = 0.7$, $\kappa = 1.3$ and $\mu = 2.9$ (dashed line); (c) $\alpha = 1.4$, $\tau = 0.6$, $\kappa = 1.6$ and $\mu = 2.9$ (dotted line); (d) $\alpha = 2.8$, $\tau = 2.7$, $\kappa = 0.6$ and $\mu = 2.2$ (dot-dashed line)

Figure 2.1: Density plots of the proposed model (2.7) for different parameter values and different weight functions. The weight functions considered are the von Mises, the sine-skewed von Mises and the wrapped Cauchy. © 2021 IEEE

parameter estimation. By considering the observed data as being incomplete and the complete data vector as $Z = (\mathbf{x}, \mathbf{u})'$ where $x_j = re(\theta_j)$ with $e(\cdot)$ as the direction cosine of θ. Considering the observed variables $X|U_j = u_j$ as independent and normally distributed and U_j as the missing variable to be independent and have PDF as defined by the weight function of choice, we can represent the log-likelihood of the complete data

as $log(L_{complete}(\Psi)) = log(L_{X|U}(\Psi)) - log(L_U(\Psi)) - log(L_R(\Psi))$. The log-likelihood functions are derived from the PDFs of the conditional distribution of $X|U$, the weight function of U and distance R respectively. A drawback of the EM algorithm for this model is the extensive runtime and as a result the maximum likelihood approach was preferred in the examples below.

2.3.3 Ants data

For the first real data application we consider the complete ants data set described in [46] based on an animal orientation experiment. The experiment recorded the direction chosen by $n = 730$ ants in response to a stimulus. The test for reflective symmetry proposed by [87] rejected the underlying distribution as being symmetric (p-value = 0.0197). Table 2.2 presents the MLL, AIC and BIC (defined in Appendix A.4) values obtained from fitting the von Mises (vM), sine-skewed von Mises (ssvM), wrapped Cauchy (wC), four-parameter distribution proposed by [57], our proposed model with weight functions von Mises (**MDM-vM**), sine-skewed von Mises (**MDM-ssvM**) and wrapped Cauchy (**MDM-wC**).

Table 2.2: Maximized log-likelihood (MLL), Akaike information criterion (AIC) and Bayesian information criterion (BIC) values for the von Mises (vM), sine-skewed von Mises, wrapped Cauchy (wC), four-parameter distribution, our proposed model with weight functions von Mises (**MDM-vM**), sine-skewed von Mises (**MDM-ssvM**) and wrapped Cauchy (**MDM-wC**) distributions fitted to the ants data © 2021 IEEE.

Model	Performance measures		
$f(\theta\|r)$	MLL	AIC	BIC
vM	-1026.20	2056.40	2065.59
ssvM	-1010.84	2027.69	2041.47
wC	-931.16	1866.32	1875.50
Four-parameter	-921.69	1851.39	1869.77
MDM-vM	**-961.82**	**1931.65**	**1950.01**
MDM-ssvM	**-961.23**	**1932.46**	**1955.43**
MDM-wC	**-919.48**	**1846.97**	**1865.34**

From the results in Table 2.2, the MLL, AIC and BIC support the proposed model

with the weight function wrapped Cauchy (MDM-wC) as the model of best fit followed by the four-parameter model of [57], wrapped Cauchy and the proposed models with weight function von Mises (MDM-vM) and sine-skewed von Mises (MDM-ssvM). The flexibility of our proposed models in capturing the skewness and shape of the data is highlighted in Figure 2.2 which illustrates the fitted PDFs superimposed on the histogram of the data.

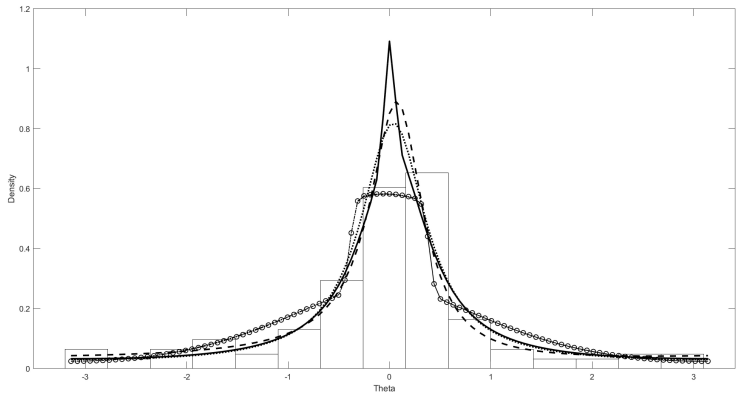

Figure 2.2: Histogram of the ants data with the five best fitted PDFs. The four-parameter model (dashed line), wrapped Cauchy (dotted line), proposed model with weight function wrapped Cauchy (solid line), proposed model with weight function von Mises (dot-dashed line) and proposed model with weight function sine-skewed von Mises (circle line) © 2021 IEEE.

2.3.4 New Caledonian laterites data

For the second real data application, we consider the pole positions determined from the palaeomagnetic study of New Caledonian laterites. The data set consists of $n = 50$ latitude and longitude measurements. The data set can be found in Appendix B1 in [31]. For this application, we consider two weight functions namely, the von Mises and Sine-skewed von Mises for our proposed model (2.6). For comparison we consider four well known spherical distributions as defined in [74] namely, the von Mises-Fisher (vMF), the Watson, Kent and the isotropic angular Gaussian (IAG) distribution on the sphere. The performance of the models is given in Table 2.3.

From the results in Table 2.3, the MDM-vM model performs best based on the MLL

Table 2.3: Performance measures from fitting the proposed distributions to the New Caledonian laterites data. The maximized log-likelihood (MLL), Akaike information criterion (AIC) and Bayesian information criterion (BIC) values for the the von Mises-Fisher (vMF), Watson, Kent, isotropic angular Gaussian (IAG) and our proposed model with weight functions von Mises (**MDM-vM**) and sine-skewed von Mises (**MDM-ssvM**) © 2021 IEEE.

Model	Performance measures		
$f(\theta\|r)$	MLL	AIC	BIC
vMF	-118.031	242.062	247.798
Watson	-135.698	277.397	283.133
IAG	-116.437	238.874	244.610
Kent	-112.052	230.103	235.839
MDM-vM	**-109.823**	**229.646**	**239.207**
MDM-ssvM	**-110.883**	**233.766**	**245.238**

and AIC. However, the Kent distribution outperforms based on the BIC. Overall the proposed MDM models compete well against the well known models. The estimated density plot of the MDM-vM model with the New Caledonian laterites data are given in Figure 2.3.

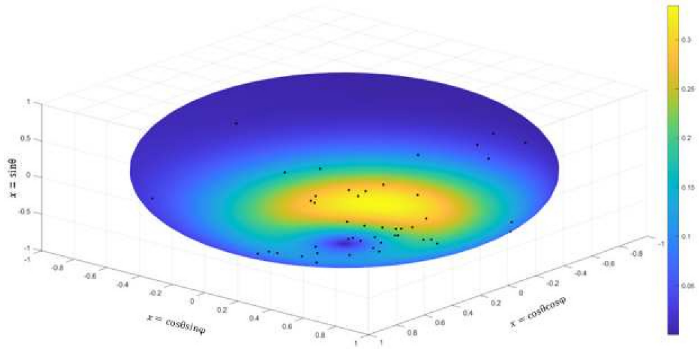

Figure 2.3: Estimated PDF plot for the model of best fit (proposed model with weight function von Mises) with the New Caledonian laterites data © 2021 IEEE.

2.3.5 Simulation study

Simulation from our proposed family is easily computable and involves a modification of a von Mises-Fisher random variable. We consider a sample size of $n = 550$ simulated values from the mean direction mixture model with weight function sine-skewed von

Mises (MDM-ssvM). The true parameter values are $\alpha = 2.22$, $\tau = 0.5$, $\kappa = 2.3$, $\mu = 2.8$ and $\lambda = 0.4$. By applying the test for symmetry proposed by [87], we can observe that the underlying distribution is rejected (p-value = 0.00001) therefore, our data is not symmetric.

Table 2.4 provides the estimated parameter values for the proposed models. From the MLEs, the identifiability discussed in Section 2.3.1 is seen as the MLEs do not necessarily converge to the true parameter values. The results from performing maximum likelihood estimation are given in Table 2.5. The likelihood value of the MDM-ssvM for the true parameters is -962.68. The histogram of the data along with the fitted models are displayed in Figure 2.4.

Table 2.4: Maximum likelihood estimates for the parameters of the proposed model (2.7) with weight functions von Mises (MDM-vM), sine-skewed von Mises (MDM-ssvM) and wrapped Cauchy (MDM-wC) for the simulated data © 2021 IEEE.

	$\hat{\alpha}$	$\hat{\tau}$	$\hat{\kappa}$	$\hat{\mu}$	$\hat{\lambda}$
MDM-vM	1.87	2.60	13.0	2.97	-
MDM-ssvM	1.84	0.59	6.94	0.81	1
MDM-wC	3.27	2.69	0.33	2.84	-

Table 2.5: Performance measures from fitting the proposed distributions to the simulated data. The maximized log-likelihood (MLL), Akaike information criterion (AIC) and Bayesian information criterion (BIC) values for von Mises (vM), sine-skewed von Mises (ssvM), wrapped Cauchy (wC), our proposed model with weight functions von Mises (MDM-vM), sine-skewed von Mises (MDM-ssvM) and wrapped Cauchy (MDM-wC) distributions © 2021 IEEE.

Model	Performance measures		
	MLL	AIC	BIC
vM	-961.46	1926.92	1935.53
ssvM	-957.53	1921.06	1933.99
wC	-958.22	1920.44	1929.06
MDM-vM	-947.95	1903.91	1921.15
MDM-ssvM	-947.65	1905.31	1926.86
MDM-wC	-948.12	1904.24	1921.48

From the results in Table 2.5, the AIC and BIC support the MDM-vM as the best fitting model followed by the MDM-wC and MDM-ssvM models.

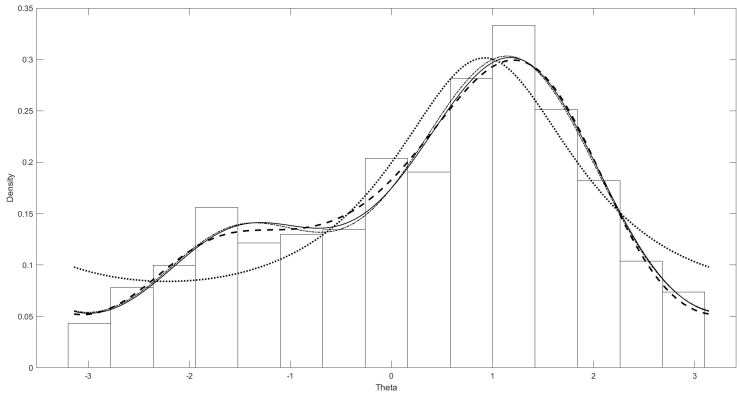

Figure 2.4: Estimated PDF plots of best fit models for the simulated data. The wrapped Cauchy (dotted line), proposed model with weight function von Mises (solid line), proposed model with weight function wrapped Cauchy (dashed line) and proposed model with weight function sine-skewed von Mises (dot-dashed line) © 2021 IEEE.

2.4 Conclusion

In this chapter, we constructed a flexible family of distributions on the unit hyper-sphere and considered the circle and sphere as the special cases for the numerical illustrations. Our proposal stems from the technique of a mean mixture of normal distributions in the linear domain, used to introduce more flexibility in models, and is adapted to only consider a mixing effect on the mean direction parameter. The construction involves the use of a weight function which can be chosen by the practitioner depending on the complexity of the data. The resulting family of distributions can account for symmetry, asymmetry, unimodality and bimodality depending on the choice of the weight function and parameter set. To alleviate the identifiability present in the model, a re-parameterization is proposed. Overall, the mean direction mixture with the von Mises and wrapped Cauchy as weight functions seem to perform the best on both the real data as well as the simulated data sets, based on the AIC and BIC when compared with alternative models, as shown in the numerical illustrations. A weakness of the proposed model arises with the interpretability of the parameters. The interpretation of the parameters cannot be done in isolation but rather as a parameter set. However, this property does not take away from the flexibility of the proposed model instead forces the practitioner to jointly view the influence of the

parameters.

The model proposed in this chapter was developed by adapting the techniques discussed in [99], where a scale mixture of the normal distribution was considered and transformed to the circular domain via spherical transformations. Other approaches which are similar to the methodology used was considered in [78] and [5], where a stereographic projection from the real line to the circle was considered. An extension to the sphere was briefly discussed. The model in this chapter differs from the aforementioned work in that we consider an adapted approach of the mean mixture of the normal distribution which is defined in terms of a weight function and thus the practitioner has more flexibility to play around with the shape and mean direction of the distribution once we move into the circular domain. As well as the proposed model can account for skewness and multimodality whereas the models in [99; 78; 5] are symmetric and unimodal.

Chapter 3

Circular-Linear Models

The joint modeling of angular and linear observations is crucial as data of this nature are prevalent in multiple disciplines, for example; the joint modeling of wind direction and another climatological variable such as wind speed or air temperature, the direction an animal moves and the distance moved, or wave direction and wave height. Hence, there is a need for developing flexible distributions on the hyper-disc, which has support of the interior of the hyper-sphere, as it allows for modeling the combination of angular and linear observations. This chapter addresses this need by developing flexible distributions for the disc that have the ability to capture any inherent bimodality present in the data. A new class of bivariate distributions is proposed which has support on the unit disc in two dimensions that includes, as a special case, the existing Möbius distribution on the disc. This class is obtained by expressing the PDF in a general form using a measurable function termed as generator. Special cases of this generator are considered to demonstrate the flexibility. By applying a conformal mapping to the generator function a new Möbius distribution class emanates. The flexible behavior of the proposed models in terms of bimodality and skewness is graphically demonstrated. Preliminary evidential analysis of the wind data observed at Marion Island reveals the absence of unimodality in the data.

This chapter is based on content that has been published in [13; 7]. [13] Reproduced with permission from A. Bekker, P. Nagar and M. Arashi, Symmetry; published by MDPI, 2019. [7] Reproduced with permission from M. Arashi, P. Nagar and A. Bekker, Sustainability; published by MDPI, 2020.

The fit of the proposed models, which account for bimodality, to the Marion Island wind data were evaluated analytically and visually.

South Africa has great potential for considering wind energy as an alternative resource as the climatology allows for significant wind energy production. An accurate joint description of the wind speed (linear) and wind direction (circular) characteristics is important for wind farm development. An application of the proposed model for the use in wind energy analysis is presented. Special cases of the proposed model are applied to wind speed and wind direction data recorded every ten minutes at two locations in South Africa. Evaluation of the models is based on three different information criteria and normalized deviation.

3.1 Introduction

A general framework for distributions which has support on the unit disc and includes the Möbius distribution on the disc [52] as a special case is proposed. This proposed class of the distributions accounts for both bimodality and skewness. We define this distribution by using a *generator function* and applying a conformal mapping, Möbius transformation, to obtain a new Möbius distribution class. This new class allows for bimodality when the generator function exhibits bimodal behavior with asymmetry introduced by the Möbius transformation.

The analytical description of wind climate is usually confined to the description of wind speed; however, the joint description of the directional and linear wind characteristics is also essential. This joint modeling of wind speed and direction is important for climatology and a variety of ocean engineering and ecological applications. Modeling of short-term wind speed is essential for evaluating wind energy potential. Typical distributions that are used in characterizing wind speed observations are, among others, Weibull, gamma, normal, Rayleigh, log-normal, Nakagami, inverse Gaussian, logistic, and Birnbaum–Saunders distributions. A review of the different distributions used to

model wind speed is given in [35] and [22]. Apart from wind speed, the importance of including wind direction in the analysis of wind energy has been emphasized in many studies [103; 90; 40; 109; 117; 102; 21; 37; 29; 96; 35; 26]. The use of a joint PDF (JPDF) of wind speed (linear variable) and wind direction (circular variable) is important in wind energy projects [103]. Further emphasis on the necessity of bivariate modeling of wind speed and wind direction was raised by [103]. Current bivariate models for wind speed and wind direction have all been defined on a cylindrical manifold. A comprehensive summary of circular–linear distributions on the cylindrical manifold can be found in [68]. Unlike the widely used Johnson–Wehrly (JW) [49] construction method used in [103; 21; 37; 96; 116; 10; 27].

One approach to capture both the linear and directional variables is by means of a disc. There are very few distributions available with support on the unit disc. The only literature that investigates distributions on the disc are those by Jones [51; 52] and Uesu, et al. [108]. In [51], the bivariate beta distribution was proposed for the disc which is a symmetric distribution. In [52], the Möbius distribution on the disc was proposed, which allowed for skewness. The multivariate extension of the Möbius distribution on the disc to the hyper-disc was then proposed by Uesu, et al. [108]. A shortcoming in the existing distributions on a disc is the ability to account for bimodality present in the data. There exists flexible distributions for cylindrical models as proposed in [49; 30; 3; 88; 2; 55; 67], but not the disc. The need for jointly modeling a linear and angular variable on a disc manifold stems from the cyclic nature of the angular variable which cannot be modeled the same as a linear variable. Many distributions have been proposed for modeling angular variables on a circle and other manifolds. For a full summary of these models, refer to [74; 68; 88].

An advantage of the proposed model is that it extends the shape characteristics of the model on the unit disc proposed by Jones [52] to account for more flexibility. This approach to modeling wind data differs from those in [20; 115; 10; 103; 37; 116; 107], by means of the correlation structure and method for obtaining the joint distribution. The

aforementioned models have been built by means of: (i) the Johnson–Wehrly (JW) [49] method; and (ii) a copula approach where the univariate models of best fit are chosen to obtain a joint bivariate distribution for the wind speed and wind direction. The proposed model in this chapter has an embedded correlation structure present to jointly account for the wind speed and wind direction. It was pointed out in [96] that the joint modeling of wind speed and wind direction is more significant than a univariate analysis of the wind speed. The univariate distribution of the wind speed or wind direction is not considered since Soukissian, et al. [103] pointed out that the best univariate distribution for wind speed does not provide the best bivariate fit for the wind speed and wind direction.

Furthermore, this proposed class of distributions accounts for bimodality and skewness present in the data. Thus, the practitioner can more accurately model the wind power density [39] for determining wind farm locations and optimal wind energy potential at various locations.

The reminder of this chapter is organized as follows, in Section 3.2 we construct the general framework for the proposed class of distributions. Special cases of the model are studied in Section 3.3. Two applications of the model are provided in Section 3.4 followed by some final remarks in Section 3.5.

3.2 Methodology

In this section, we define the *general Möbius class* and consider an algorithm to estimate the generator function and the parameters using a semi-parametric approach.

3.2.1 Möbius transformation

The Möbius transformation is defined on the extended complex plane denoted by $\tilde{\mathbb{C}}$ [94]. Hence, we rewrite the cartesian coordinates in polar coordinates. Considering the polar coordinate form of the unit disc, we write $z = (x, y)$ and $w = (u, v)$ as complex numbers with $w = re^{i\theta},\ 0 \leq r \leq 1,\ -\pi < \theta \leq \pi$ and i the unit imaginary number. The Möbius

transformation is defined by [61] as

$$z = M_c(w) = \frac{w-c}{1-\bar{c}w} \quad \text{with inverse} \quad w = M_{-c}(z) = \frac{z+c}{1+\bar{c}z}$$

where $c = ae^{i\mu}$, $0 \leq a < 1$ and $\bar{c}$ denotes the complex conjugate. The only conformal mapping from the unit disc to itself is the Möbius transformation [61]. Using this Möbius transformation, we can develop probability distributions [78; 52; 56].

Further details on the Möbius transformation utilized in the next sections is given in Appendix B.1.

3.2.2 Cartesian coordinate configuration of the general class

Consider the general bivariate PDF,

$$f(x,y) = Cg\left(x^2+y^2\right), \tag{3.1}$$

where $0 \leq x^2+y^2 \leq 1$ and $g(\cdot)$ is a measurable and continuous function termed as the "generator" that admits the Taylor's series expansion. The normalizing constant C can be obtained from the polar form of (3.1) as

$$C^{-1} = \int_0^{2\pi}\int_0^1 sg\left(s^2\right)dsd\phi = 2\pi\int_0^1 \frac{1}{2}g(u)\,du = \pi\int_0^1 g(u)\,du, \tag{3.2}$$

when the $g(\cdot)$ function is infinitely differentiable at the point zero. Numerical computation of the integral in (3.2) is given by

$$\int_0^1 g(u)\,du = E_U[g(X)]. \tag{3.3}$$

where $E[\cdot]$ denotes the expected value with respect to the random variable U. Writing the Taylor's series expansion (defined in Appendix A.1) of $g(u)$ in (3.2) around zero gives

$$C^{-1} = \pi \sum_{j=0}^{\infty} \frac{g^{(j)}(0)}{j!} \int_0^1 u^j du = \pi \sum_{j=0}^{\infty} \frac{g^{(j)}(0)}{(j+1)!},$$

which allows the computation of the normalizing constant by derivatives of $g(\cdot)$ around zero.

3.2.3 General Möbius distribution on the disc

By applying the Möbius transformation in Section 3.2.1 (see Appendix B.1), we obtain the class of general Möbius distributions on the disc as,

$$f(r,\theta) = \frac{C\left(1-a^2\right)^2 r}{\pi\left[1-2ar\cos\left(\theta-\mu\right)+a^2r^2\right]^2} g\left(\frac{a^2-2ar\cos\left(\theta-\mu\right)+r^2}{1-2ar\cos\left(\theta-\mu\right)+a^2r^2}\right), \tag{3.4}$$

where $0 \leq a < 1$, $-\pi < \mu \leq \pi$ and $0 \leq r \leq 1$, $-\pi < \theta \leq \pi$. We denote this class as $(r,\theta) \sim GM(a,\mu,g)$.

Trivial calculations reveal for a strictly increasing generator function, $L < f(r,\theta) < U$, where

$$L = \frac{C(1-a^2)^2 r}{\pi(1+ar)^4} g\left[\frac{(a+r)^2}{(1+ar)^2}\right], \quad U = \frac{C(1-a^2)^2 r}{\pi(1-ar)^4} g\left[\frac{(a-r)^2}{(1-ar)^2}\right]. \tag{3.5}$$

These bounds are achieved when $\theta = \mu(+\pi)$. For the limiting case $a \to 0$, the joint distribution tends to $Crg\left(r^2\right)/\pi$. We can rewrite the PDF in (3.4) in the Cartesian space by performing the transformation: $u = r\cos\theta$ and $v = r\sin\theta$. Then, the resulting PDF is

$$\begin{aligned} f(u,v) = & \frac{C\left(1-a^2\right)^2}{\pi\left[1-2au\cos\mu-2av\sin\mu+a^2\left(u^2+v^2\right)\right]^2} \\ & \times g\left(\frac{a^2-2au\cos\mu-2av\sin\mu+u^2+v^2}{1-2au\cos\mu-2av\sin\mu+a^2\left(u^2+v^2\right)}\right), \end{aligned} \tag{3.6}$$

where $0 \leq u^2+v^2 \leq 1$, $0 \leq a < 1$ and $-\pi < \mu \leq \pi$.

3.2.4 Maximum likelihood estimation

In this section, we derive the maximum likelihood (ML) estimates of the parameters. Let $S = \{(r_i, \theta_i)\}_{i=1}^{n}$ be a random sample from $GM(a, \mu, g)$, where all parameters are unknown. From (3.4) the likelihood function has the form

$$L(a, \mu, g) = \left(\frac{C(1-a^2)^2}{\pi} \right)^n \prod_{j=1}^{n} \frac{r_j g\left(\frac{a^2 - 2ar_j \cos(\theta_j - \mu) + r_j^2}{1 - 2ar_j \cos(\theta_j - \mu) + a^2 r_j^2} \right)}{\left[1 - 2ar_j \cos(\theta_j - \mu) + a^2 r_j^2\right]^2}. \tag{3.7}$$

Computational stages for estimating $g(\cdot)$ and the parameters are given by Algorithm 1.

Algorithm 1 Generic maximum likelihood estimation algorithm

Step 1. Create a grid of the parameter space of a and μ. Set the starting values for the parameters to $\hat{a} = 0$ and $\hat{\mu} = -\pi$. These values are chosen as they are the lower bounds of the respective parameter domain.

Step 2. Given the observations $(r_1, \theta_1), (r_2, \theta_2), \ldots, (r_n, \theta_n)$, we estimate $g(\cdot)$ via

$$\hat{g}(x) = \frac{1}{nh} \sum_{j=0}^{n} K\left(\frac{x - x_j}{h} \right),$$

where $x_j = (a^2 - 2ar_j \cos(\theta_j - \mu) + r_j^2)/(1 - 2ar_j \cos(\theta_j - \mu) + a^2 r_j^2)$, h is the bandwidth and $K(\cdot)$ is the kernel function.

Step 3. Compute the likelihood function, (3.7), using the estimated $\hat{g}(\cdot)$, $\hat{a}$ and $\hat{\mu}$.

Step 4. Repeat Steps 2 and 3, by sequentially updating the set of parameter values of a and μ in the predefined grid. The estimated values are those that result in the maximized likelihood function.

Step 5. Repeat steps 1 o 4 for a grid with decreased spacing to ensure that the estimated parameters represent the maximum of the likelihood function over the space of interest. Continue to decrease grid spacing until parameters converge.

In Algorithm 1, the bandwidth h can be obtained using existing methods since the values in the argument of $g(\cdot)$ function belong to the Cartesian space. In Algorithm 1, the computation time can be improved by considering a grid approach in Step 4 over the domain of the two parameters.

Remark 2. *The mathematical expressions for the modality of the model (3.4) are intractable.*

3.3 Special cases of the general model

In this section, we consider three special cases of the generator function, $g(\cdot)$. The first generator function, Pearson Type II distribution [50], results in the well known Möbius distribution on the disc proposed by Jones [52]. The second generator function, Kummer beta distribution [82], results in the Kummer beta Möbius distribution and the third generator function, beta type III distribution [19], results in the beta type III Möbius distribution. The Pearson Type II distribution was used for comparison purposes and to show that the proposed new class of distributions include the well known distribution on the disc [52]. The other special cases are considered due to their flexibility and the capacity of the distribution to handle bimodality [82].

3.3.1 Möbius distribution on the disc

By defining the generator function as

$$g(w) = (1-w)^{\gamma-1},$$

we obtain the bivariate spherically symmetric beta (Pearson Type II) distribution [50], with PDF,

$$f_\gamma(x,y) = \frac{\gamma}{\pi}\left(1-x^2-y^2\right)^{\gamma-1}, \tag{3.8}$$

where $C = \frac{\gamma}{\pi} > 0, \;\; 0 \leq x^2+y^2 \leq 1$.

The PDF and marginal distribution graphs in Figures 3.1 and 3.2 illustrate the symmetrical and unimodal behavior of the generator function in (3.8).

After applying the Möbius transformation, this choice of generator function in (3.8) simplifies to the well known Möbius distribution on the disc defined by Jones [52].

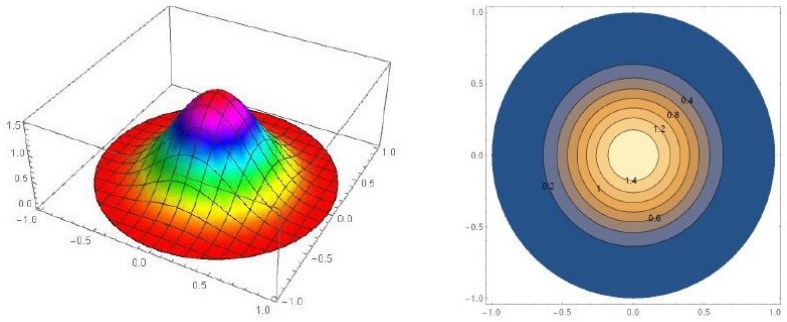

Figure 3.1: The PDF and contour plot of the bivariate Pearson Type II distribution in (3.8) for $\gamma = 5$.

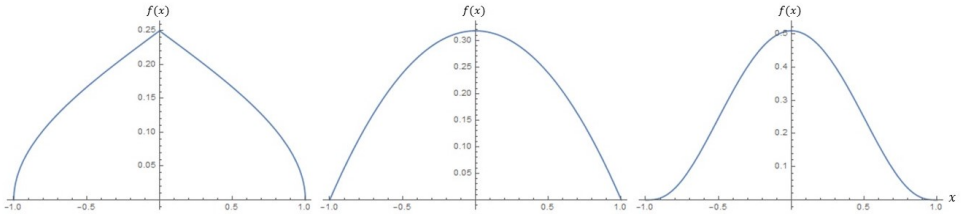

Figure 3.2: The marginal PDF of the bivariate Pearson Type II distribution in (3.8) for $\gamma = 0.5, 1, 3$ from left to right.

The polar form PDF is given as

$$f(r,\theta) = \frac{\gamma\left(1-a^2\right)^{\gamma+1} r\left(1-r^2\right)^{\gamma-1}}{\pi\left(1-2ar\cos\left(\theta-\mu\right)+a^2r^2\right)^{\gamma+1}}, \tag{3.9}$$

where $0 \leq a < 1$, $-\pi < \mu \leq \pi$, $0 \leq r \leq 1$ and $-\pi < \theta \leq \pi$. The PDF in terms of Cartesian coordinates is

$$f(u,v) = \frac{\gamma\left(1-a^2\right)^{\gamma+1}\left(u^2+v^2\right)^{\frac{1}{2}}\left(1-u^2-v^2\right)^{\gamma-1}}{\pi\left(1-2au\cos\mu-2av\sin\mu+a^2\left(u^2+v^2\right)\right)^{\gamma+1}}, \tag{3.10}$$

where $0 \leq a < 1$, $-\pi < \mu \leq \pi$ and $0 \leq u^2+v^2 \leq 1$.

The parameters can be interpreted as γ controls the concentration, a controls the skewness (or the asymmetry for the length from the center of the disc) and μ controls the orientation of the distribution (see Figure 3.3).

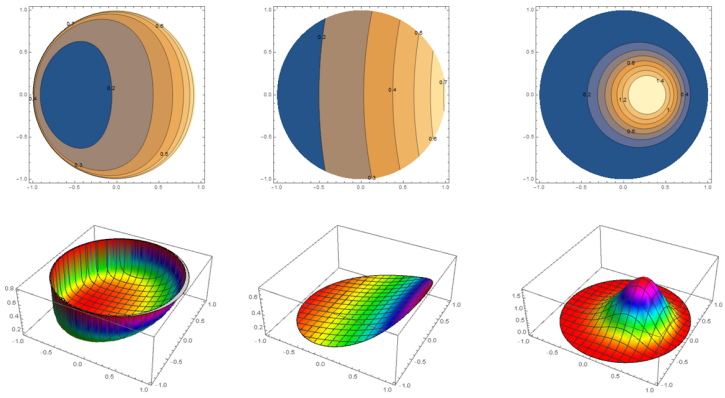

(a) PDF and contour plots of (3.10) for $a = 0.2$, $\mu = 0$ and $\gamma = 0.7, 1, 5$ (from left to right).

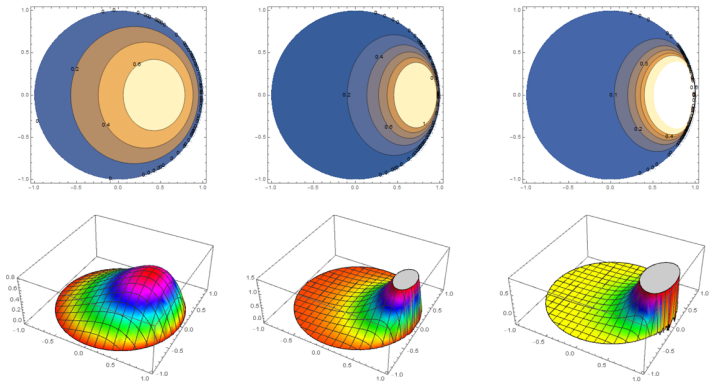

(b) PDF and contour plots of (3.10) for $\gamma = 2$, $\mu = 0$ and $a = 0.2, 0.5, 0.7$ (from left to right).

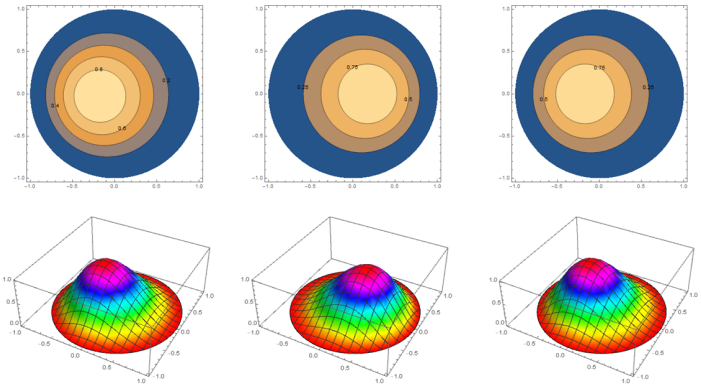

(c) PDF and contour plots of (3.10) for $\gamma = 3$, $a = 0.1$ and $\mu = -3, 0, \pi$ (from left to right).

Figure 3.3: PDF and contour plots of the Möbius distribution on the disc, (3.10), for varying parameter values.

Maximum likelihood estimation

The log-likelihood of the polar PDF, (3.9), is obtained for the ML as:

$$\begin{aligned}\log\left[L\left(f\left(r,\theta\right)\right)\right] &= n\log\left[\gamma\right]+n\left(\gamma+1\right)\log\left[1-a^2\right]+\sum_{j=1}^{2}\log\left[r_j\right]\\ &\quad+\sum_{j=1}^{2}\left(\gamma-1\right)\log\left[1-r_j^2\right]-n\log\left[\pi\right]\\ &\quad-\sum_{j=1}^{2}\left(\gamma+1\right)\log\left[1-2ar_j\cos\left(\theta_j-\mu\right)+a^2r_j\right].\end{aligned} \tag{3.11}$$

While closed form expressions for the MLEs of (3.9) are intractable, a set of expressions that can be used to derive the MLEs is given in Appendix B.2.1.

3.3.2 Kummer beta Möbius distribution on the disc

Consider the following generator function

$$g(w)=w^{\beta-1}\left(1-w\right)^{\gamma-1}\exp\left\{-\lambda w\right\},$$

where $\gamma,\beta,\lambda>0$. By substituting the generator function in (3.1), the resulting distribution is a bivariate Kummer beta distribution [82] with PDF

$$f_{\gamma,\lambda,\beta}\left(x,y\right)=C\left(x^2+y^2\right)^{\beta-1}\left(1-x^2-y^2\right)^{\gamma-1}\exp\left\{-\lambda\left(x^2+y^2\right)\right\}, \tag{3.12}$$

where $\gamma,\beta,\lambda>0$, $0\leq x^2+y^2\leq 1$ and

$$C=\frac{\Gamma\left(\beta+\gamma\right)}{\pi\Gamma\left(\beta\right)\Gamma\left(\gamma\right)\ {}_1F_1\left(\beta,\beta+\gamma,-\lambda\right)} \tag{3.13}$$

is the normalizing constant where ${}_1F_1(\cdot)$ is the confluent hypergeometric function of the first kind defined in Appendix A.1.

The PDF and marginal distribution graphs in Figures 3.4 and 3.5 illustrate the symmetrical behavior of the generator function and the bimodal behavior is observed in Figure 3.5.

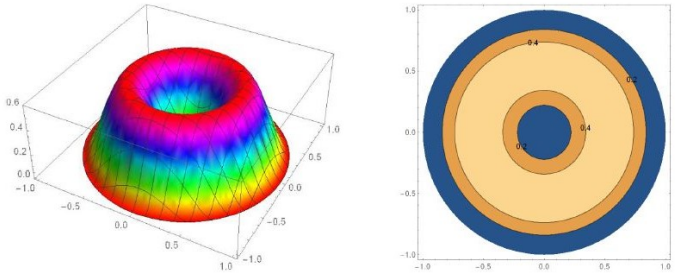

Figure 3.4: The PDF and contour plot of the bivariate Kummer beta distribution in (3.12) for $\gamma = 3, \beta = 2$ and $\lambda = 0.5$.

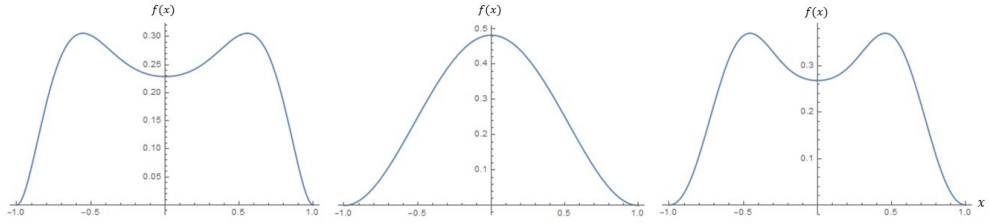

Figure 3.5: The marginal PDF plot of the bivariate Kummer beta distribution in (3.12) for $\gamma = 2, 2, 2, \beta = 3, 1, 3$ and $\lambda = 1, 1, 4$ from left to right.

After applying the inverse Möbius transformation in Section 3.2.1, the *Kummer beta Möbius distribution* is obtained from (3.4) with the PDF in terms of the polar coordinates as

$$\begin{aligned} f(r,\theta) &= Cr\left(1-a^2\right)^{\gamma+1}\left(1-r^2\right)^{\gamma-1}\left[a^2-2ar\cos(\theta-\mu)+r^2\right]^{\beta-1} \\ &\quad \times \exp\left\{\frac{-\lambda\left[a^2-2ar\cos(\theta-\mu)+r^2\right]}{1-2ar\cos(\theta-\mu)+a^2r^2}\right\} \\ &\quad \times \left[1-2ar\cos(\theta-\mu)+a^2r^2\right]^{-\gamma-\beta}, \end{aligned} \tag{3.14}$$

where $0 \leq a < 1$, $-\pi < \mu \leq \pi$, $0 \leq r \leq 1$, $-\pi < \theta \leq \pi$ and C given by (3.13).

We can obtain the PDF in terms of Cartesian coordinates (u, v) by using (3.6), thus

the PDF is

$$\begin{aligned} f(u,v) &= C\left(1-a^2\right)^{\gamma+1}\left(1-u^2-v^2\right)^{\gamma-1}\left[a^2-2au\cos\mu-2av\sin\mu+\left(u^2+v^2\right)\right]^{\beta-1} \\ &\quad\times\exp\left\{\frac{-\lambda\left[a^2-2au\cos\mu-2av\sin\mu+\left(u^2+v^2\right)\right]}{1-2au\cos\mu-2av\sin\mu+a^2\left(u^2+v^2\right)}\right\} \\ &\quad\times\left[1-2au\cos\mu-2av\sin\mu+a^2\left(u^2+v^2\right)\right]^{-\gamma-\beta}, \end{aligned} \tag{3.15}$$

where $0 \leq u^2+v^2 \leq 1$, $0 \leq a < 1$, $-\pi < \mu \leq \pi$ and C is given by (3.13).

The parameters can be interpreted as γ controls the concentration, while β contributes to the concentration by adding bimodality. As the value of β increases, the model introduces another mode in the form of an antimode, as seen in the plots of the generator function in Figure 3.4. The parameter λ controls the steepness of the concentration, a controls the skewness (or the asymmetry for the length from the center of the disc) and μ controls the orientation of the distribution (see Figure 3.6).

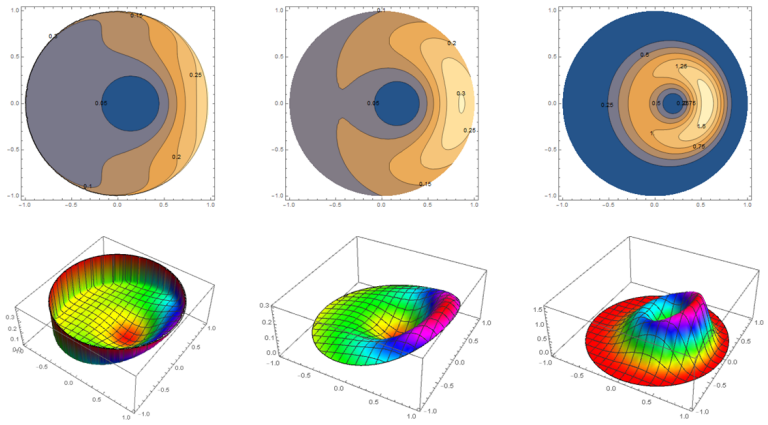

(a) PDF and contour plots (3.16) for $a = 0.2$, $\mu = 0$, $\beta = 2$, $\lambda = 2$ and $\gamma = 0.8, 1, 5$ (from left to right).

Figure 3.6: PDF and contour plots of the Kummer beta Möbius distribution, (3.16), for varying parameter values.

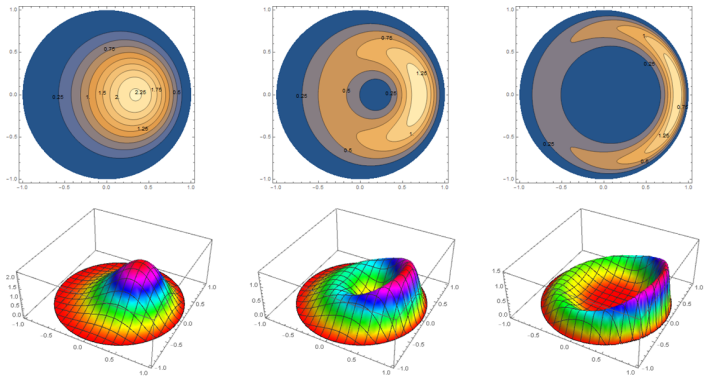

(b) PDF and contour plots (3.16) for $a = 0.2$, $\mu = 0$, $\gamma = 3$, $\lambda = 0.5$ and $\beta = 1, 2, 5$ (from left to right).

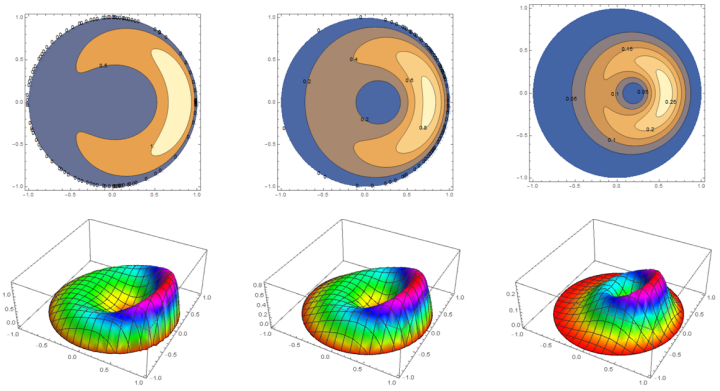

(c) PDF and contour plots (3.16) for $a = 0.2$, $\mu = 0$, $\gamma = 2$, $\beta = 2$ and $\lambda = 0, 1, 5$ (from left to right).

Figure 3.6: PDF and contour plots of the Kummer beta Möbius distribution, (3.16), for varying parameter values. (cont.)

Maximum likelihood estimation

While closed form expressions for the MLEs of (3.15) are intractable, a set of expressions that can be used to derive the MLEs is given in Appendix B.2.2.

The log-likelihood of the polar PDF, (3.15), is obtained for the ML as:

$$\begin{aligned}\log\left[L\left[f\left(r,\theta\right)\right]\right] &= n\log\left[\Gamma\left(\gamma+\beta\right)\right]-n\log\left[\Gamma\left(\beta\right)\right]-n\log\left[\Gamma\left(\gamma\right)\right]\\ &\quad -n\log\left[{}_1F_1\left(\beta,\beta+\gamma,-\lambda\right)\right]-n\log\left[\pi\right]+n\left(\gamma+1\right)\log\left[1-a^2\right]\\ &\quad +\left(\gamma-1\right)\sum_{j=1}^{n}\log\left(1-r_j^2\right)+\sum_{j=1}^{n}\log\left(r_j\right)\\ &\quad +\left(\beta-1\right)\sum_{j=1}^{n}\log\left[a^2-2ar_j\cos\left(\theta_j-\mu\right)+r_j^2\right]\\ &\quad -\left(\gamma+\beta\right)\sum_{j=1}^{n}\log\left[1-2ar_j\cos\left(\theta_j-\mu\right)+a^2r_j^2\right]\\ &\quad -\lambda\sum_{j=1}^{n}\frac{\left[a^2-2ar_j\cos\left(\theta_j-\mu\right)+r_j^2\right]}{\left[1-2ar_j\cos\left(\theta_j-\mu\right)+a^2r_j^2\right]}.\end{aligned} \tag{3.16}$$

3.3.3 Beta type III Möbius distribution on the disc

Consider the following generator function

$$g(w)=w^{\beta-1}\left(1-w\right)^{\gamma-1}\left(1+w\right)^{-(\gamma+\beta)},$$

where $\gamma,\beta>0$. By substituting the generator in (3.1), the resulting distribution is a bivariate beta type III distribution [19] with PDF

$$f_{\gamma,\beta}\left(x,y\right)=C\left(x^2+y^2\right)^{\beta-1}\left(1-x^2-y^2\right)^{\gamma-1}\left(1+x^2+y^2\right)^{-(\gamma+\beta)}, \tag{3.17}$$

where $\gamma,\beta>0$, $0\leq x^2+y^2\leq 1$ and

$$C=\frac{2^{\beta}\Gamma\left(\beta+\gamma\right)}{\pi\Gamma\left(\beta\right)\Gamma\left(\gamma\right)} \tag{3.18}$$

is the normalizing constant.

The PDF and marginal distribution graphs in Figures 3.7 and 3.8 illustrate the symmetrical and bimodal behavior of the generator function.

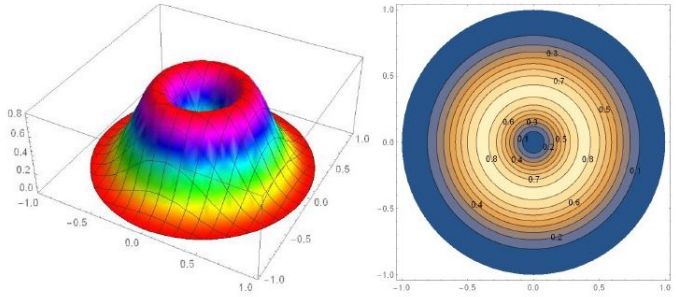

Figure 3.7: The PDF and contour plot of the bivariate beta type III distribution in (3.17) for $\gamma = 3$ and $\beta = 2$.

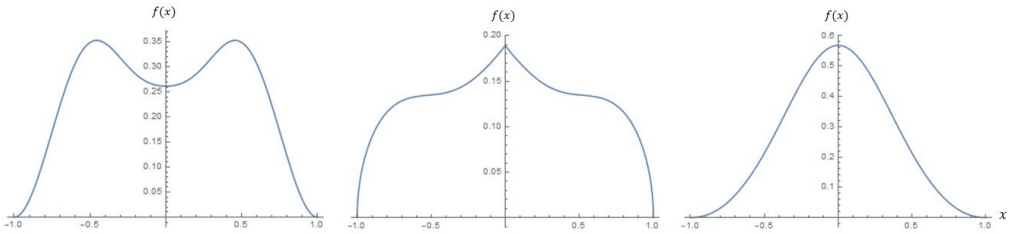

Figure 3.8: The marginal PDF plot of the bivariate beta type III distribution in (3.17) for $\gamma = 2, 0.5, 2$ and $\beta = 3, 3, 1$. from left to right.

After applying the inverse Möbius transformation in Section 3.2.1, the *beta type III Möbius distribution* is obtained from (3.4) with the PDF in terms of the polar coordinates as

$$\begin{aligned} f(r,\theta) &= Cr\left(1-a^2\right)^{\gamma+1}\left(1-r^2\right)^{\gamma-1}\left[a^2-2ar\cos\left(\theta-\mu\right)+r^2\right]^{\beta-1} \\ &\quad \times\left[\left(1+r^2\right)\left(1+a^2\right)-4ar\cos\left(\theta-\mu\right)\right]^{-\gamma-\beta}, \end{aligned} \tag{3.19}$$

where $0 \leq a < 1$, $-\pi < \mu \leq \pi$, $0 \leq r \leq 1$, $-\pi < \theta \leq \pi$ and C as given in (3.18).

We can obtain the PDF in terms of Cartesian coordinates (u, v) by using (3.6), thus the PDF is

$$\begin{aligned} f(u,v) &= C\left(1-a^2\right)^{\gamma+1}\left(1-u^2-v^2\right)^{\gamma-1}\left[a^2-2au\cos\mu-2av\sin\mu+\left(u^2+v^2\right)\right]^{\beta-1} \\ &\quad \times\left[\left(1+u^2+v^2\right)\left(1+a^2\right)-4au\cos\mu-4av\sin\mu\right]^{-\gamma-\beta}, \end{aligned} \tag{3.20}$$

where $0 \leq u^2+v^2 \leq 1$, $0 \leq a < 1$, $-\pi < \mu \leq \pi$ and C is given in (3.18).

The parameters can be interpreted as γ controls the steepness of the concentration, while β contributes to the concentration by adding bimodality. As the value of β increases ($\beta > 1$), the model introduces another mode in the form of an antimode, as seen in the generator function plots in Figure 3.7. The parameters a controls the skewness (or the asymmetry for the length from the center of the disc) and μ controls the orientation of the distribution (see Figure 3.9).

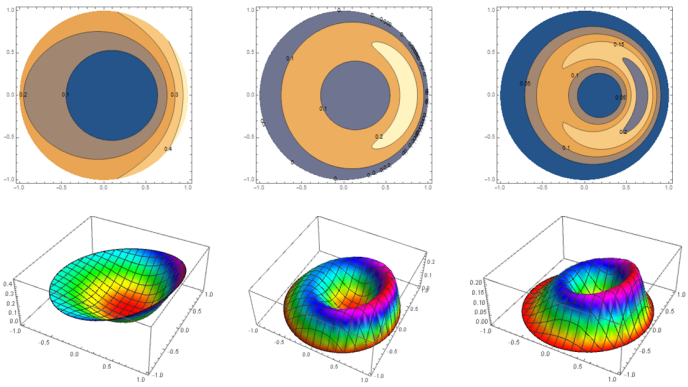

(a) PDF and contour plots of (3.20) for $a = 0.2$, $\mu = 0$, $\beta = 2$ and $\gamma = 1, 2, 3$ (from left to right).

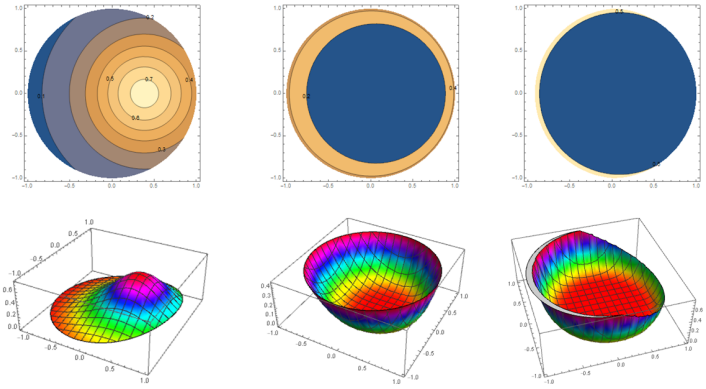

(b) PDF and contour plots of (3.20) for $a = 0.2$, $\mu = 0$, $\gamma = 1$ and $\beta = 1, 3, 5$ (from left to right).

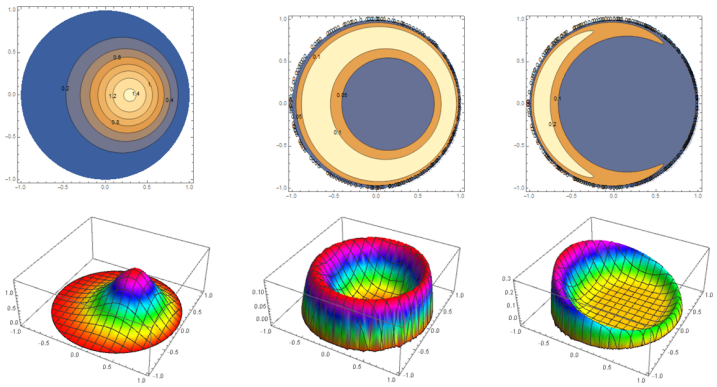

(c) PDF and contour plots of (3.20) for $a = 0.2$, $\mu = 0$, $\gamma = 2$ and $\beta = 1, 3, 5$ (from left to right).

Figure 3.9: PDF plot and contour plots of beta type III Möbius distribution, (3.20), for varying parameter values. (cont.)

Maximum likelihood estimation

The log-likelihood of the polar PDF, (3.19), is obtained for the ML as:

$$\begin{aligned}\log\left[L\left[f\left(r,\theta\right)\right]\right] &= n\beta\log\left[2\right] + n\log\left[\Gamma\left(\lambda+\beta\right)\right] - n\log\left[\Gamma\left(\beta\right)\right] - n\log\left[\Gamma\left(\lambda\right)\right] - n\log\left[\pi\right] \\ &\quad + \sum_{j=1}^{n}\log\left(r_j\right) + n\left(\gamma+1\right)\log\left[1-a^2\right] + \left(\gamma-1\right)\sum_{j=1}^{n}\log\left(1-r_j^2\right) \\ &\quad + \left(\beta-1\right)\sum_{j=1}^{n}\log\left[a^2 - 2ar_j\cos\left(\theta_j-\mu\right) + r_j^2\right] \\ &\quad - \left(\gamma+\beta\right)\sum_{j=1}^{n}\log\left[\left(1+a^2\right)\left(1+r_j^2\right) - 4ar_j\cos\left(\theta_j-\mu\right)\right]. \end{aligned} \tag{3.21}$$

While closed form expressions for the MLEs of (3.19) are intractable, a set of expressions that can be used to derive the MLEs is given in Appendix B.2.3.

3.4 Application

In this section we consider two different application studies. The first study focuses on modeling the wind description at Marion Island. The second study focuses on evaluating the wind energy potential at two different locations in South Africa, namely Humansdorp

and Noupoort.

For modeling data on the disc, the restriction of the domain of the linear variable requires that the observations fall in the interval $[0, 1)$. To ensure the data in the applications in this section adhere to this restriction we make use of the scaling approach. We scale the linear observations based on the maximum wind speed for each location. The maximum wind speed used to scale the data was obtained based on historic data and knowledge from experts in the domain.

The criteria used to evaluate the models are first defined followed by the respective application studies.

3.4.1 Evaluation criteria

In this chapter, four goodness-of-fit metrics are defined to evaluate the models. The AIC, BIC and HQC (as defined in Appendix A.4) are considered. The fourth goodness-of-fit measure is the normalized deviation, which is used for circular–linear models [103]. This performance measure was proposed by Mathisen, et al. [76], which is used to evaluate the fits of bivariate models. This method is based on the normalized deviation, d_{ij} between the observed number of data points, $N_{ij}^{(o)}$, falling in a cell and the expected number of points, $np_{ij}^{(e)}$. The mathematical expression for the normalized deviation, d_{ij}, is given by

$$d_{ij} = \frac{N_{ij}^{(o)} - np_{ij}^{(e)}}{\sigma_{ij}^{(e)}}, \tag{3.22}$$

where $\sigma_{ij}^{(e)}$ is the normalizing factor and the expected standard deviation for the number of data points falling in the cell. Values of normalized deviation close to zero indicate a good fit of the estimated models. The normalized deviation identify the areas in the (r, θ) plane where the model either underperforms or overperforms.

Remark 3. *It is appropriate to compare parametric with semi-parametric models via AIC or BIC. We can motivate this in two ways. The process in this application of implementing kernel density estimation on the unknown function $g(\cdot)$ and then maximum likelihood*

estimation on the model is similar to that in [25], where they used the AIC and BIC for model selection in a semi-parametric context. Secondly, from the profile likelihood viewpoint [80], by substituting the estimated $g(\cdot)$ into the PDF (3.4), we obtain a parametric form for which we can then apply maximum likelihood estimation as in [114; 32; 118].

Remark 4. *On the use of AIC, BIC, and HQC in order to compare parametric and semi-parametric models, one must make some regularity assumptions. As such, we will be assuming the estimation of the nonparametric component $g(\cdot)$, using the kernel density estimation for a finite-dimensional problem in this case. Once we estimate the nonparametric component, we apply the plugin approach into the likelihood (as outlined in Algorithm 1) and then maximize the log-likelihood to obtain the estimate of the parameters; indeed, this is a maximization over a restricted parameter space. There is no guarantee that using this method will provide good estimates for the parameters. Therefore, in order to make sure the estimates fulfill satisfactory conditions, we need to use other measures in addition to the aforementioned information criteria. As such, we computed the normalized deviation for a valid comparison.*

3.4.2 Wind description - Marion Island

There has been much attention in wind power assessment worldwide, however, there has been no analysis of the wind speed and wind direction data for Marion Island. The proposed models were used to analyze the wind data for Marion Island. These models were compared to the only known model on the disc, which is a special case of the proposed class.

The Prince Edward Island group (PEI) consist of two small volcanic islands: (1) Marion Island; and (2) Prince Edward Island. These islands are located in the sub-Antarctic Indian Ocean at latitude 46°49′–46°59′ South and longitude 37°35′–37°55′ East (see Figure 3.10a). Both island territories belong to South Africa, which is situated 1900 km to the northwest of the island group [106]. The recently declared PEIs Marine Protected Area (MPA) is one of the largest of its kind in the world and serves as a research area for

South Africa as well as the world.

With an area of about 290 km^2, a circumference of 72 km and the highest peak at 1300 m, Marion Island is the larger of the Prince Edward Islands. With its geographic isolation, Marion Island's climate is highly oceanic in nature, coupled with the influence of passing frontal weather systems. This creates conditions of high temperature variability and where gale force winds can blow during most weeks of the year. In 1948, South Africa established a fully operational weather station on Marion Island (see Figure 3.10b) with continuous weather data records available since the early 1950s [24]. Due to its duration and the scarcity of weather data from the sub-Antarctic region, these weather records provide valuable and unique opportunities for research.

Data from the Marion Island describe climate variability collected by a weather station that is located near the coast on the eastern side of the island [98]. Wind differences between the eastern (predominantly leeward winds) and western (windward) parts of the island, both within the larger scale prevalence of westerly winds, have long been speculated about [98; 64; 93]. It has been suggested that winds at the western side of the island, where no consistent data collection exists, are stronger and less variable, in comparison to winds at the eastern weather station. Despite these orographically induced differences, wind recordings of the weather should capture the larger scale variability of climate at Marion Island.

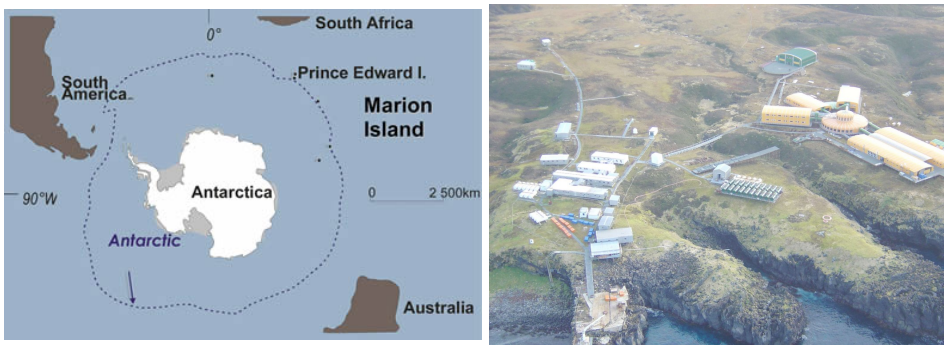

Figure 3.10: Images of the location and weather station of Marion Island. (**a**) An image of the location of Marion Island[1]. (**b**) An image of the Marion Island weather station[2].

Data description

The data used in this study were obtained from Marion Island and recorded daily at 08:00, 14:00 and 20:00 SAST (relates to the main synoptic hours). The daily averages were obtained and the wind speed and wind direction investigated for nine different years. These nine years were considered in two-year intervals from 2001 to 2017. Figure 3.11 provides visual displays of the data to the reader with some background to the behavior of the data. A scatter plot of the wind direction and wind speed is given in Figure 3.12.

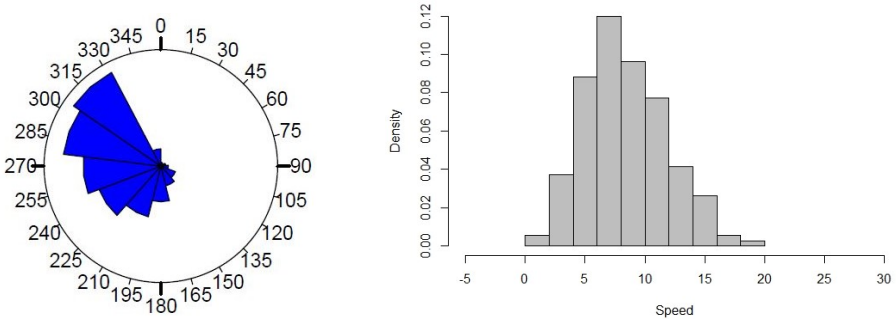

Figure 3.11: A rose diagram of the wind direction (**left**); and histogram of the wind speed (**right**) from the data observed at Marion Island for 2017.

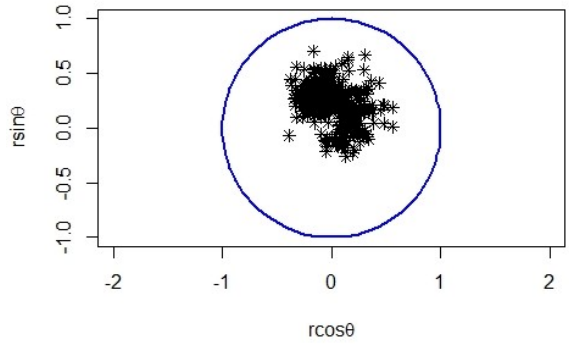

Figure 3.12: A scatter plot of the wind speed and wind direction data from Marion Island for 2017.

In Table 3.1, the values of the main circular statistics [74] of the wind direction for the nine years are given. Specifically, the mean resultant length ($\bar{\omega}$), mean direction ($\bar{\theta}$),

[1]Image obtained from https://www.environment.gov.za/mediarelease/princeedwardislands_declaredmarineprotectedarea on 9 February 2019

[2]Image obtained from http://blogs.sun.ac.za/antarcticlegacy/about-2/marion-station on 9 February 2019

circular variance (V_Θ), circular standard deviation (ν_Θ), circular dispersion (δ), circular skewness (s) and circular kurtosis (k) are shown.

Table 3.1: Circular statistics for the wind direction at Marion Island for nine years.

Year	$\bar{\omega}$	$\bar{\theta}$	V_Θ	ν_Θ	δ	s	k
2001	0.59	−1.38	0.40	0.89	1.14	−1.60	−3.38
2003	0.58	−1.43	0.41	0.90	1.18	−1.67	−3.02
2005	0.58	−1.52	0.41	0.91	1.21	−1.70	−2.84
2007	0.48	1.48	0.52	1.02	2.20	−0.84	−1.59
2009	0.57	−1.56	0.43	0.93	1.35	−1.55	−2.41
2011	0.57	1.56	0.43	0.93	1.33	−1.58	−2.45
2013	0.56	1.53	0.44	0.94	1.39	−1.56	−2.24
2015	0.56	1.52	0.43	0.93	1.36	−1.58	−2.32
2017	0.53	1.45	0.47	0.97	1.71	−1.11	−2.04

Results and discussion

For this application, to obtain the MLEs for the general Möbius distribution we applied the commonly used cross validation method to optimize h in Algorithm 1. Furthermore, we considered the standard Gaussian model for the kernel function, $K(\cdot)$.

The normalized deviation, d_{ij} (3.22), is presented in Figure 3.13, for the model of best fit for each year according to the performance measures in Table 3.2. In Table 3.3, the range and median of the d_{ij} for the models of best fit for each year are given. If the values of d_{ij} are close to zero it is indicative of a good fit of the model. Positive and negative values indicate underestimation and overestimation, respectively. In Table 3.4, a summary of the normalized deviations for the model of best fit for each year, based on Table 3.2, are provided. Figure 3.13 illustrates the normalized deviation plots for the model of best fit for each year.

In Table 3.2, the estimated values of the parameters of the models and their performances are summarized.

The following inferences can be drawn from Table 3.2:

1. The general Möbius distribution performs fairly well most of the time and has the advantage of no distributional assumptions. However, it is worth noting that the selection of the bandwidth plays an important role in the directional analysis.

2. The Möbius distribution on the disc outperforms when there is unimodal behavior inherent in the data. This can be seen for the years 2003, 2005, 2007, 2013, 2015 and 2017.

3. The beta type III Möbius distribution outperforms when there is bimodal behavior inherent in the data. This can be seen for the years 2001, 2009 and 2011. It is also worth noting that the beta type III Möbius distribution has the ability to model unimodality as well as bimodality. Hence, the performance of this model fairs well against the Möbius distribution on the disc.

4. It is interesting to note that the parameters introduced by the Möbius transformation, a and μ, have the same estimated values for the three parametric models. This highlights the influence of the Möbius transformation to the generator models.

Table 3.2: Results from fitting the proposed distributions to the Marion Island data.

Model	**Estimates**					**Performance**		
$f_{R,\Theta}(r,\theta)$	$\hat{a}$	$\hat{\mu}$	$\hat{\gamma}$	$\hat{\beta}$	$\hat{\lambda}$	log(L)	**AIC**	**BIC**
Year 2001								
General Möbius distribution (h = 0.0109)	0.3	1.88	-	-	-	−295.68	595.37	602.85
Möbius distribution on disc	0.17	1.95	9.46	-	-	−293.38	592.75	603.97
Kummer beta	0.16	1.97	2.66	1.42	12.52	−286.85	583.71	602.41
Beta type III	0.15	1.93	6.89	1.40	-	−286.87	581.74	596.69
Year 2003								
General Möbius distribution (h = 0.0088)	0.4	1.88	-	-	-	−281.06	566.11	573.91

Möbius distribution on disc	0.21	1.74	11.55	-	-	−276.29	558.57	570.27
Kummer beta	0.21	1.76	11.86	1.15	1.86	−274.16	558.31	577.81
Beta type III	0.21	1.78	7.41	1.24	-	−275.01	558.01	573.61
Year 2005								
General Möbius distribution (h = 0.0096)	0.3	1.26	-	-	-	−277.18	558.36	566.08
Möbius distribution on disc	0.20	1.28	11.39	-	-	−271.14	548.27	559.85
Kummer beta	0.20	1.27	9.13	1.03	3.25	−271.39	552.77	572.06
Beta type III	0.20	1.28	6.45	1.04	-	−272.18	552.36	567.79
Year 2007								
General Möbius distribution (h = 0.0107)	0.2	1.26	-	-	-	−354.05	712.10	719.89
Möbius distribution on disc	0.18	1.59	9.33	-	-	−349.50	705.01	716.70
Kummer beta	0.18	1.60	1.18	1.17	11.69	−346.84	703.68	723.17
Beta type III	0.17	1.61	6.22	1.23	-	−347.00	702.01	717.59
Year 2009								
General Möbius distribution (h = 0.0079)	0.3	1.26	-	-	-	−282.38	568.77	576.57
Möbius distribution on disc	0.19	1.59	11.91	-	-	−280.42	566.83	578.53
Kummer beta	0.19	1.61	7.69	1.34	9.16	−274.04	558.08	577.58
Beta type III	0.20	1.62	8.67	1.38	-	−274.31	556.63	572.23
Year 2011								
General Möbius distribution (h = 0.0078)	0.2	1.88	-	-	-	−277.24	558.48	566.27
Möbius distribution on disc	0.18	1.51	13.54	-	-	−275.09	556.19	567.88
Kummer beta	0.18	1.47	14.84	1.24	1.88	−270.37	550.74	570.22
Beta type III	0.18	1.48	9.36	1.29	-	−270.53	549.06	564.65
Year 2013								
General Möbius distribution (h = 0.0089)	0.3	1.88	-	-	-	−258.28	520.56	528.32
Möbius distribution on disc	0.19	1.56	12.55	-	-	−251.43	508.86	520.51
Kummer beta	0.19	1.55	10.22	1.19	4.99	−249.76	509.52	528.92
Beta type III	0.20	1.56	8.27	1.25	-	−250.50	509.00	524.52

Year 2015								
General Möbius distribution (h = 0.0073)	0.2	1.88	-	-	-	−261.57	527.15	534.95
Möbius distribution on disc	0.19	1.59	13.79	-	-	−253.29	512.58	524.27
Kummer beta	0.19	1.54	13.28	1.04	0.61	−253.79	517.57	537.06
Beta type III	0.19	1.56	8.15	1.12	-	−253.77	515.55	531.14
Year 2017								
General Möbius distribution (h = 0.00818)	0.2	1.26	-	-	-	−261.99	527.98	535.77
Möbius distribution on disc	0.22	1.59	12.14	-	-	−258.51	523.01	534.69
Kummer beta	0.21	1.57	11.59	1.15	2.44	−257.25	524.50	543.97
Beta type III	0.21	1.61	7.56	1.15	-	−257.91	523.82	539.39

Table 3.3: Normalized deviation ranges for model of best fit for each year.

Year	Best Fit Model	Range	Median
2001	Beta type III Möbius	(−2.651791; 5.920593)	−0.1554433
2003	Möbius distribution on the disc	(−2.312973; 6.288503)	−0.147436
2005	Möbius distribution on the disc	(−3.453434; 12.743586)	−0.1662767
2007	Möbius distribution on the disc	(−2.610813; 7.522888)	−0.3437355
2009	Beta type III Möbius	(−3.000686; 7.984593)	−0.05206841
2011	Beta type III Möbius	(−2.482695; 12.845301)	−0.08473761
2013	Möbius distribution on the disc	(−2.404983; 9.312558)	−0.05009261
2015	Möbius distribution on the disc	(−2.516891; 9.782227)	−0.03193083

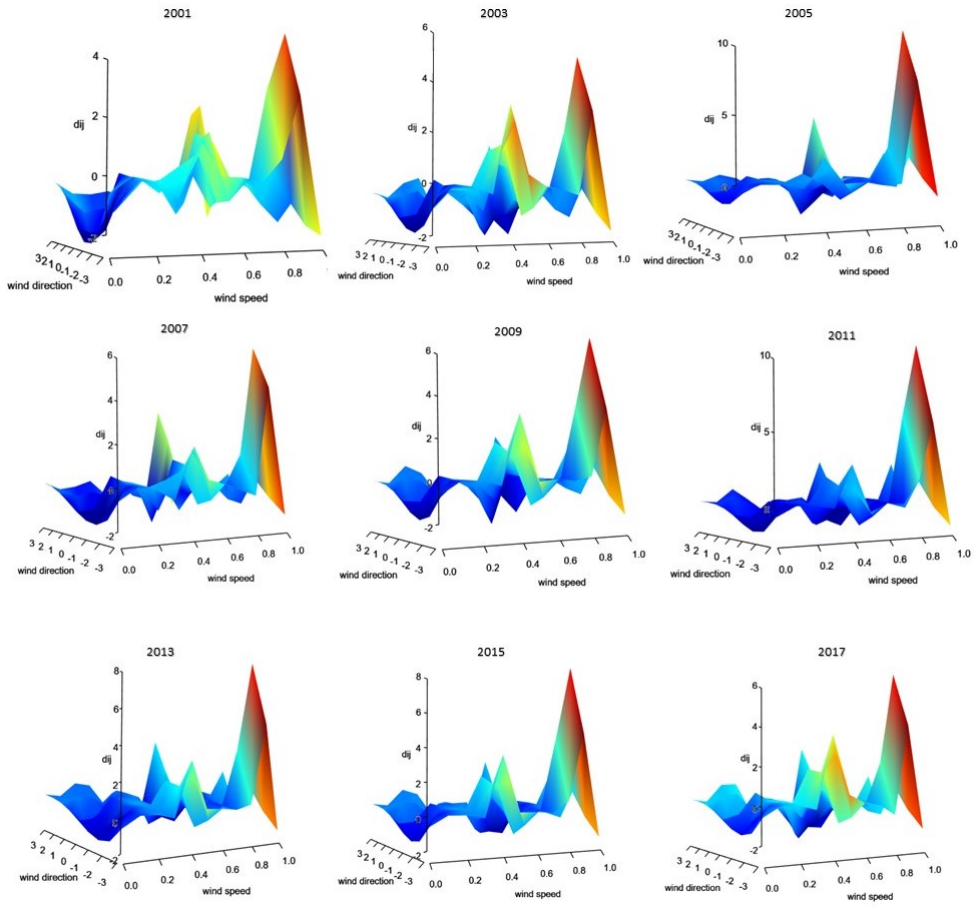

Figure 3.13: The normalized deviation for the model of best fit for each year.

For the year 2017, the estimated PDF plot of the Möbius distribution on the disc is given in Figure 3.14. In Table 3.4, the range and median of the normalized deviation for the proposed parametric models are compared and the plots of these normalized deviation are illustrated in Figure 3.15.

Table 3.4: Normalized deviation ranges for the parametric models for 2017.

Model	**Range**	**Median**
Möbius distribution on disc	$(-2.933306; 7.795678)$	-0.07912035
Kummer beta Möbius	$(-2.859249; 8.231555)$	-0.06817048
Beta type III Möbius	$(-2.964023\ 8.259554)$	-0.100007

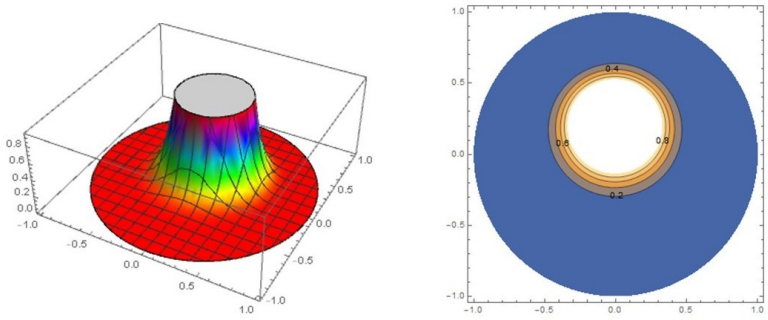

Figure 3.14: The PDF plot and contour plot of the Möbius distribution on the disc for the estimated parameter values $\hat{a} = 0.22$, $\hat{\mu} = 1.59$ and $\hat{\gamma} = 12.14$.

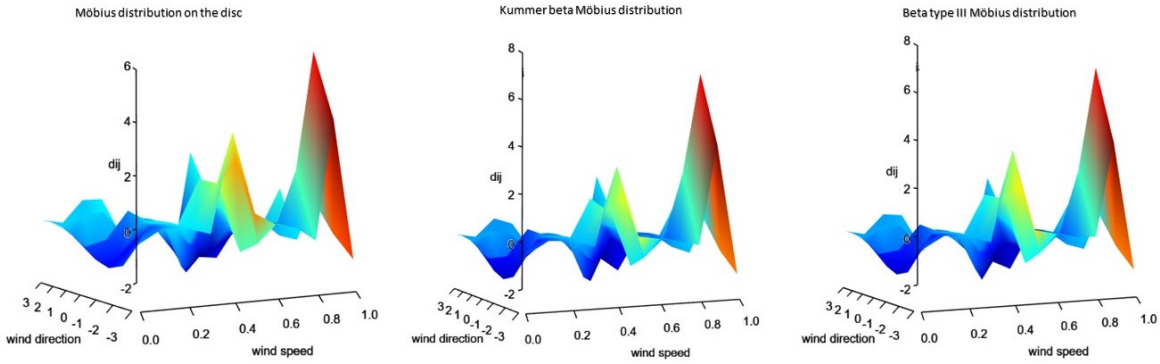

Figure 3.15: The normalized deviation for the parametric models for 2017.

3.4.3 Wind energy potential - Humansdorp and Noupoort

In South Africa, fossil fuels are the main form of energy supply. This results in emissions causing local and global environmental complications. Fossil fuels are not sustainable and, therefore, it is of importance to investigate renewable energy resources. Eskom (the electricity supply commission of South Africa) is a South African electricity public utility that generates approximately 95% of electricity used in South Africa [3]. It is also well known that Eskom's current fleet of power stations is old and suffers from reliability problems, resulting in frequent load shedding (a controlled blackout to respond to unplanned events to protect the electricity power system from a total blackout), with a negative im-

[3] https://world-nuclear.org/information-library/country-profiles/countries-o-s/south-africa.aspx (accessed 19 January 2023)

pact on the South African economy. Renewable resources also have inherent constraints; for example, solar power is limited to the availability of the sun rays and is costly. Considering the climatology of South Africa, wind energy stands out as a viable option. At the South African Investment Conference 2022 [4], a pledge to increase the use of renewable energy sources to generate electricity was made. For this objective, it was pointed out that 884.9 million rand would be invested in the 100MW Sere wind farm (Western Cape, South Africa) and 1.45 billion rand to be invested in the 100MW Xina solar plant (Northern Cape, South Africa). From an environmental impact perspective, wind energy is superior in comparison to other energy sources [36; 95]. As reported by [95], even though wind energy is popular due to the cost efficiency, there are some unfavorable environmental impacts of wind energy, such as the noise produced by the windmills, its impact on the ecology (bird hits), etc. To overcome these negative impacts, the design of the wind farms is of utmost importance.

The overall capacity of all wind turbines installed worldwide reached 597 GW by the end of 2018 [5]. This covers 6% of the global electricity demand. As emphasized in [54], a total of 98 countries can be provided with electricity produced by wind energy. Furthermore, there is a great interest in expanding wind energy.

Site location and wind data

As of 2022, in South Africa, there are 33 wind farms: 22 fully operational and 11 in construction [6]. In order to assess the competence of the proposed models, two stations situated in South Africa, namely Humansdorp and Noupoort, have been selected. These locations already have a fully operational wind farm; however, they were chosen due to the availability of data. The wind speed and wind direction provided by the Wind Atlas for South Africa project (WASA) [7] were recorded every 10 min at 20 and 60 m

[4] https://www.sainvestmentconference.co.za/ (accessed 19 January 2023)
[5] Global Wind Energy Council: Global wind statistics, 2019; https://gwec.net/wp-content/uploads/2019/04/GWEC-Global-Wind-Report-2018.pdf (accessed 22 August 2019)
[6] based on the South African Wind Energy Association https://sawea.org.za/
[7] http://wasadata.csir.co.za/wasa1/WASAData (accessed 29 August 2019)

heights. For each location, the main characteristics were reported by the WASA [8]; these characteristics include a photographic documentation of mast design, installation, and surroundings, as well as elevation maps that have been constructed for each site from Shuttle Radar Topography Mission (SRTM) 3 arc-second data. These reported images provide an overall view of the location and terrain. Figure 3.16 shows the locations of the stations and Table 3.5 provides the geographical details for the locations.

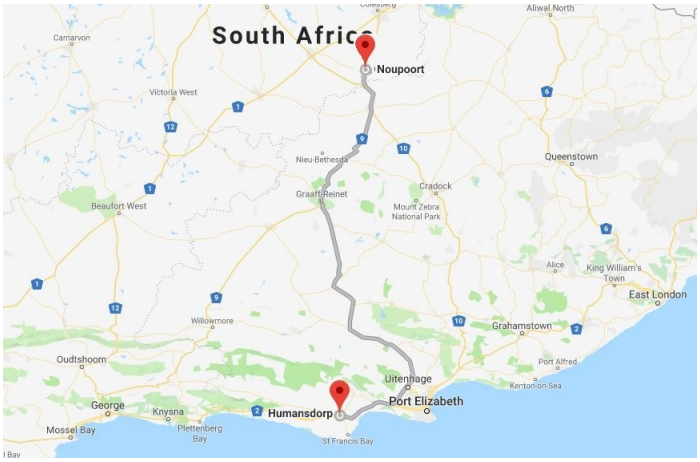

Figure 3.16: Locations of the two stations in South Africa [9].

Table 3.5: Geographical details of the two stations.

Station	**Latitude (°S)**	**Longitude (°E)**	**Elevation (m)**
Humansdorp	−34.109965	24.514360	110
Noupoort	31.252540	25.028380	1806

In Table 3.6, information on the quantity and quality of the measured wind data for the two locations is given. The period of utilized data, the total number of observations, the number of expected data, and absent data are presented, respectively. The record contained no calm data, as the average of the wind speed over a ten-minute interval

[8] http://stel-apps.csir.co.za/wasa-data/docs/WASA1Station_and_Site_Description_Report_April2014.pdf (accessed 29 August 2019)

[9] Google Maps, 2020. Google Maps (online). Available through: https://www.google.com/maps (Accessed 05 March 2020).

was recorded.

Table 3.6: Information of the wind data for the two locations.

Station	Data Period (dd/mm/yyyy)	Total Data	Expected Data	Absent Data
Humansdorp	01/01/2016–28/02/2019	166,226	166,320	94
Noupoort	01/01/2016–28/02/2019	137,660	166,320	28,660

In Table 3.7, the descriptive statistics for the wind speed for the two locations are given; specifically, the maximum (Max), mean, standard deviation (std), skewness, and kurtosis. In Table 3.8, the values of the main circular statistics [74] of the wind direction for the two locations are given. Specifically, the mean resultant length ($\bar{\omega}$), mean direction ($\bar{\theta}$), circular variance (V_Θ), circular standard deviation (ν_Θ), circular dispersion (δ), circular skewness (s), and circular kurtosis (k) are shown.

Table 3.7: Descriptive statistics of the wind speed data.

Station	Height (m)	Max (m/s)	Mean (m/s)	std (m/s)	Skewness	Kurtosis
Humansdorp	20	24.40	6.01	3.40	0.68	0.16
Humansdorp	60	26.66	7.13	3.65	0.63	0.26
Noupoort	20	21.37	6.93	3.09	0.64	0.19
Noupoort	60	24.79	7.91	3.50	0.57	0.13

Table 3.8: Descriptive circular statistics for the wind direction data.

Station	Height (m)	$\bar{\omega}$	$\bar{\theta}$ (rad)	V_Θ	ν_Θ	δ	s	k
Humansdorp	20	0.24	−1.21	0.76	1.68	8.10	0.55	−0.65
Humansdorp	60	0.28	−1.16	0.72	1.60	6.22	0.60	−0.71
Noupoort	20	0.14	−0.82	0.86	1.99	23.92	0.04	−0.72
Noupoort	60	0.15	−0.88	0.85	1.95	20.69	−0.08	−0.74

From Table 3.7, Noupoort has the highest mean wind speed with the value of 7.91 m/s, while Humansdorp has the lowest mean wind speed with the value of 6.01 m/s.

Since the skewness is positive for both the stations, we can conclude that the distributions are skewed to the right. The wind direction data for the Humansdorp location seems to be more concentrated based on the $\bar{\omega}$, as seen in Table 3.8. Based on the $\bar{\theta}$, the Humansdorp location is dominated by winds blowing from the WNW (for $\theta \in [1.77; 2.16]$) sector while for Noupoort the dominant wind direction is NW (for $\theta \in [1.57; 2.36]$).

Fitting of the system of wind distributions

For the estimation of the parameters of the general Möbius distribution (3.4), the computational stages for estimating $g(\cdot)$ and the parameters are given by Algorithm 2. For the parameter estimation of the Möbius distribution on the disc (3.9) and beta type III Möbius model (3.19), ML estimation is performed. Since closed-form expressions for the MLE could not be obtained for the parameters, numerical optimization of the ML is performed using the "optimization" package available in the R software.

A general algorithm for estimating the parameters of the general Möbius distribution is given in Algorithm 1. In this application, a specific case of the general algorithm was used and is described in Algorithm 2.

Take note that, in Algorithm 2 Step 1, the kernel function is estimated using the argument r^2. This was chosen as it is the argument before the Möbius transformation and, since the transformation applies to the variable, the function of $g(\cdot)$ can be estimated using the original argument. In Algorithm 2, the starting values for a and μ are obtained using a randomized technique of simulating random numbers for $a \in [0, 1)$ and $\mu \in [-\pi, \pi)$ and selecting the set of parameters that maximize the likelihood function.

Influence of wind speed and wind direction data

The bivariate relationship between the wind speed and wind direction is measured by the linear-circular correlation coefficient, $cor_{r,\theta}$, defined in Appendix A.2. The correlation coefficients for the two locations are given in Table 3.9, emphasizing the need for a joint model with an embedded correlation structure.

Algorithm 2 Maximum likelihood estimation algorithm for the general Möbius distribution (3.4).

Step 1. Select a set of starting values for a and μ by using a randomized technique of simulating random numbers from $a \in [0, 1)$ and $\mu \in [-\pi, \pi)$..

Step 2. Given the observations $r_1, r_2, \ldots, r_n$, we estimate $g(\cdot)$ in (3.4) using kernel density estimation as follows:

$$\hat{g}(w) = \frac{1}{nh} \sum_{j=0}^{n} K\left(\frac{w - w_j}{h}\right),$$

where $w_j = r_j^2$, h is the bandwidth, and $K(\cdot)$ is the kernel function. For this application, we assume a Gaussian kernel with restricted support of $r \in [0, 1]$ and use a plugin bandwidth selection technique to obtain the optimal h value.

Step 3. For given a and μ, compute the value of the argument of $g(\cdot)$ in (3.4), i.e., compute the value of $q_j = (a^2 - 2ar_j \cos(\theta_j - \mu) + r_j^2)/(1 - 2ar_j \cos(\theta_j - \mu) + a^2 r_j^2)$. Using the function estimated in Step 1, $\hat{g}(\cdot)$, calculate the corresponding function of $\hat{g}(q_j)$.

Step 4. Compute the likelihood function based on (3.4) using the estimated $\hat{g}(q_j)$, $\hat{a}$, and $\hat{\mu}$.

Step 5. Repeat Steps 2 and 3 using a numerical optimization technique to maximize the likelihood function by updating the parameter set until convergence for the parameters a and μ is achieved. The final estimated values are those that maximize the likelihood function.

Table 3.9: Correlation coefficient for the wind speed and wind direction.

Station	Height (m)	Correlation Coefficient
Humansdorp	20	0.2487562
Humansdorp	60	0.1711075
Noupoort	20	0.2688977
Noupoort	60	0.2677411

Subsequently, in Figures 3.17 and 3.18, the wind speed and wind direction for the two locations are given to assist the practitioner in choosing an appropriate model. Figures 3.17a–d and 3.18a–d illustrate the wind speed and wind direction histograms, respectively. From the histograms, the bimodality in the wind direction and the skewness in the

wind speed can be seen. Figures 3.17e–h and 3.18e–h illustrate the wind speed and wind direction boxplots, respectively.

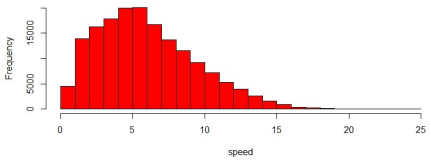

(a) A histogram of the wind speed at 20 m.

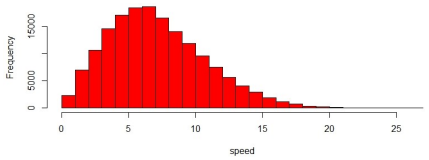

(b) A histogram of the wind speed at 60 m.

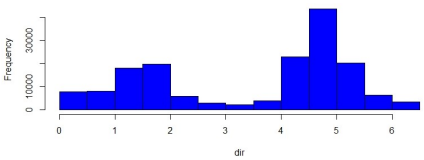

(c) A histogram of the wind direction at 20 m.

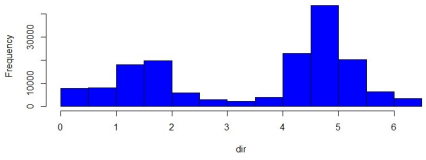

(d) A histogram of the wind direction at 60 m.

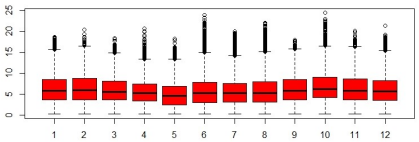

(e) A boxplot of the wind speed at 20 m.

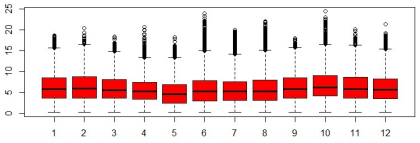

(f) A boxplot of the wind speed at 60 m.

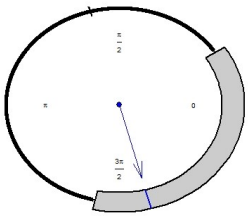

(g) A boxplot of the wind direction at 20 m.

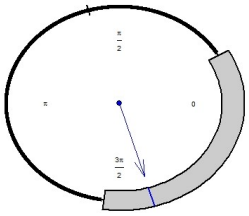

(h) A boxplot of the wind direction at 60 m.

Figure 3.17: Data plots for the Humansdorp location.

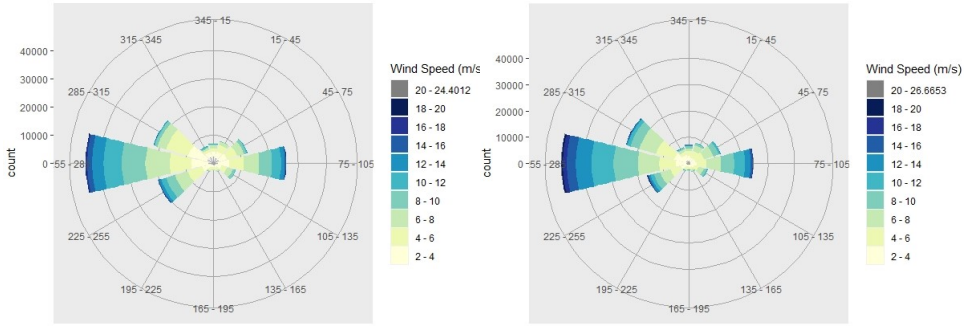

(i) A windrose diagram of the wind speed and wind direction at 20 m.

(j) A windrose diagram of the wind speed and wind direction at 60 m.

Figure 3.17: Data plots for the Humansdorp location (cont.).

The boxplots for the wind speed (Figures 3.17e,f and 3.18e,f) are plotted by month of the year and indicate the seasonality of the wind behavior. The circular boxplots in Figures 3.17g,h and 3.18g,h were constructed using the methodology proposed by [18]. The circular boxplots display the skewness present in the wind direction. The windrose diagrams in Figures 3.17i and 3.18j illustrate the intensity of the wind speed in the specific wind directions.

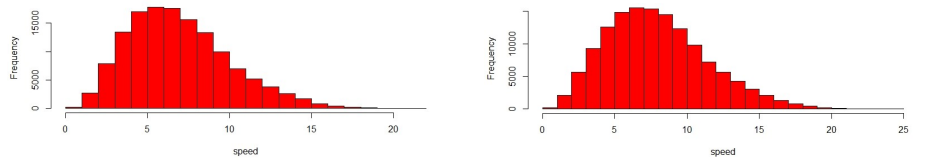

(a) A histogram of the wind speed at 20 m.

(b) A histogram of the wind speed at 60 m.

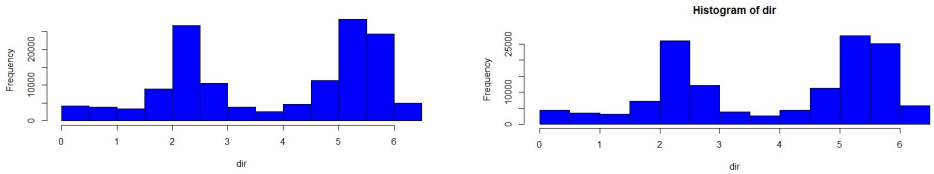

(c) A histogram of the wind direction at 20 m.

(d) A histogram of the wind direction at 60 m.

Figure 3.18: Data plots for the Noupoort location.

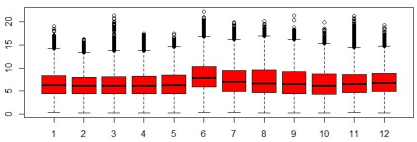

(e) A boxplot of the wind speed at 20 m.

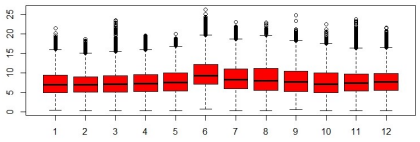

(f) A boxplot of the wind speed at 60 m.

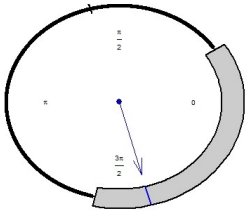

(g) A boxplot of the wind direction at 20 m.

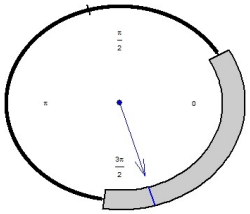

(h) A boxplot of the wind direction at 60 m.

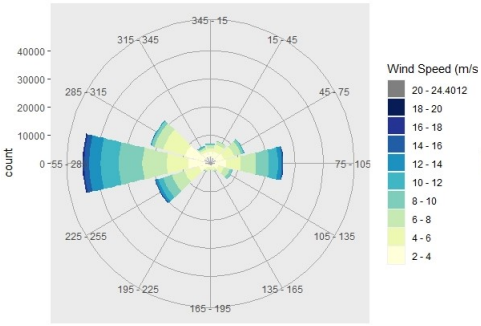

(i) A windrose diagram of the wind speed and wind direction at 20 m.

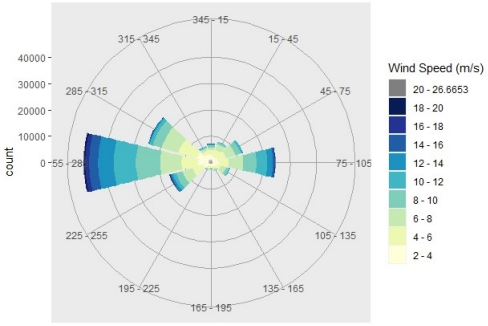

(j) A windrose diagram of the wind speed and wind direction at 60 m.

Figure 3.18: Data plots for the Noupoort location (cont.).

Results and discussion

Based on the assumption that the air density[10], ρ_A, is constant, the wind power PDF is expressed as [103]

$$P(r,\theta) = \frac{1}{2}\rho_A f_{R,\Theta}(r,\theta) r^3. \tag{3.23}$$

The wind power density defined in (3.23) is used to evaluate the wind energy at the two locations. For this application study we consider three special cases of the proposed model, namely (i) the general Möbius distribution on the disc (3.4), (ii) the Möbius distribution on the disc (3.9), and (iii) the beta type III Möbius distribution on the disc (3.19),

[10] air density is dependent on altitude, humidity, and temperature; we consider the air density to be independent of the wind characteristics and be equal to a constant value of 1.225 kg/m^3

to jointly model the wind speed and wind direction for the wind data observed at Humansdorp and Noupoort.

The results from estimating the joint wind speed and wind direction distributions are presented and discussed in this section. In Table 3.10, the MLEs of the parameters and the performance measures for the proposed models are given. The following inferences can be drawn from Table 3.10:

1. For the Humansdorp location at 20 m, the general Möbius distribution performs the best overall. The beta type III Möbius model performs the best from the parametric models.

2. For the Humansdorp location at 60 m, the general Möbius distribution performs the best overall. The Möbius distribution on the disc model performs the best from the parametric models.

3. For the Noupoort location at 20 m, the general Möbius distribution performs the best overall. The beta type III Möbius model performs the best from the parametric models.

4. For the Noupoort location at 60 m, the general Möbius distribution performs the best overall. The beta type III Möbius model performs the best from the parametric models.

5. The general Möbius distribution outperforms overall based on the performance measures. This model has the advantage of limited distributional assumptions. However, it is worth noting that the selection of the bandwidth plays an important role in statistical analysis.

6. The beta type III Möbius model performs the best from the parametric models based on the performance measures. This is a result of the model's flexibility in capturing bimodality and skewness present in the data. The presence of bimodality and skewness can be seen in the data plots (see Figure 3.17 and Figure 3.18).

Table 3.10: Parameter estimates from fitting the proposed distributions to the two locations at 20 and 60 m height.

Model	**Estimates**					**Performance measures**		
$f_{R,\Theta}(r,\theta)$	$\hat{a}$	$\hat{\mu}$	$\hat{\gamma}$	$\hat{\beta}$	$log(\hat{L})$	**AIC**	**BIC**	**HQC**
Humansdorp at 20 m								
General Möbius distribution	0.06	1.643	-	-	−50,073.496	100,150.992	100,171.034	100,161.912
Möbius distribution on the disc	0.06	1.61	19.99	-	−137,147.608	274,301.217	274,331.280	274,310.136
Beta type III Möbius	0.05	1.84	12.58	0.82	−128,863.955	257,735.910	257,775.994	257,747.8033
Humansdorp at 60 m								
General Möbius distribution	0.06	1.71	-	-	−134,644.097	269,292.195	269,312.237	269,303.114
Möbius distribution on the disc	0.06	1.75	19.06	-	−143,268.526	286,543.052	286,573.115	286,551.972
Beta type III Möbius	0.07	1.94	10.43	0.89	−143,270.191	286,548.383	286,588.467	286,560.2753
Noupoort at 20 m								
General Möbius distribution	0.03	2.26	-	-	−98,121.666	196,247.332	196,266.997	196,258.1571
Möbius distribution on the disc	0.05	2.20	19.92	-	−105,008.477	210,022.953	210,052.451	210,031.7791
Beta type III Möbius	0.04	2.28	13.69	1.23	−102,044.187	204,096.373	204,135.704	204,108.1408
Noupoort at 60 m								
General Möbius distribution	0.05	2.33	-	-	−119,253.019	238,510.038	238,529.703	238,520.8631
Möbius distribution on the disc	0.05	2.33	15.89	-	−121,825.312	243,656.624	243,686.122	243,665.4491
Beta type III Möbius	0.03	2.67	12.24	1.4	−120,573.788	241,155.575	241,194.905	241,167.3428

For comparison purposes, it is important to note that, since our model is fitted using the maximum-likelihood method (for the parameters), we can use the AIC and/or BIC, which are based on the likelihood method.

In Table 3.11, a summary of the normalized deviations (3.22) for the parametric models for each location is provided. Figure 3.13 illustrates the normalized deviation plots for the parametric models for each location. Using this metric from Table 3.11, we can conclude that the Möbius distribution on the disc model has a better fit for the Humansdorp location and the beta type III Möbius model fits better for the Noupoort location, as the median of the normalized deviation is closer to zero.

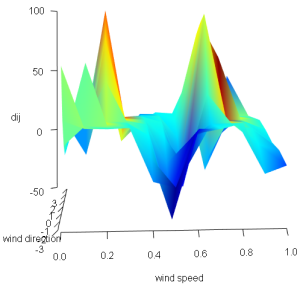

(a) The normalized deviation for the Möbius distribution on the disc model for Humansdorp at 20 m.

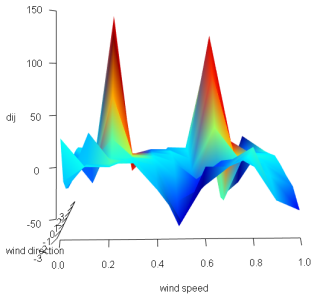

(b) The normalized deviation for the beta type III Möbius model for Humansdorp at 20 m.

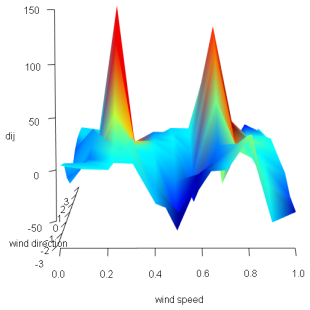

(c) The normalized deviation for the Möbius distribution on the disc model for Humansdorp at 60 m.

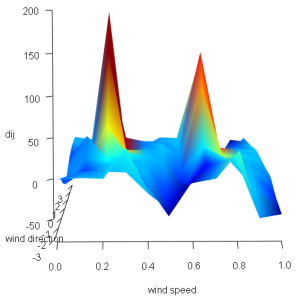

(d) The normalized deviation for the beta type III Möbius model for Humansdorp at 60 m.

Figure 3.19: The normalized deviations for the parametric models for the Humansdorp location (**a**–**d**) . The normalized deviations for the parametric models for the Noupoort location (**e**–**h**).

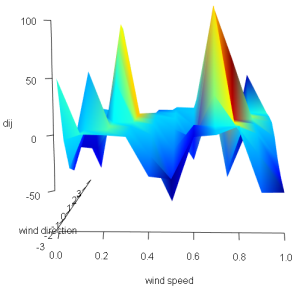

(e) The normalized deviation for the Möbius distribution on the disc model for Noupoort at 20 m.

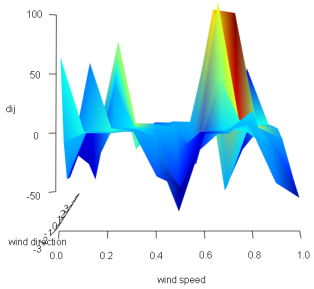

(f) The normalized deviation for the beta type III Möbius model for Noupoort at 20 m.

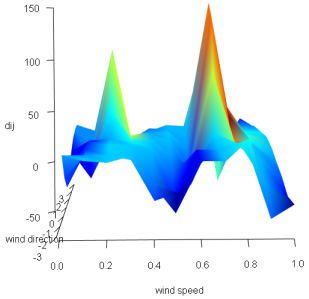

(g) The normalized deviation for the Möbius distribution on the disc model for Noupoort at 60 m.

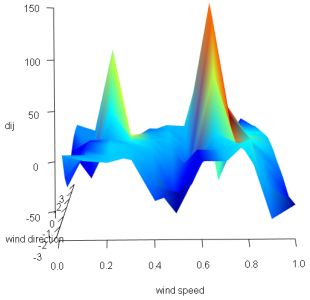

(h) The normalized deviation for the beta type III Möbius model for Noupoort at 60 m.

Figure 3.19: The normalized deviations for the parametric models for the Humansdorp location (**a**–**d**) . The normalized deviations for the parametric models for the Noupoort location (**e**–**h**) (Cont.).

Table 3.11: Normalized deviations for parametric models for each location.

Station	Height (m)	Model	Median	Range
Humansdorp	20	Möbius distribution on the disc	−0.2708471	(−86.41038; 114.30956)
Humansdorp	20	Beta type III Möbius	−0.2757685	(−66.82174; 168.59107)
Humansdorp	60	Möbius distribution on the disc	−0.3938287	(−73.57794; 154.53348)
Humansdorp	60	Beta type III Möbius	−0.8428266	(−74.65866; 201.50158)
Noupoort	20	Möbius distribution on the disc	−0.4002134	(−84.15884; 116.17518)
Noupoort	20	Beta type III Möbius	−0.2386832	(−80.73554; 126.18355)
Noupoort	60	Möbius distribution on the disc	−0.3757053	(−76.41617; 162.44165)
Noupoort	60	Beta type III Möbius	−0.08373657	(−73.58869; 179.88564)

For the wind power density, (3.23), we substitute the proposed parametric base models $f_{R,\Theta}(r,\theta)$ (joint model of wind speed and wind direction) to evaluate the wind energy.

Based on the parametric models of best fit in Table 3.10, the wind power density is plotted in Figure 3.20 for the estimated parameter values given in Table 3.10.

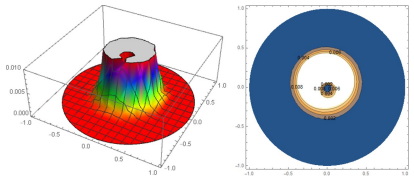

(a) Wind power density with the beta type III Möbius model as the base model for Humansdorp at 20 m.

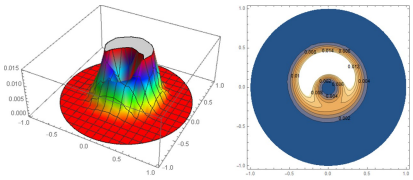

(b) Wind power density with the Möbius distribution on the disc model as the base model for Humansdorp at 60 m.

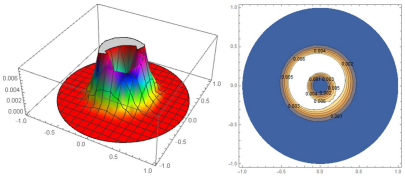

(c) Wind power density with the beta tyep III Möbius model as the base model for Noupoort at 20 m.

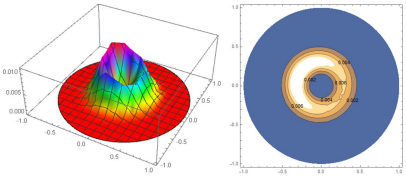

(d) Wind power density with the beta tyep III Möbius model as the base model for Noupoort at 60 m.

Figure 3.20: Plots and contour plots of the estimated wind power density (3.23) for each location with the parametric model of best fit as the base joint model of wind speed and wind direction.

The intensity plots for the estimated wind power density (3.23) for when the base model is considered as the general Möbius distribution (model of best fit) are given in Figure 3.21 for various values of θ and r.

Figure 3.21 illustrates that the estimated wind power density is maximal when the wind is blowing in a North Westerly direction (for θ between 1.57 to 2.36, given that $-\pi$ is the North direction) and when the wind speed is low to moderate. It can also be noted that at the Humansdorp location a height of 20 m displays a stronger wind power density compared to the height of 60 m, and at the Noupoort location, a height of 60 m displays a stronger wind power density compared to the height of 20 m.

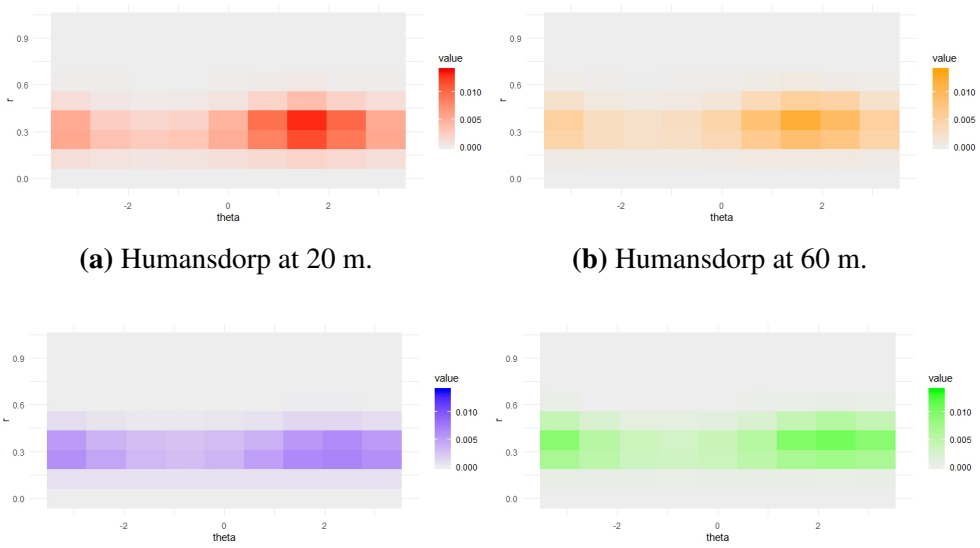

(a) Humansdorp at 20 m.

(b) Humansdorp at 60 m.

(c) Noupoort at 20 m.

(d) Noupoort at 60 m.

Figure 3.21: Estimated intensity plots of wind power density (3.23) values of the general Möbius distribution for various values of r and θ.

3.5 Conclusion

In this chapter, we developed a new general Möbius distribution class on the disc which has support on the unit disc that includes the well-known Möbius distribution on the disc proposed by [52] as a special case. This new class can assume either a semi-parametric or parametric form depending on the choice of the practitioner. This class of distributions is suitable when there exists skewness and bimodal patterns hidden in the data structure. Using the Marion Island climate data, model evaluation showed the performance of the different proposed models and the flexibility of this new class of distributions in capturing the bimodality and asymmetry present in the data. The Möbius transformation introduces asymmetry to the model in terms of off-centeredness as well as an orientation for the asymmetry. The ability of this new class to capture the bimodal behavior is a result of the generator function. To illustrate the proposed models validity we considered two applications; modeling the wind description at Marion Island and the evaluation of wind energy potential at two different locations in South Africa. Considering the situation sur-

rounding the supply of electricity in South Africa, the need for investigating and investing in alternative renewable energy sources is of utmost importance to the socioeconomic development of the country.

For the purpose of model comparison it is important to note that comparisons between the models proposed in this chapter and existing joint wind speed and wind direction models are inappropriate due to the differences in the definitions of the manifolds (cylindrical vs disc manifold). Existing joint models have been defined on the cylindrical manifold, where the linear random variable is defined on the real line and is not restricted to the interval $[0, 1]$. Hence, the proposed model was compared to the only existing distribution on the disc. For the models on the disc, the restriction of the domain of the linear variable requires the observation to be scaled for certain applications like the wind studies in this chapter. This could be viewed as a weakness of defining models on the disc manifold as some information could be lost as a result of scaling the observations. However, in applications where there is a predefined finite upper bound the use of models defined on the disc could prove beneficial. As future work, one could consider applying a one-to-one transformation (such as $r = 1 - e^{-x}$) to transform the linear variable variable from $\mathbb{R}$ to $[0, 1)$.

Chapter 4

Multivariate Circular-Linear Models

This chapter is motivated by an applied statistical study in the biomechanical domain. For the first time in this domain the use of directional statistics within a multivariate dependent modeling framework is considered to examine the mechanical behavior of external fixators. Complex data containing circular and linear variables is common in biomechanical and orthopedic studies. In most cases the circular and linear variables are considered in isolation. The joint distribution modeling based on multivariate data containing circular and linear data is vital given the large amounts of directional data and the vast applications thereof.

The work in this chapter is motivated by the modeling of biomechanical data, i.e. the fracture displacements, that is used as a measure in external fixator comparisons. Fracture healing is inevitably influenced by the complex interplay of biology and biomechanics - i.e. inter-fragmentary motion and inter-fragmentary biomechanics. The stiffness of a construct of an external fixator is determined by the configuration of the hardware. The construct's configuration may lead to different inter-fragmentary motion and it is therefore important to compare constructs to obtain the most appropriate construct for optimal healing. Therefore, our approach in this chapter is to propose a modeling framework applicable to the 6D joint distribution of circular-linear data based on vine copulas. The pair-copula decomposition concept of vine copulas represents the dependence structure as

a combination of circular-linear, circular-circular and linear-linear pairs modeled by their respective copulas. This allows us to assess the dependencies in the joint distribution. The need for joint dependence models is emphasized in this chapter through a comparison with the independent model and a new approach for accurate modeling of mechanical behavior for Ilizarov ring fixators and other data of this nature is imparted.

4.1 Data and motivation

External fixators is a medical instrument used to immobilize fracture or heavy damage to the bone structure. Healing of a fracture is influenced by the amount of strain at the fracture site as discussed in [34]. The strain is related to the amount of motion of the fracture under loading. The motion of the fracture rely on the combination of rings, bars, pins and wires. Different configuration of external fixators can be compared by measuring the displacement of the fracture. In this application the motion of the fracture is quantified by the displacement of the proximal fracture end to the distal fracture end. The translational displacement in the three translation directions as well as the rotational displacement about the three axis is measured as illustrated in Figure 4.1.

Let X, Y and Z denote the linear (translational) variables defined on $\mathbb{R}$ where X is the displacement in the $x-axis$, Y the displacement in the $y-axis$ and Z the displacement in the $z-axis$. Let Θ_X, Θ_Y and Θ_Z denote the circular (rotational) variables defined on the unit circle $\mathbb{S}^1$ where Θ_X is the angular displacement about the $x-axis$, Θ_Y the angular displacement about the $y-axis$, and Θ_Z the angular displacement about the $z-axis$. For this application we consider two different constructs of an Ilizarov ring fixator which we refer to as configuration 1 and configuration 2.

In Table 4.1, the descriptive statistics for the translational (linear) variables of configuration 1 and configuration 2 are given; specifically, the mean, standard deviation (sd), interquartile range (IQR), skewness, and kurtosis.

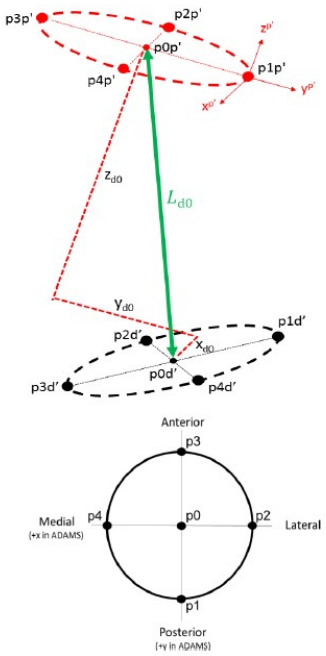

Figure 4.1: Model of fracture with extraction of points of interest after displacement.

Table 4.1: Descriptive statistics of the translational variables for each configuration.

Configuration	Variable	Mean	sd	IQR	skewness	kurtosis
1	X	-0.2708	0.4475	0.5192	-0.3707	-0.0128
	Y	0.2948	0.4565	0.5646	-0.4791	0.2707
	Z	5.1039	3.6230	6.9932	0.0084	-1.4289
2	X	0.0455	0.4760	0.5915	-0.7638	2.573
	Y	1.5551	2.2361	3.1523	1.0108	-0.0973
	Z	6.7993	4.4999	8.9947	-0.0029	-1.5106

In Table 4.2, the values of the main circular statistics [74] are given for the rotational variables of configuration 1 and configuration 2. Specifically, the mean resultant length ($\bar{\omega}$), mean direction ($\bar{\theta}$), circular standard deviation (V_Θ), circular skewness (s) and circular kurtosis (k) are shown. The unit of measurement for the circular variables is considered as radians.

Table 4.2: Descriptive statistics of the rotational variables for each configuration.

Configuration	Variable	$\bar{\omega}$	$\bar{\theta}$	V_Θ	s	k
1	Θ_X	0.9999	0.0011	0.0143	0.3286	-1.1368
	Θ_Y	0.9999	-0.0056	0.0127	-0.1026	0.2556
	Θ_Z	0.9999	0.0008	0.0119	0.0048	-1.2235
2	Θ_X	0.9992	-0.0642	0.0397	2.7537	6.0765
	Θ_Y	0.9999	0.0166	0.0165	-0.0424	0.1532
	Θ_Z	0.9998	0.0194	0.0209	-1.7600	1.4948

In Figures 4.2 and 4.3, the data plots of the translation and rotational variables for configuration 1 and configuration 2 are provided, respectively. From Figures 4.2 and 4.3, bimodality and slight skewness is observed in some of the data plots indicating the need for a model that can account for multimodality, for example the use of finite mixture models for specific variables. Based on these model requirements, a copula approach where the marginal distributions can be specified separately from the dependence structure is a useful technique to build a joint model. From the results in Table 4.2 and the histograms in Figures 4.2 and 4.3, we note that the rotational variables are highly concentrated which raises questions on the assumption of the periodicity of the variables. However, due to the nature of the variables we consider them to be circular in the modeling approach as the concentration might differ for various manufacturers and configurations but the nature of the variable remains unchanged.

Pearson's correlation coefficient was considered for the paired translational variables. The bivariate relationship between the translational and rotational variables is measured by the linear-circular correlation coefficient, $cor_{x,\theta}$, defined in Appendix A.2. For the paired rotational variables we consider the correlation coefficient, $cor^2_{\theta,\phi}$, as defined in Appendix A.3. The correlation plots for configuration 1 and configuration 2 are given in Figure 4.4 and Figure 4.5 respectively. From Figures 4.4 and 4.5 and Tables 4.3 and 4.4 it is observed that the assumption of independence is violated by the data. Thus, a joint dependent model is required.

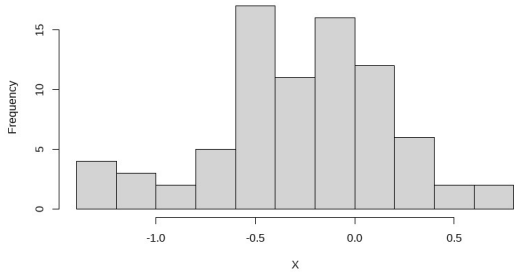

(a) Histogram of the translational variable X.

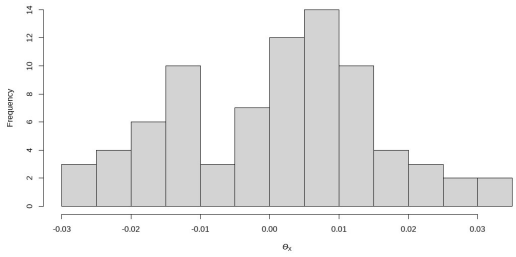

(b) Histogram of the rotational variable Θ_X.

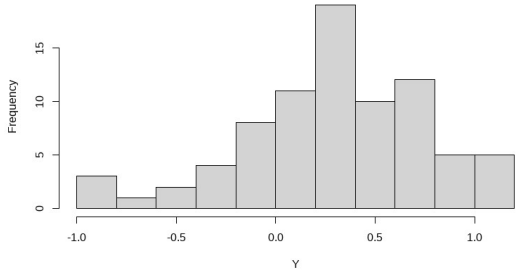

(c) Histogram of the translational variable Y.

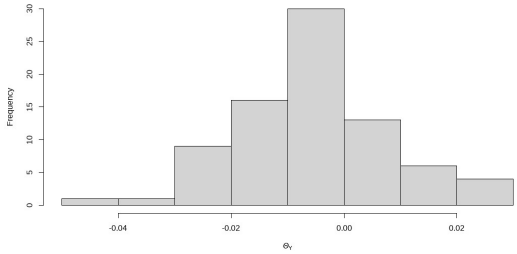

(d) Histogram of the rotational variable Θ_Y.

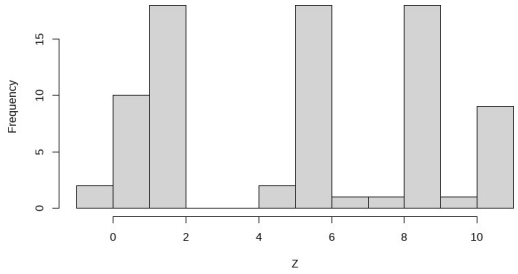

(e) Histogram of the translational variable Z.

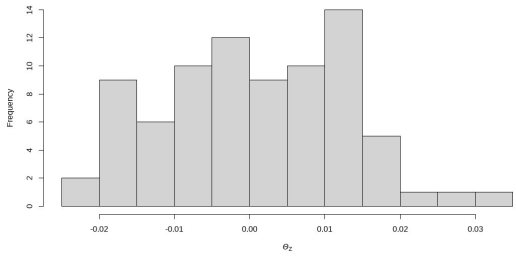

(f) Histogram of the rotational variable Θ_Z.

Figure 4.2: Histograms of the translational (left) and rotational (right) variables for configuration 1.

A significance test was performed to evaluate the necessity of accounting for a dependence structure between the variables. Table 4.3 and Table 4.4 provide the significant (at a 5% significance level) correlation coefficients for configuration 1 and configuration 2, respectively, where the null hypothesis is independency among the respective variables. The results from the correlation tests further emphasize the need for a joint model that accounts for dependencies.

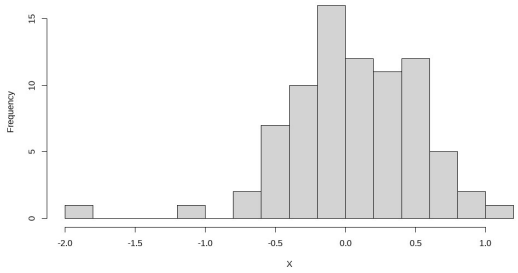

(a) Histogram of the translational variable X.

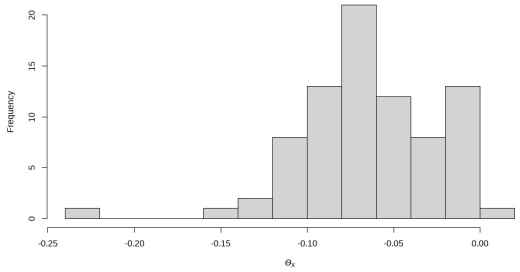

(b) Histogram of the rotational variable Θ_X.

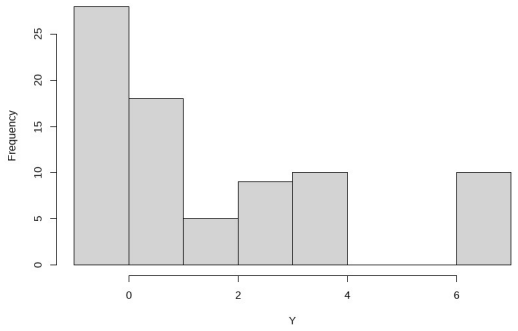

(c) Histogram of the translational variable Y.

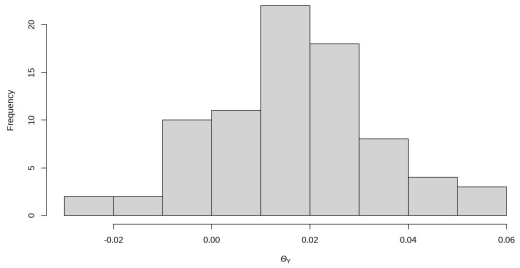

(d) Histogram of the rotational variable Θ_Y.

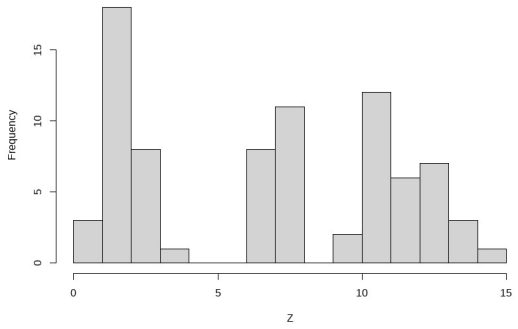

(e) Histogram of the translational variable Z.

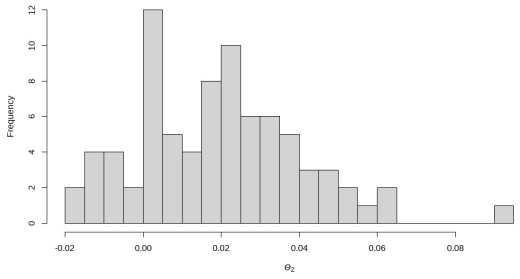

(f) Histogram of the rotational variable Θ_Z.

Figure 4.3: Histograms of the translational (left) and rotational (right) variables for configuration 2.

In the literature various studies can be found which compare configurations of constructs to determine strain at a fracture site and thus the most appropriate configuration for optimal healing (see [33] and [38]). To the best of the author's knowledge, all studies in this area follow a similar statistical procedure; the assumption of independence among

Figure 4.4: Correlation plot for configuration 1.

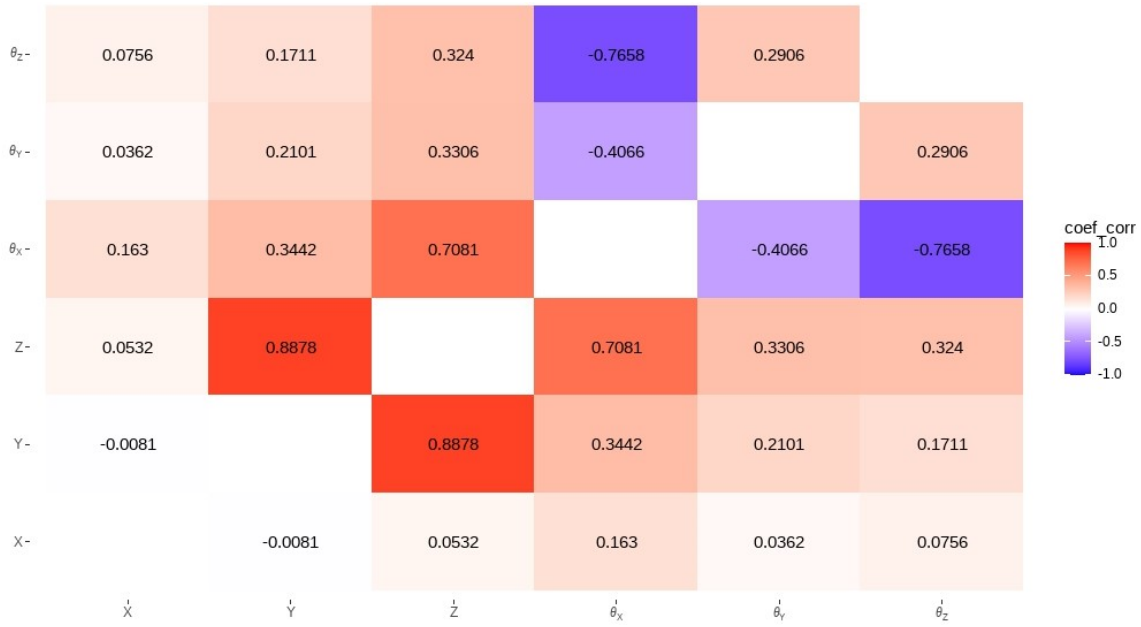

Figure 4.5: Correlation plot for configuration 2.

the variables and all variables are linear variables. There are two main shortfalls of this approach: (i) disregard of the dependence structure between the variables which may impair the accuracy of the model and (ii) the cyclicity of the rotational variables is neglected and mistreated as a linear variable which may produce misleading results. In the biome-

Table 4.3: Paired variables for configuration 1 with correlation coefficients significant at a 5% significance level.

Variable 1	**Variable 2**	*cor*	**p-value**
X	Y	0.3662	0.0017
Y	Z	0.5758	0.000
Y	Θ_X	0.1196	0.0001
Y	Θ_Y	0.078	0.0024
X	Θ_Z	0.0961	0.0006
Z	Θ_Z	0.1001	0.0004

Table 4.4: Paired variables for configuration 2 with correlation coefficients significant at a 5% significance level.

Variable 1	**Variable 2**	*cor*	**p-value**
Y	Z	0.8878	0.000
Θ_X	Θ_Y	-0.4066	0.0218
Θ_X	Θ_Z	-0.7658	0.0007
X	Θ_X	0.163	0.000
Y	Θ_X	0.3442	0.000
Z	Θ_X	0.7081	0.000
Y	Θ_Y	0.2101	0.000
Z	Θ_Y	0.3306	0.000
X	Θ_Z	0.0756	0.0029
Y	Θ_Z	0.1711	0.000
Z	Θ_Z	0.324	0.000

chanical domain, studies including the use of directional statistical techniques have been limited to the univariate and bivariate setting as seen in [91; 92; 86; 105].

In this chapter we propose a modeling framework applicable to the 6D joint distribution to address the above shortcomings. For modeling the displacement of a fracture site, we consider the use of six variables of which three are translational and three rotational. Our proposed model makes use of directional statistics to account for the cyclicity of the rotational variables and is constructed based on vine copulas. The pair-copula decomposition concept of vine copulas represents the dependence structure as a combination of circular-linear, circular-circular and linear-linear pairs modeled by their respective copulas. This allows us to capture the dependencies in the joint distribution. An advantage of using vine copulas is the flexibility to build multivariate distributions via bivariate copulas

that model the dependence between pairs of random variables.

The remainder of this chapter follows as, Section 4.2 provides some background on the statistical techniques required to build our proposed model defined in Section 4.3. Section 4.4 contains the results and discussion of the real data application. Section 4.5 concludes with some final remarks.

4.2 Background

In many studies, the cyclicity of a circular variable is often neglected and mistreated as a linear variable as pointed out in [113; 119; 101; 66]. Modeling of circular-linear (C-L) data is limited to the bivariate C-L joint distribution. Various bivariate C-L distributions have been proposed and studied, specifically with focus on meteorology and climatology studies. A well-known method to obtain a C-L distribution is via the conditional modeling approach. This approach combines the von Mises and normal distribution to obtain a joint model with conditional independence [75]. Thereafter many other models have been proposed, however, this approach restricts the choice of the marginal distribution and may neglect the dependence structure between the variables. This concern becomes even more complicated when extending the C-L distribution to the multivariate setting. Even with the assumption of independence among the circular and linear variables, extending a C-L distribution past the bivariate setting is difficult due to the normalizing constant being intractable in most cases as well as the restricted circumstances for the normalizing constant to be approximated. This results in additional complexity with regards to efficient estimation methods. An attempt to extend the model proposed by [75] to the multivariate setting is given in [70]. In these studies, dependencies between linear variables were considered however, every circular variables was considered independent of all the other variables.

One of the most commonly used C-L distributions is the model proposed by [50], known as the JW model. This model was constructed using copulas. Copulas are used to link the marginal distribution of variables to their multivariate distribution [85]. Using copulas to build multivariate distributions is a flexible and convenient approach. In the

linear domain, substantial amount of literature can be found on multivariate copulas as given in [85; 48]. However, these copulas cannot directly be applied to our problem as we need to consider the directional variables and account for their cyclicity. In the directional domain at present only bivariate copulas have been studied for circular-circular (C-C) variables as discussed in [53; 60] and circular-linear (C-L) variables. The JW model being the most extensively considered and used. The JW model allows the distribution of the C-L variable pair to be written as a function of the marginals and the JW copula function. Since copula functions in the directional domain is limited to the bivariate case an alternative model needs to be considered to obtain our joint 6D model.

A possible solution for the shortfall of multivariate C-L copulas is vine copulas. The origin of vine copulas stem from the hierarchical copula-based structure, specifically the pair-copula construction proposed by [47] and then investigated by [11; 12]. There has been a growing interest in vine copulas due to their flexibility and intuitive decomposition. Vine copulas allow the construction of multivariate joint probability distributions by decomposing the multivariate function into simple building blocks comprising of bivariate copulas (pair-copulas) based on conditional probabilities as discussed in [1]. Hence, the need for a multivariate C-L copula function is avoided. A vine is usually divided into D-vine and canonical vine (C-vine) structures where the latter is more suitable for situations where a variable is key in controlling the dependency. A $d-$dimensional vine contains $(d-1)$ trees, where the trees are represented with nodes and edges. The nodes are used to determine the edge label. The edge label corresponds to the subscript of each pair-copula density and each edge corresponds to one pair-copula. Thus the final $d-$dimensional copula can be obtained from the product of the pair-copula densities given by all the edges.

By considering vine copulas with our linear-linear (L-L) variable pairs, C-C variable pairs and C-L variable pairs we can construct a multivariate joint probability model while also taking into account the cyclicity of the directional variables. For the trivariate case of a circular-linear-linear joint model this approach has proven to be useful in meteorology and oceanography, see [112] and [41].

With the flexibility offered by vine copulas comes an increase in the complexity in

larger dimensions. This results in the computational effort required to estimate all the parameters growing exponentially with dimension. Given that our dataset is 6D we consider a truncated vine copula. Truncated vine copulas have been proposed by [63] and [16]. Truncated vine copulas are helpful as they can be constructed by using only pair-wise copulas and a lower number of conditional pair-wise copulas. This method is applied by considering a vine copula structure where all pair-wise copulas with conditioning set equal to or larger than K are replaced with independence copulas. Various approaches for obtaining the optimal K exists and are discussed in [63] and [16].

In this chapter we propose a modeling framework applicable to the 6D joint distribution. Our proposed model makes use of directional statistics to account for the cyclicity of the rotational variables and is constructed based on truncated vine copulas. The pair-copula decomposition concept of vine copulas represents the dependence structure as a combination of L-L, C-C and C-L pairs modeled by their respective copulas. This allows us to assess the dependencies in the joint distribution. An advantage of using vine copulas is the flexibility to build multivariate distributions via bivariate copulas that model the dependence between pairs of random variables. The truncation of the vine copula assists with the computation effort required to estimate our model.

4.3 Methodology

In this section we define the proposed modeling framework applicable to the 6D joint distribution. The linear and circular PDFs considered are given as well as the copula functions.

4.3.1 Linear and circular distributions

Let X, Y and Z denote the linear (translational) variables defined on $\mathbb{R}$ with PDFs $f_X(x), f_Y(y)$ and $f_Z(z)$, respectively. Let Θ_X, Θ_Y and Θ_Z denote the circular (rotational) variables defined on the unit circle $\mathbb{S}^1$ with PDFs $f_{\Theta_X}(\theta_x), f_{\Theta_Y}(\theta_y)$ and $f_{\Theta_Z}(\theta_z)$, respec-

tively. The CDFs of the variables are represented as $F_X(X)$ for the linear variables and $F_{\Theta_X}(\theta_x)$ for the circular variables.

Based on the preliminary analysis of the data, and the histograms of the variables provided in Figures 4.2 and 4.3, for the translational variables, the normal (N) distribution and a two component mixture of the normal (MN) distributions were considered to be most appropriate. A two component mixture of the normal distribution was considered to accommodate for the multimodality. The expression for the PDF of a finite mixture model is given as

$$f_X(x) = \sum_{j=1}^{m} \omega_j f(x|\boldsymbol{\beta_j}), \tag{4.1}$$

where m is the number of mixture components, $0 < \omega_j \leq 1$ with $\sum_{j=1}^{m} \omega_j = 1$ representing the mixing proportions and $\boldsymbol{\beta_j}$ is the j^{th} parameter components of the finite mixture distribution.

For the rotational variables we considered various circular distributions and found the wC and a two component mixture of the wC (MwC) to be most appropriate. The peakedness of the wC makes it an appealing choice for this study. The PDF of the wC is defined in Table 2.1.

To build our model we consider the defined linear and circular distributions as the marginal distributions for our framework based on the analysis of the data. Various other distributions may also be considered depending on the complexity of the data.

4.3.2 Copulas

The copula approach allows us to consider the marginal distributions separately from the dependence structure between the variables. Consider $F_{X_1,X_2,...,X_d}(x_1, x_2, .., x_d)$ and $f_{X_1,X_2,...,X_d}(x_1, x_2, .., x_d)$ to be the JCDF and JPDF of the $d-$dimensional random variables $(X_1, X_2, ..., X_d)$, respectively. Then we define the copula, $\mathcal{C}$, as

$$F_{X_1,X_2,...,X_d}(x_1, x_2, .., x_d) = \mathcal{C}(u_1, u_2, ..., u_d), \tag{4.2}$$

and thus

$$f_{X_1,X_2,...,X_d}(x_1,x_2,..,x_d) = c(u_1,u_2,...,u_d)\prod_{j=1}^{d} f_{X_j}(x_j), \tag{4.3}$$

where $u_j = F_{X_j}(x_j), j = 1,2,...,d$ with $x_j \in \mathbb{R}$, $u_j \in [0,1]$ and $f_{X_j}(x_j)$ the marginal PDF of each variable.

In the linear domain, various multivariate copula functions have been defined as mentioned by [85], however, in directional statistics copula functions are limited to the bivariate case. Thus, we consider the use of vine copulas.

For the L-L pair-copula we consider the conventional Farlie-Gumbel-Morgenstern (FGM) defined as

$$c_{X_1,X_2}(u_1,u_2) = 1 + q(1-2u_1)(1-2u_2), \tag{4.4}$$

where $q \in [-1,1]$.

For the C-L pair copula we consider the most common function proposed by [50], the JW copula, defined as

$$c_{\Theta,X}(u_1,u_2) = 2\pi g(\eta), \tag{4.5}$$

where

$$\eta = 2\pi(u_1 - qu_2), \tag{4.6}$$

and $\eta \in [0,2\pi]$ is a circular random variable with $g(\cdot)$ defined as a circular PDF with $q \in \{-1,1\}$.

In order to obtain a bivariate circular copula, Jones et al. [53] proposed a similar approach to Johnson-Wehrly [50]. The resulting copula function simplifies to a circular PDF where the argument is defined as in (4.6).

4.3.3 Proposed model

Based on the concept of vine copulas our proposed model is built using the L-L, C-L and C-C pair-copulas and their respective marginal distributions.

In Figure 4.6 the illustrated canonical vine structure considered is given and from this

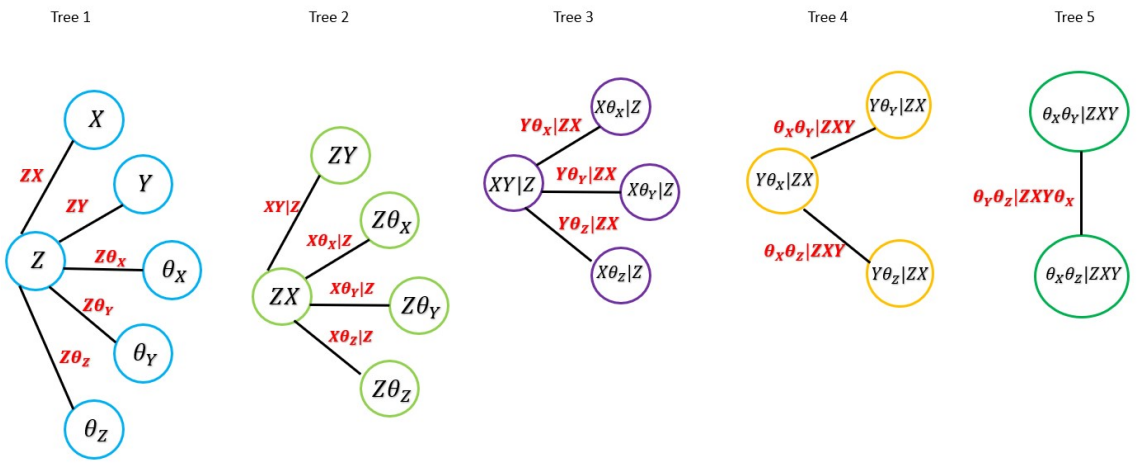

Figure 4.6: A schematic diagram of the canonical vine structure considered for the proposed model.

structure the resulting JPDF can be extracted as follows:

It is important to note that different vine structures may lead to different results. As mentioned in [1], the decomposition should be selected by determining which pair relationships are most important. Thus, for the purposes of this application we considered a structure where the variable Z is identified as most important and is linked to all the variables and is considered the conditional variable.

$$\begin{aligned} f(x,y,z,\theta_x,\theta_y,\theta_z) = {} & f(x)f(y)f(z)f(\theta_x)f(\theta_y)f(\theta_z) \\ & \times c_{xz}(F_X,F_Z)c_{yz}(F_Y,F_Z)c_{z\theta_x}(F_Z,F_{\theta_X})c_{z\theta_y}(F_Z,F_{\theta_Y})c_{z\theta_z}(F_Z,F_{\theta_Z}) \\ & \times c_{xy|z}(F_{X|Z},F_{Y|Z})c_{x\theta_x|z}(F_{X|Z},F_{\theta_X|Z})c_{x\theta_y|z}(F_{X|Z},F_{\theta_Y|Z}) \\ & \times c_{x\theta_z|z}(F_{X|Z},F_{\theta_Z|Z})c_{y\theta_x|z}(F_{Y|Z},F_{\theta_X|Z})c_{y\theta_y|z}(F_{Y|Z},F_{\theta_Y|Z}) \\ & \times c_{y\theta_z|z}(F_{Y|Z},F_{\theta_Z|Z})c_{\theta_x\theta_y|z}(F_{\theta_X|Z},F_{\theta_Y|Z}) \\ & \times c_{\theta_x\theta_z|z}(F_{\theta_X|Z},F_{\theta_Z|Z})c_{\theta_y\theta_z|z}(F_{\theta_Y|Z},F_{\theta_Z|Z}) \end{aligned} \tag{4.7}$$

For the parameter estimation of (4.7) the method of MLE is considered. Closed form expressions for the MLEs cannot be obtained due to the complex functional form. Advanced optimization algorithms are required to numerically compute the ML and thus the MLEs.

4.4 Application

In this section we illustrate the validity of our proposed model by considering the fracture displacements data discussed in Section 4.1. The necessity for a joint dependence model is highlighted in this section though a comparison to the norm of an independence assumption.

The flexibility offered by vine copulas come at a computational cost for high dimensions. As a result, we consider a *simplified* form of the JPDF given in (4.7) namely a truncated vine copula. For the purposes of this application we considered $K = 2$ for the truncation of our vine copula. Our motivation for the choice of $K = 2$ stems from the dependence structure desired, the correlations observed from the data analysis as well as the practical implications of the relationships between the variables and their interactions.

To compute our joint distribution model we first need to specify the marginal and copula functions for each variable and variable-pair, respectively. Based on the preliminary analysis of the data and models defined in Section 4.3, for the linear variables we consider the N distribution as well as the MN distribution (see Section 4.3.1). For the circular variables we consider the wC distribution as well as the MwC distribution. Table 4.5 provides a summary of the different cases evaluated for each configuration. We consider two cases, A and B, for each configuration (1 and 2). The cases are labeled with the case option and configuration, for example the second case of configuration 1 is denoted as case B1. The cases were chosen in consultation with the biomechanical domain experts and the need for a parsimonious model.

Table 4.5: Cases denoting the combination of marginal and copula functions considered for each configuration.

		Function										
Configuration	**Case**	X	Y	Z	Θ_X	Θ_Y	Θ_Z	ZX	ZY	$Z\Theta_X$	$Z\Theta_Y$	$Z\Theta_Z$
1	**A1**	N	N	N	wC	wC	wC	FGM	FGM	wC (JW)	wC (JW)	wC (JW)
	B1	N	N	N	MwC	wC	MwC	FGM	FGM	wC (JW)	wC (JW)	wC (JW)
2	**A2**	N	N	N	wC	wC	wC	FGM	FGM	wC (JW)	wC (JW)	wC (JW)
	B2	N	MN	N	wC	wC	MwC	FGM	FGM	wC (JW)	wC (JW)	wC (JW)

Table 4.6: The number of parameters (p), Maximized log-likelihood (MLL), Akaike information criterion (AIC) and Bayesian information criterion (BIC) values for the different combinations of marginal and copula functions.

Configuration	Case	p	MLL	AIC	BIC
1	**A1**	17	169.4548	-304.9096	-264.4152
	B1	23	170.6057	-295.2114	-240.4248
2	**A2**	17	37.7123	-41.4246	-0.9302
	B2	23	103.2792	-160.5584	-105.7718

For the parameter estimation the method of MLE is utilized. For the finite mixture models, the expectation-maximization (EM) algorithm may be utilized. Due to the high dimensional space of the parameter set, advanced optimization algorithms such as the particle swarm optimization (PSO) discussed in [111] and genetic algorithm (GA) summarized in [23] were used to efficiently estimate the parameters of the joint model.

In Table 4.6, the performance measures for the different cases specified in Table 4.5, are provided. For the performance evaluation two goodness-of-fit metrics are applied to evaluate the models. The AIC and BIC are considered (as defined in Appendix A.4). Based on the performance measures in Table 4.6, we can conclude that case B1 and case B2 are the best models for configuration 1 and configuration 2, respectively.

To illustrate the validity of the proposed model in comparison to the conventional use of an independent model, we consider a likelihood ratio test (LRT). We consider the model under the null hypothesis to be the independent model and case B1 and case B2 to be the model under the alternative hypothesis, respectively. For the independent model, we consider the same distributions as specified for case B1 and case B2 for the six variables, respectively. For configuration 1, independent model vs case B1, we obtain a LRT value of 80.4512 and reject the null hypothesis at a 5% significance level (p-value = $6.66e^{-16}$). For configuration 2, independent model vs case B2, we obtain a LRT value of 22.1448 and reject the null hypothesis at a 5% significance level (p-value = 0.0005). Thus, we can conclude that the joint dependent model is a more suitable fit for the data.

4.5 Conclusion

In this chapter we proposed a modeling framework applicable to the 6D joint distribution. This model accounted for the cyclicity of the rotational variables by means of directional statistics as well as accounted for a dependence structure between the variables. The framework was constructed based on vine copulas. The pair-copula decomposition concept of vine copulas represents the dependence structure as a combination of circular-linear, circular-circular and linear-linear pairs modeled by their respective copulas. This allowed us to assess the dependencies in the joint distribution. An advantage of using vine copulas is the flexibility to build multivariate distributions via bivariate copulas that model the dependence between pairs of random variables. For efficient estimation a truncation of the vine copula was considered. The analysis of this data motivated the need for a dependence structure to be accounted for when modeling this type of data. From the results in the application the advantage to applying the joint dependence model was observed. Based on the likelihood ratio test we can conclude that the joint dependent model was a better choice for modeling the fracture displacements and will thus be more informative for evaluations of these devices and the design thereof. The proposed modeling framework can be adjusted for other practical cases depending on the desired dependency structure required and relationship between the variables.

Chapter 5

Summary and future work

In this thesis we considered multivariate models defined on three different manifolds, namely the hyper-sphere, the disc and the poly-cylinder. The proposed multivariate directional models serve to fill some of the gaps identified in literature and considered contemporary applications for manifolds that have previously been neglected and/or instances where directional statistics techniques have been overlooked.

In Chapter 2, we constructed a flexible family of distributions on the unit hyper-sphere and considered the circle and sphere as the special cases for the numerical illustrations. This approach was inspired by the scale mixture model proposed by Shimizu and Iida [99]. Our proposal stems from the technique of a mean mixture of normal distributions in the linear domain, used to introduce more flexibility in models. The construction involves the use of a weight function which can be chosen by the practitioner depending on the complexity of the data. For the purposes of this thesis the weight functions were chosen as known circular PDFs. However, the choice of weight function is not limited to PDFs but do have to satisfy certain conditions (as in the linear domain). The resulting family of distributions can account for symmetry, asymmetry, unimodality and bimodality depending on the choice of the weight function and parameter set. The proposed model on the circle was shown to account for bimodality, however, as future work we propose the investigation of finite mixture models of this distribution for accounting for multimodality.

This will allow the practitioner broader insight into the structure of the data. As future work we propose considering the mean-scale mixture modeling approach as an extension and combination of the work proposed in this chapter and that by Shimizu and Iida [99].

In Chapter 3, we have developed a new general Möbius distribution class on the disc which has support on the unit disc. This new class can assume either a semi-parametric or parametric form depending on the choice of the practitioner. This class of distributions is suitable when there exists skewness and bimodal patterns hidden in the data structure. The work emanating from this chapter was served to revive the disc manifold and focused on an application domain that is of utmost importance to the socioeconomic development of not only South Africa but globally. We considered two applications; modeling the wind description at Marion Island and the evaluation of wind energy potential at two different locations in South Africa. Considering the situation surrounding the supply of electricity in South Africa, the need for investigating and investing in alternative renewable energy sources is of paramount importance. As future work we propose the extension of this model to the multivariate setting similarly to the work proposed by Uesu et al. [108]. Since the disc manifold has not been extensively explored in literature other questions that emerged during this work related to the simulation of observations from disc models as well as goodness-of-fit measures. A suggested technique for simulation was proposed by [14] in which the acceptance-rejection algorithm was utilized for a simple density function, however, the method is not very effective for more complex functions and thus other methods should be investigated. The normalized deviation was considered as a goodness-of-fit measure in this study as it was proposed for circular-linear observations, however, this measure only gives an indication of the overall fit of the model and cannot be used for model comparison.

In Chapter 4, we propose a modeling framework applicable to the 6D joint distribution. This model accounts for the cyclicity of the rotational variables as well as for a dependence structure between the variables. The framework is constructed based on vine copulas. An advantage of using vine copulas is the flexibility to build multivariate

distributions via bivariate copulas that model the dependence between pairs of random variables. The joint dependent model is a better choice for modeling the fracture displacements and will thus be more informative for evaluations of these devices and the design thereof. The proposed modeling framework can be adjusted for other practical cases depending on the desired dependency structure required and relationship between the variables. This can be easily adjusted by changing the canonical vine structure and selecting the most important pair relationships based on the experimental design. Various other distributions may also be considered depending on the complexity of the data resulting in this approach being very flexible. As future work we propose investigating and developing additional multivariate joint circular-linear models that can be used for general cases and allow for easier interpretability of the dependence structure and model parameters. Two possible avenues for this include (i) developing multivariate copulas for circular variables and/or circular-linear variables and then considering a multivariate circular-linear copula and (ii) developing a joint multivariate model for circular-linear data. Other future work also includes investigating techniques for comparison of different configurations with each other as well as entropy analysis for different constructions and configurations. The biomechanical domain is ripe with many other opportunities for future work as the use of directional statistics has been overlooked mainly due to the previous unfamiliarity of directional statistics and the lack of readily available computer software packages that can easily assist with the computational requirements of implementation. However, with the recent popularity and increased awareness of directional statistics these hurdles can be easily overcome.

The societal impact of this thesis can be divided into two main areas, namely renewable energy and health care. Exploitation of wind has long been recognized as one of the key aspects among renewable energy sources for reducing carbon emissions and securing a sustainable energy supply. The analytic knowledge and modeling of wind climate in a candidate area is a critical issue in wind energy assessment in order to optimize the layout of a wind farm, improve system efficiency, estimate accurately wind energy potential and reduce costs. In South Africa, there is an increasing transition towards an environmentally

sustainable, climate-change resilient and low-carbon economy. The models proposed in Chapter 3 have the possibility of bringing about change not only in wind energy avenues but also with the detection of climate change and climate patterns.

Chapter 4 is motivated by the biomechanical domain with focus on external fixators. The primary goal within the biomechanical domain are injury prevention and/or rehabilitation and performance enhancement. Patients are generally inoperative during the time in which a fracture heals, which impacts their functionality and quality of life. Some may even be impacted in the long term, due to long lasting damage caused by the fracture. Fracture healing is inevitably influenced by the complex interplay of biology and biomechanics - i.e. inter-fragmentary motion and biomechanics. The construct of an external fixator is determined by the configuration of the hardware. The construct's configuration may lead to different inter-fragmentary motions and it is therefore important to accurately model and understand the motions in play to obtain the most appropriate construct for optimal healing. The modeling framework proposed in this thesis provides a more accurate view for fracture displacements thus leading to improved evaluations and design of these devices.

The models developed in this thesis are just a drop in the ocean of possibility in the world of multivariate directional models with innumerable prospects for future work.

Appendix A

Definitions

A.1 Mathematical expressions

Result 1. *The confluent hypergeometric function of the first kind is defined by [6, equation 13.1.2] for* $|x| < 1$ *as*

$$ {}_1F_1\left(\alpha;\beta;x\right) = \sum_{j=0}^{\infty} \frac{\left(\alpha\right)_j}{\left(\beta\right)_j} \frac{x^j}{j!}, $$

where $\left(\alpha\right)_j$ *is the Pochhammer symbol.*

Result 2. *The modified Bessel function of the first kind and order* v *can be expressed as an infinite series as defined by [6, equation 9.6.10],*

$$ I_v\left(x\right) = \sum_{j=0}^{\infty} \left(\frac{x}{2}\right)^v \frac{\left(\frac{1}{4}x^2\right)^j}{j!\,\Gamma\left(v+j+1\right)}. $$

Result 3. *Let a function* $f(x)$ *be infinitely differentiable. The Taylor series of* $f(x)$*, centered at* 0 *is defined by [6, equation 25.2.24] as*

$$ f(x) = \sum_{j=0}^{\infty} \frac{f^{(j)}(0)}{j!} x^j. $$

A.2 Linear-circular correlation

The bivariate relationship between the linear and circular variables is measured by the linear-circular correlation coefficient, $cor_{x,\theta}$, defined by [74, equation 11.2.1] as

$$cor_{r,\theta} = \sqrt{\frac{c_{rc}^2 + c_{rs}^2 - 2c_{rc}c_{rs}c_{cs}}{1 - c_{cs}^2}},$$

where $c_{rc} = cor(r, \cos\theta)$, $c_{rs} = cor(r, \sin\theta)$, and $c_{cs} = cor(\cos\theta, \sin\theta)$ are the sample correlation coefficients.

A.3 Circular-circular correlation

The bivariate relationship between a pair of circular variables is measured by the circular-circular correlation coefficient as specified by [74, equation 11.2.8] is defined as

$$\begin{aligned} cor_{\theta,\phi}^2 = \big[&\left(cor_{cc}^2 + cor_{cs}^2 + cor_{sc}^2 + cor_{ss}^2\right) + 2\left(cor_{cc}cor_{ss} + cor_{cs}cor_{sc}\right)cor_1 cor_2 \\ &-2\left(cor_{cc}cor_{cs} + cor_{sc}cor_{ss}\right)cor_2 - 2\left(cor_{cc}cor_{sc} + cor_{cs}cor_{ss}\right)cor_1\big] \\ &\times \frac{1}{\left(1 - cor_1^2\right)\left(1 - cor_2^2\right)} \end{aligned}$$

where $cor_{cc} = cor(\cos\theta, \cos\phi)$, $cor_{ss} = cor(\sin\theta, \sin\phi)$, $cor_{cs} = cor(\cos\theta, \sin\phi)$, $cor_{sc} = cor(\sin\theta, \cos\phi)$, $cor_1 = cor(\cos\theta, \sin\theta)$ and $cor_2 = cor(\cos\phi, \sin\phi)$ are the sample correlation coefficients.

A.4 Goodness-of-fit measures

We define the following three goodness-of-fit metrics for the evaluation of the models in this thesis. The Akaike information criterion (AIC) estimates the relative amount of information lost by a given model. The Bayesian information criterion (BIC) is widely

used for model selection and is similar to the AIC. The Hannan–Quinn information criterion (HQC) is similar to the BIC and is strongly consistent. These three measures differ in terms of the amount of model complexity penalization. The two measures BIC and HQC penalize more severely than AIC [17]. The BIC attempts to find the true model among the set of candidates; however, this is not the case for the AIC [28]. The conclusion made using the AIC and BIC will only differ when the AIC chooses a larger model (more complex model) than the BIC. From a statistical viewpoint, information criteria are commonly used when assessing the accuracy of a probabilistic model [110]. These three strict criteria are considered most significant in measuring performance accuracy of distributions. These three metrics are defined in Table A.1, where p is the number of estimated parameters in the model, n the total number of data points, and $\hat{L}$ the maximum value of the likelihood function for a specific model.

Table A.1: Evaluated goodness-of-fit metrics.

Metric	**Equation**
AIC	$2p - 2\log(\hat{L})$
BIC	$p\log(n) - 2\log(\hat{L})$
HQC	$2p\log[\log(n)] - 2\log(\hat{L})$

A.5 Code

The code for the applications in this thesis are available on request via Github `https://github.com/nagar-priyanka/PhD-Thesis.git`.

Appendix B

Circular-Linear Models

B.1 Derivation of Möbius transformation

Considering the polar coordinate form of the unit disc, we write $z = (x, y)$ and $w = (u, v)$ as complex numbers with $w = re^{i\theta}$, $0 \leq r \leq 1$, $-\pi < \theta \leq \pi$. The Möbius transformation is defined by [61] as

$$z = M_c(w) = \tfrac{w-c}{1-\bar{c}w} \quad \text{with inverse} \quad w = M_{-c}(z) = \tfrac{z+c}{1+\bar{c}z},$$

where $c = ae^{i\mu}$, $0 \leq a < 1$ and $\bar{c}$ denotes the complex conjugate.

Let s and ϕ denote the polar coordinates of z, i.e. $z = se^{i\phi}$, then we can obtain the expressions for s and ϕ. To obtain an expression for s;

$$\begin{aligned} s^2 &= z\bar{z} = \left(\frac{w-c}{1-\bar{c}w}\right)\left(\frac{\bar{w}-\bar{c}}{1-c\bar{w}}\right) \\ &= \frac{r^2 + a^2 - ar\left[e^{i(\theta-\mu)} + e^{i(\mu-\theta)}\right]}{1 + a^2r^2 - ar\left[e^{i(\mu-\theta)} - e^{i(\theta-\mu)}\right]}. \end{aligned} \tag{B.1}$$

Since $e^{i\theta} = \cos\theta + i\sin\theta$, we can rewrite $(B.1)$ as

$$= \frac{r^2 + a^2 - ar\left[\{\cos(\theta-\mu) + i\sin(\theta-\mu)\} + \{\cos(\mu-\theta) + i\sin(\mu-\theta)\}\right]}{1 + a^2r^2 - ar\left[\{\cos(\mu-\theta) + i\sin(\mu-\theta)\} - \{\cos(\theta-\mu) + i\sin(\theta-\mu)\}\right]}.$$

Then using the trigonometric properties, $\cos(-\theta) = \cos(\theta)$ and $\sin(-\theta) = -\sin(\theta)$, we can simplify further to obtain

$$\begin{aligned} s^2 &= \frac{r^2 + a^2 - ar\left[\cos(\theta-\mu) + i\sin(\theta-\mu) + \cos(\theta-\mu) - i\sin(\theta-\mu)\right]}{1 + a^2r^2 - ar\left[\cos(\theta-\mu) - i\sin(\theta-\mu) - \cos(\theta-\mu) + i\sin(\theta-\mu)\right]} \\ &= \frac{a^2 - 2ar\cos(\theta-\mu) + r^2}{1 - 2ar\cos(\theta-\mu) + a^2r^2}. \end{aligned}$$

To obtain an expression for ϕ:

$$\begin{aligned} z\left(\frac{1-c\bar{w}}{1-c\bar{w}}\right) &= \left(\frac{w-c}{1-\bar{c}w}\right)\left(\frac{1-c\bar{w}}{1-c\bar{w}}\right) \\ &= \frac{w - wc\bar{w} - c + cc\bar{w}}{1 - c\bar{w} - \bar{c}w + \bar{c}wc\bar{w}} \\ &= \frac{re^{i\theta} - \left(re^{i\theta}\right)\left(re^{-i\theta}\right)\left(ae^{i\mu}\right) - \left(ae^{i\mu}\right) + \left(ae^{i\mu}\right)\left(ae^{i\mu}\right)\left(re^{-i\theta}\right)}{1 - \left(ae^{i\mu}\right)\left(re^{-i\theta}\right) - \left(ae^{-i\mu}\right)\left(re^{i\theta}\right) + \left(ae^{-i\mu}\right)\left(ae^{i\mu}\right)\left(re^{i\theta}\right)\left(re^{-i\theta}\right)} \\ &= \frac{re^{i\theta} - r^2ae^{i\mu} - ae^{i\mu} + a^2re^{i(2\mu-\theta)}}{1 - are^{i(\mu-\theta)} - are^{i(\theta-\mu)} + a^2r^2}. \end{aligned} \tag{B.2}$$

Since $e^{i\theta} = \cos\theta + i\sin\theta$, we get

$$\begin{aligned} &= \frac{r\cos\theta + i\sin\theta - a\left(1+r^2\right)\left(\cos\mu + i\sin\mu\right) + a^2r\left[\left(\cos(2\mu-\theta) + i\sin(2\mu-\theta)\right)\right]}{1 + a^2r^2 - ar\left[2\cos(\theta-\mu)\right]} \\ &= p + iq. \end{aligned}$$

Using the trigonometric relation $\tan(\phi) = \frac{Im(z)}{Re(z)}$, we get

$$\tan\phi = \frac{\sin\theta - a\left(1+r^2\right)\sin\mu + a^2r\sin(2\mu-\theta)}{r\cos\theta - a\left(1+r^2\right)\cos\mu + a^2r\cos(2\mu-\theta)},$$

and, thus we obtain an expression for ϕ,

$$\phi = \arctan\left(\frac{\sin\theta - a\left(1+r^2\right)\sin\mu + a^2r\sin(2\mu-\theta)}{r\cos\theta - a\left(1+r^2\right)\cos\mu + a^2r\cos(2\mu-\theta)}\right). \tag{B.3}$$

The Jacobian for transformation of (s, ϕ) to (r, θ) is:

$$\begin{aligned} |J(s,\phi) \longrightarrow (r,\theta)| &= \begin{vmatrix} \frac{\partial s}{\partial r} & \frac{\partial s}{\partial \theta} \\ \frac{\partial \phi}{\partial r} & \frac{\partial \phi}{\partial \theta} \end{vmatrix} \\ &= \left(\frac{\partial s}{\partial r}\right)\left(\frac{\partial \phi}{\partial \theta}\right) - \left(\frac{\partial s}{\partial \theta}\right)\left(\frac{\partial \phi}{\partial r}\right). \end{aligned}$$

Thus, we obtain

$$|J| = \frac{r(1-a^2)^2}{s\left[1 - 2ar\cos(\theta - \mu) + a^2r^2\right]^2}. \tag{B.4}$$

The PDF of (r, θ) in polar coordinates is obtained as follows

$$f(r,\theta) = f_{s,\phi}(r,\theta)\,|J|\,. \tag{B.5}$$

We can transform the PDF of polar coordinates (r, θ) to Cartesian coordinates (u, v) using the following results:

$$u = r\cos\theta \quad , \quad v = r\sin\theta$$

and

$$r^2 = u^2 + v^2,$$

with the Jacobian as

$$|J(r,\theta) \longrightarrow (u,v)| = \left(u^2 + v^2\right)^{-\frac{1}{2}}.$$

B.2 Maximum likelihood estimators

B.2.1 Möbius distribution on the disc

For the Möbius distribution on the disc, assuming that $a \neq 0$, the maximum likelihood estimators can be obtained by estimating the equations below derived from (3.12),

$$0 = \sum_{i=1}^{n} \frac{(\gamma+1)\left(2ar_i \sin\left(\theta_i - \mu\right)\right)}{1 - 2ar_i \cos\left(\theta_i - \mu\right) + a^2 r_i},$$

$$0 = \sum_{i=1}^{n} \frac{(\gamma+1)\left(2ar_i^2 - 2r_i \cos\left(\theta_i - \mu\right)\right)}{1 - 2ar_i \cos\left(\theta_i - \mu\right) + a^2 r_i},$$

$$0 = \sum_{i=1}^{n} \log\left[1 - 2ar_i \cos\left(\theta_i - \mu\right) + a^2 r_i\right] - \sum_{i=1}^{n} \log\left(1 - r_i^2\right) - n \log\left(1 - a^2\right).$$

B.2.2 Kummer beta Möbius distribution

For the Kummer beta Möbius distribution, assuming that $a \neq 0$, the maximum likelihood estimators can be obtained by estimating the equations below derived from (3.16),

$$0 = -\sum_{i=1}^{n} \frac{[a^2 - 2ar_i \cos(\theta_i - \mu) + r_i^2]}{[1 - 2ar_i \cos(\theta_i - \mu) + a^2 r_i^2]},$$

$$\begin{aligned} 0 \;=\; & n\Psi(\beta+\gamma) - n\Psi(\beta) + \sum_{i=1}^{n} \log[a^2 - 2ar_i \cos(\theta_i - \mu) + r_i^2] \\ & - \sum_{i=1}^{n} \log[1 - 2ar_i \cos(\theta_i - \mu) + a^2 r_i^2] \\ & - \frac{n[{}_1F_1^{(0,1,0)}\left(\beta, \beta+\gamma; -1\right) + {}_1F_1^{(1,0,0)}\left(\beta, \beta+\gamma; -1\right)]}{{}_1F_1\left(\beta, \beta+\gamma; -1\right)}, \end{aligned}$$

$$
\begin{aligned}
0 &= n\Psi(\beta+\gamma) - n\Psi(\gamma) + n\log[1-a^2] + \sum_{i=1}^{n}\log(1-r_i^2) \\
&\quad - \sum_{i=1}^{n}\log[1-2ar_i\cos(\theta_i-\mu)+a^2r_i^2] - \frac{n[{}_1F_1^{(0,1,0)}(\beta,\beta+\gamma;-1)]}{{}_1F_1(\beta,\beta+\gamma;-1)},
\end{aligned}
$$

$$
\begin{aligned}
0 &= \sum_{i=1}^{n}\frac{2(\beta-1)ar_i\sin(\mu-\theta_i)}{a^2-2ar_i\cos(\theta_i-\mu)+r_i^2} - \sum_{i=1}^{n}\frac{2(\gamma+\beta)ar_i\sin(\mu-\theta_i)}{1-2ar_i\cos(\theta_i-\mu)+a^2r_i^2} \\
&\quad -\lambda\sum_{i=1}^{n}\frac{2ar_i[a^2-r_i^2+a^2r_i^2]\sin(\mu-\theta_i)}{[1-2ar_i\cos(\theta_i-\mu)+a^2r_i^2]^2},
\end{aligned}
$$

$$
\begin{aligned}
0 &= \frac{-2an(\gamma+1)}{(1-a^2)} + \sum_{i=1}^{n}\frac{(\beta+1)(2a-2r_i\cos(\theta_i-\mu))}{(a^2-2ar_i\cos(\theta_i-\mu)+r_i^2)} \\
&\quad -\sum_{i=1}^{n}\frac{(\gamma+\beta)(2ar_i^2-2r_i\cos(\theta_i-\mu))}{(1-2ar_i\cos(\theta_i-\mu)+a^2r_i^2)} \\
&\quad -\lambda\sum_{i=1}^{n}\frac{2(r_i^2-1)\left[a^2r_i\cos(\theta_i-\mu)+r_i\cos(\theta_i-\mu)-a^2(r_i^2+1)\right]}{[1-2ar_i\cos(\theta_i-\mu)+a^2r_i^2]^2},
\end{aligned}
$$

where $\Psi(\cdot)$ is the digamma function and ${}_1F_1^{(\cdot)}(\cdot)$ is the derivative of the confluent hypergeometric function.

B.2.3 Beta type III Möbius distribution

For the beta type III Möbius distribution, assuming that $a \neq 0$, the maximum likelihood estimators can be obtained by estimating the equations below derived from (3.21),

$$
\begin{aligned}
0 &= n\log(2) + n\Psi(\beta+\gamma) - n\Psi(\beta) + \sum_{i=1}^{n}\log[a^2-2ar_i\cos(\theta_i-\mu)+r_i^2] \\
&\quad -\sum_{i=1}^{n}\log[(1+a^2)(1+r^2)-4ar_i\cos(\theta_i-\mu)],
\end{aligned}
$$

$$\begin{aligned} 0 &= n\Psi(\beta+\gamma) - n\Psi(\gamma) + n\log[1-a^2] + \sum_{i=1}^{n}\log(1-r_i^2) \\ &\quad - \sum_{i=1}^{n}\log[(1+a^2)(1+r^2) - 4ar_i\cos(\theta_i-\mu)], \end{aligned}$$

$$0 = \sum_{i=1}^{n}\frac{4ar_i(\beta+\gamma)\sin(\theta_i-\mu)}{(1+a^2)(1+r^2)-4ar_i\cos(\theta_i-\mu)} - \sum_{i=1}^{n}\frac{2ar_i(\beta-1)\sin(\theta_i-\mu)}{a^2-2ar_i\cos(\theta_i-\mu)+r_i^2},$$

$$0 = \sum_{i=1}^{n}\frac{(\beta-1)(2a-2r_i\cos(\theta_i-\mu))}{a^2-2ar_i\cos(\theta_i-\mu)+r_i^2} - \frac{2na(\gamma+1)}{1-a^2} - \sum_{i=1}^{n}\frac{(\gamma+\beta)(2a(1+r_i^2)-4ar_i\cos(\theta_i-\mu))}{(1+a^2)(1+r^2)-4ar_i\cos(\theta_i-\mu)},$$

where $\Psi(\cdot)$ is the digamma function.

Bibliography

[1] AAS, K., CZADO, C., FRIGESSI, A., AND BAKKEN, H. Pair-copula constructions of multiple dependence. *Insurance: Mathematics and Economics 44*, 2 (2009), 182–198.

[2] ABE, T., IMOTO, T., SHIOHAMA, T., AND MIYATA, Y. On some flexible models for circular, toroidal, and cylindrical data. In *Directional Statistics for Innovative Applications*. Springer, 2022, pp. 229–243.

[3] ABE, T., AND LEY, C. A tractable, parsimonious and flexible model for cylindrical data, with applications. *Econometrics and Statistics 4* (2017), 91–104.

[4] ABE, T., AND PEWSEY, A. Sine-skewed circular distributions. *Statistical Papers 52*, 3 (2011), 683–707.

[5] ABE, T., SHIMIZU, K., AND PEWSEY, A. Symmetric unimodal models for directional data motivated by inverse stereographic projection. *Journal of the Japan Statistical Society 40*, 1 (2010), 045–061.

[6] ABRAMOWITZ, M., AND STEGUN, I. A. *Handbook of mathematical functions: with formulas, graphs, and mathematical tables*, vol. 55. Courier Corporation, 1965.

[7] ARASHI, M., NAGAR, P., AND BEKKER, A. Joint probabilistic modeling of wind speed and wind direction for wind energy analysis: A case study in Humansdorp and Noupoort. *Sustainability 12*, 11 (2020).

[8] ARSLAN, O. Variance-mean mixture of the multivariate skew normal distribution. *Statistical Papers 56*, 2 (2015), 353–378.

[9] BARNDORFF-NIELSEN, O., KENT, J., AND SØRENSEN, M. Normal variance-mean mixtures and z distributions. *International Statistical Review/Revue Internationale de Statistique* (1982), 145–159.

[10] BASILE, S., BURLON, R., AND MORALES, F. Joint probability distributions for wind speed and direction. a case study in sicily. In *2015 International Conference on Renewable Energy Research and Applications (ICRERA)* (2015), IEEE, pp. 1591–1596.

[11] BEDFORD, T., AND COOKE, R. M. Probability density decomposition for conditionally dependent random variables modeled by vines. *Annals of Mathematics and Artificial Intelligence 32*, 1 (2001), 245–268.

[12] BEDFORD, T., AND COOKE, R. M. Vines–a new graphical model for dependent random variables. *The Annals of Statistics 30*, 4 (2002), 1031–1068.

[13] BEKKER, A., NAGAR, P., ARASHI, M., AND RAUTENBACH, H. From symmetry to asymmetry on the disc manifold: Modeling of Marion island data. *Symmetry 11*, 8 (2019).

[14] BERRY, T., AND SAUER, T. Density estimation on manifolds with boundary. *Computational Statistics & Data Analysis 107* (2017), 1–17.

[15] BORIS CHOY, S., AND CHAN, J. S. Scale mixtures distributions in statistical modelling. *Australian & New Zealand Journal of Statistics 50*, 2 (2008), 135–146.

[16] BRECHMANN, E. C., CZADO, C., AND AAS, K. Truncated regular vines in high dimensions with application to financial data. *Canadian Journal of Statistics 40*, 1 (2012), 68–85.

[17] BURNHAM, K. P., AND ANDERSON, D. R. Practical use of the information-theoretic approach. In *Model selection and inference*. Springer, 1998, pp. 75–117.

[18] BUTTARAZZI, D., PANDOLFO, G., AND PORZIO, G. C. A boxplot for circular data. *Biometrics 74*, 4 (2018), 1492–1501.

[19] CARDENO, L., NAGAR, D. K., AND SÁNCHEZ, L. E. Beta type 3 distribution and its multivariate generalization. *Tamsui Oxford Journal of Mathematical Sciences 21*, 2 (2005), 225–242.

[20] CARTA, J. A., AND RAMIREZ, P. Analysis of two-component mixture Weibull statistics for estimation of wind speed distributions. *Renewable Energy 32*, 3 (2007), 518–531.

[21] CARTA, J. A., RAMIREZ, P., AND BUENO, C. A joint probability density function of wind speed and direction for wind energy analysis. *Energy Conversion and Management 49*, 6 (2008), 1309–1320.

[22] CARTA, J. A., RAMIREZ, P., AND VELAZQUEZ VELAZQUEZ, S. A review of wind speed probability distributions used in wind energy analysis: Case studies in the canary islands. *Renewable and Sustainable Energy Reviews 13*, 5 (2009), 933–955.

[23] CHATTERJEE, S., LAUDATO, M., AND LYNCH, L. A. Genetic algorithms and their statistical applications: an introduction. *Computational Statistics & Data Analysis 22*, 6 (1996), 633–651.

[24] CHOWN, S., AND FRONEMAN, P. W. *The Prince Edward Islands: land-sea interactions in a changing ecosystem*. African Sun Media, 2008.

[25] CLAESKENS, G., AND CARROLL, R. J. An asymptotic theory for model selection inference in general semiparametric problems. *Biometrika 94*, 2 (2007), 249–265.

[26] DEEP, S., SARKAR, A., GHAWAT, M., AND RAJAK, M. K. Estimation of the wind energy potential for coastal locations in India using the Weibull model. *Renewable Energy 161* (2020), 319–339.

[27] ERDEM, E., AND SHI, J. Comparison of bivariate distribution construction approaches for analysing wind speed and direction data. *Wind Energy 14*, 1 (2011), 27–41.

[28] FABOZZI, F. J., FOCARDI, S. M., RACHEV, S. T., AND ARSHANAPALLI, B. G. *The basics of financial econometrics: Tools, concepts, and asset management applications*. John Wiley & Sons, 2014.

[29] FENG, J., AND SHEN, W. Modelling wind for wind farm layout optimization using joint distribution of wind speed and wind direction. *Energies 8*, 4 (2015), 3075–3092.

[30] FERNÁNDEZ-DURÁN, J. J. Models for circular–linear and circular–circular data constructed from circular distributions based on nonnegative trigonometric sums. *Biometrics 63*, 2 (2007), 579–585.

[31] FISHER, N. I., LEWIS, T., AND EMBLETON, B. J. *Statistical analysis of spherical data*. Cambridge university press, 1993.

[32] FU, Y.-Z., AND CHEN, X.-D. Model selection of generalized partially linear models with missing covariates. *Journal of Statistical Planning and Inference 142*, 1 (2012), 126–138.

[33] GESSMANN, J., CITAK, M., JETTKANT, B., SCHILDHAUER, T. A., AND SEYBOLD, D. The influence of a weight-bearing platform on the mechanical behavior of two Ilizarov ring fixators: tensioned wires vs. half-pins. *Journal of Orthopaedic Surgery and Research 6*, 1 (2011), 1–11.

[34] GLATT, V., EVANS, C. H., AND TETSWORTH, K. A concert between biology and biomechanics: the influence of the mechanical environment on bone healing. *Frontiers in Physiology 7* (2017), 678.

[35] GUGLIANI, G. K., SARKAR, A., LEY, C., AND MANDAL, S. New methods to assess wind resources in terms of wind speed, load, power and direction. *Renewable Energy 129* (2018), 168–182.

[36] HAMED, T. A., AND ALSHARE, A. Environmental impact of solar and wind energy-a review. *Journal of Sustainable Development of Energy, Water and Environment Systems 10*, 2 (2022), 1–23.

[37] HAN, Q., HAO, Z., HU, T., AND CHU, F. Non-parametric models for joint probabilistic distributions of wind speed and direction data. *Renewable Energy 126* (2018), 1032–1042.

[38] HENDERSON, D. J., RUSHBROOK, J. L., STEWART, T. D., AND HARWOOD, P. J. What are the biomechanical effects of half-pin and fine-wire configurations on fracture site movement in circular frames? *Clinical Orthopaedics and Related Research® 474*, 4 (2016), 1041–1049.

[39] HENNESSEY JR, J. P. A comparison of the Weibull and Rayleigh distributions for estimating wind power potential. *Wind Engineering* (1978), 156–164.

[40] HERBERT-ACERO, J., PROBST, O., RÉTHORÉ, P.-E., LARSEN, G., AND CASTILLO-VILLAR, K. A review of methodological approaches for the design and optimization of wind farms. *Energies 7*, 11 (2014), 6930–7016.

[41] HEREDIA-ZAVONI, E., AND MONTES-ITURRIZAGA, R. Modeling directional environmental contours using three dimensional vine copulas. *Ocean Engineering 187* (2019), 106102.

[42] HOLZMANN, H., MUNK, A., AND STRATMANN, B. Identifiability of finite mixtures-with applications to circular distributions. *Sankhyā: The Indian Journal of Statistics* (2004), 440–449.

[43] JAMALIZADEH, A., AND BALAKRISHNAN, N. Conditional distributions of multivariate normal mean–variance mixtures. *Statistics & Probability Letters 145* (2019), 312–316.

[44] JAMMALAMADAKA, S. R., AND KOZUBOWSKI, T. J. A general approach for obtaining wrapped circular distributions via mixtures. *Sankhya A 79*, 1 (2017), 133–157.

[45] JAMMALAMADAKA, S. R., AND SENGUPTA, A. *Topics in circular statistics*, vol. 5. World Scientific, 2001.

[46] JANDER, R. The optical directional orientation of the red wood ant (formica ruea l.). *Magazine for Comparative Physiology 40*, 2 (1957), 162–238.

[47] JOE, H. m (m-1)/2 bivariate dependence parameters. *Distributions with Fixed Marginals and Related Topics 28* (1996), 120.

[48] JOE, H. *Dependence Modeling with Copulas*. CRC Press, 2014.

[49] JOHNSON, R. A., AND WEHRLY, T. Measures and models for angular correlation and angular–linear correlation. *Journal of the Royal Statistical Society: Series B (Methodological) 39*, 2 (1977), 222–229.

[50] JOHNSON, R. A., AND WEHRLY, T. E. Some angular-linear distributions and related regression models. *Journal of the American Statistical Association 73*, 363 (1978), 602–606.

[51] JONES, M. Marginal replacement in multivariate densities, with application to skewing spherically symmetric distributions. *Journal of Multivariate Analysis 81*, 1 (2002), 85–99.

[52] JONES, M. The Möbius distribution on the disc. *Annals of the Institute of Statistical Mathematics 56*, 4 (2004), 733–742.

[53] JONES, M., PEWSEY, A., AND KATO, S. On a class of circulas: copulas for circular distributions. *Annals of the Institute of Statistical Mathematics 67*, 5 (2015), 843–862.

[54] JUNG, C., AND SCHINDLER, D. Sensitivity analysis of the system of wind speed distributions. *Energy Conversion and Management 177* (2018), 376–384.

[55] KALAYLIOGLU, Z. Analysis of correlated circular and extremal data with a flexible cylindrical distribution. *Environmental and Ecological Statistics 29*, 1 (2022), 207–222.

[56] KATO, S., AND JONES, M. A family of distributions on the circle with links to, and applications arising from, möbius transformation. *Journal of the American Statistical Association 105*, 489 (2010), 249–262.

[57] KATO, S., AND JONES, M. A tractable and interpretable four-parameter family of unimodal distributions on the circle. *Biometrika 102*, 1 (2015), 181–190.

[58] KATO, S., MCCULLAGH, P., ET AL. Some properties of a Cauchy family on the sphere derived from the Möbius transformations. *Bernoulli 26*, 4 (2020), 3224–3248.

[59] KATO, S., AND SHIMIZU, K. *A further study of t-distributions on spheres*. Keio University. Department of Mathematics, 2004.

[60] KATO, S., AND SHIMIZU, K. Dependent models for observations which include angular ones. *Journal of Statistical Planning and Inference 138*, 11 (2008), 3538–3549.

[61] KRANTZ, S. G. *Handbook of complex analysis*. Birkhäuser, 1999.

[62] KUBOKAWA, T., STRAWDERMAN, W. E., AND YUASA, R. Shrinkage estimation of location parameters in a multivariate skew-normal distribution. *Communications in Statistics-Theory and Methods 49*, 8 (2020), 2008–2024.

[63] KUROWICKA, D. Optimal truncation of vines. In *Dependence modeling: Vine copula handbook*. World Scientific, 2010, pp. 233–247.

[64] LE ROUX, P. C. *Azorella selago (Apiaceae) as a model for examining climate change effects in the sub-Antarctic*. PhD thesis, Stellenbosch: Stellenbosch University, 2004.

[65] LEE, S. X., AND MCLACHLAN, G. J. On mean and/or variance mixtures of normal distributions. In *Scientific Meeting of the Classification and Data Analysis Group of the Italian Statistical Society* (2019), Springer, pp. 117–127.

[66] LEGUEY, I., LARRAÑAGA, P., BIELZA, C., AND KATO, S. A circular-linear dependence measure under Johnson–Wehrly distributions and its application in Bayesian networks. *Information Sciences 486* (2019), 240–253.

[67] LEY, C., BABIĆ, S., AND CRAENS, D. Flexible models for complex data with applications. *Annual Review of Statistics and Its Application 8* (2021), 369–391.

[68] LEY, C., AND VERDEBOUT, T. *Modern directional statistics*. Chapman and Hall/CRC, 2017.

[69] LEY, C., AND VERDEBOUT, T. Skew-rotationally-symmetric distributions and related efficient inferential procedures. *Journal of Multivariate Analysis 159* (2017), 67–81.

[70] LUENGO-SANCHEZ, S., BIELZA, C., AND LARRAÑAGA, P. Hybrid Gaussian and von Mises model-based clustering. In *Proceedings of the Twenty-Second European Conference on Artificial Intelligence* (NLD, 2016), ECAI'16, IOS Press, p. 855–862.

[71] MADADI, M., BALAKRISHNAN, N., JAMALIZADEH, A., ET AL. Family of mean-mixtures of multivariate normal distributions: properties, inference and assessment of multivariate skewness. *Journal of Multivariate Analysis* (2020), 104679.

[72] MAHBUDI, S., JAMALIZADEH, A., AND FARNOOSH, R. Mixture of extended Birnbaum-Saunders distributions: an approach via the mean-mixture of normal models. *Journal of Mathematical Extension 15* (2020).

[73] MARDIA, K. V. Distribution theory for the von Mises-Fisher distribution and its application. In *A Modern Course on Statistical Distributions in Scientific Work*. Springer, 1975, pp. 113–130.

[74] MARDIA, K. V., AND JUPP, P. E. *Directional statistics*, vol. 494. John Wiley & Sons, 2009.

[75] MARDIA, K. V., AND SUTTON, T. A model for cylindrical variables with applications. *Journal of the Royal Statistical Society: Series B (Methodological) 40*, 2 (1978), 229–233.

[76] MATHISEN, J., AND BITNER-GREGERSEN, E. Joint distributions for significant wave height and wave zero-up-crossing period. *Applied Ocean Research 12*, 2 (1990), 93–103.

[77] THE MATHWORKS, INC. *MATLAB version 9.8.0.1417392 (R2020a) Update 4*. Natick, Massachusetts, 2020.

[78] MINH, D. L., AND FARNUM, N. R. Using bilinear transformations to induce probability distributions. *Communications in Statistics-Theory and Methods 32*, 1 (2003), 1–9.

[79] MIYATA, Y., SHIOHAMA, T., AND ABE, T. Identifiability of asymmetric circular and cylindrical distributions. *Sankhya A* (2022), 1–21.

[80] MURPHY, S. A., AND VAN DER VAART, A. W. On profile likelihood. *Journal of the American Statistical Association 95*, 450 (2000), 449–465.

[81] NADERI, M., HUNG, W.-L., LIN, T.-I., AND JAMALIZADEH, A. A novel mixture model using the multivariate normal mean–variance mixture of Birnbaum–Saunders distributions and its application to extrasolar planets. *Journal of Multivariate Analysis 171* (2019), 126–138.

[82] NAGAR, D. K., AND GUPTA, A. K. Matrix-variate Kummer-beta distribution. *Journal of the Australian Mathematical Society 73*, 1 (2002), 11–26.

[83] NAGAR, P., BEKKER, A., AND ARASHI, M. Mean mixtures in directional statistics. In *2021 IEEE International Conference on Multisensor Fusion and Integration for Intelligent Systems (MFI)* (2021), pp. 1–6.

[84] NEGARESTANI, H., JAMALIZADEH, A., SHAFIEI, S., AND BALAKRISHNAN, N. Mean mixtures of normal distributions: properties, inference and application. *Metrika 82*, 4 (2019), 501–528.

[85] NELSEN, R. B. *An introduction to copulas*. Springer Science & Business Media, 2007.

[86] PATAKY, T. C., AND CHALLIS, J. H. Using directional statistics to test hypotheses regarding rigid body attitude: Comparison to univariate and multivariate cardan angle tests. *Journal of Biomechanics 111* (2020), 109976.

[87] PEWSEY, A. Testing circular symmetry. *Canadian Journal of Statistics 30*, 4 (2002), 591–600.

[88] PEWSEY, A., AND GARCÍA-PORTUGUÉS, E. Recent advances in directional statistics. *Test 30*, 1 (2021), 1–58.

[89] PEWSEY, A., NEUHÄUSER, M., AND RUXTON, G. D. *Circular statistics in R*. Oxford University Press, 2013.

[90] PORTÉ-AGEL, F., WU, Y.-T., AND CHEN, C.-H. A numerical study of the effects of wind direction on turbine wakes and power losses in a large wind farm. *Energies 6*, 10 (2013), 5297–5313.

[91] RIVEST, L.-P. A directional model for the statistical analysis of movement in three dimensions. *Biometrika 88*, 3 (2001), 779–791.

[92] RIVEST, L.-P., BAILLARGEON, S., AND PIERRYNOWSKI, M. A directional model for the estimation of the rotation axes of the ankle joint. *Journal of the American Statistical Association 103*, 483 (2008), 1060–1069.

[93] ROUAULT, M., MÉLICE, J.-L., REASON, C. J., AND LUTJEHARMS, J. R. Climate variability at Marion island, southern ocean, since 1960. *Journal of Geophysical Research: Oceans 110*, C5 (2005).

[94] RUDIN, W. *Real and complex analysis*. Tata McGraw-hill education, 2006.

[95] SAIDUR, R., RAHIM, N., ISLAM, M., AND SOLANGI, K. Environmental impact of wind energy. *Renewable and Sustainable Energy Reviews 15*, 5 (2011), 2423–2430.

[96] SANUSI, N., ZAHARIM, A., MAT, S., AND SOPIAN, K. Comparison of univariate and bivariate parametric model for wind energy analysis. *Journal of Advanced Research in Fluid Mechanics and Thermal Sciences 49*, 1 (2018), 1–10.

[97] SASAEI, M., POURMOUSA, R., BALAKRISHNAN, N., AND JAMALIZADEH, A. A robust class of multivariate fatigue distributions based on normal mean-variance mixture model. *Journal of the Korean Statistical Society* (2020), 1–25.

[98] SCHULZE, B. The climate of Marion island. *Marion and Prince Edward Islands 16* (1971), 31.

[99] SHIMIZU, K., AND IIDA, K. Pearson type VII distributions on spheres. *Communications in Statistics-Theory and Methods 31*, 4 (2002), 513–526.

[100] SIEW, H.-Y., AND SHIMIZU, K. The generalized symmetric Laplace distribution on the sphere. *Statistical Methodology 5*, 6 (2008), 487–501.

[101] SOLARI, S., AND ÁNGEL LOSADA, M. Simulation of non-stationary wind speed and direction time series. *Journal of Wind Engineering and Industrial Aerodynamics 149* (2016), 48–58.

[102] SONG, M., CHEN, K., ZHANG, X., AND WANG, J. Optimization of wind turbine micro-siting for reducing the sensitivity of power generation to wind direction. *Renewable Energy 85* (2016), 57–65.

[103] SOUKISSIAN, T. H., AND KARATHANASI, F. E. On the selection of bivariate parametric models for wind data. *Applied Energy 188* (2017), 280–304.

[104] TAMANDI, M., NEGARESTANI, H., JAMALIZADEH, A., AND AMIRI, M. Skew–normal mean–variance mixture of Birnbaum–Saunders distribution and its associated inference and application. *Journal of The Iranian Statistical Society 18*, 2 (2019), 87–113.

[105] TELSCHOW, F. J., PIERRYNOWSKI, M. R., AND HUCKEMANN, S. F. Functional inference on rotational curves under sample-specific group actions and identification of human gait. *Scandinavian Journal of Statistics 48*, 4 (2021), 1256–1276.

[106] TRUSWELL, J. Marion island, South Indian Ocean. *Nature 205*, 4966 (1965), 64–65.

[107] TUGAC, S., AND YILDIRAK, K. Wind speed and wind direction prediction: An implementation of a deep learning algorithm enriched by SWT and circular PCA. In *Directional Statistics for Innovative Applications*. Springer, 2022, pp. 475–488.

[108] UESU, K., SHIMIZU, K., AND SENGUPTA, A. A possibly asymmetric multivariate generalization of the möbius distribution for directional data. *Journal of Multivariate Analysis 134* (2015), 146–162.

[109] WAEWSAK, J., CHAICHANA, T., CHANCHAM, C., LANDRY, M., AND GAGNONC, Y. Micro-siting wind resource assessment and near shore wind farm analysis in Pakpanang district, Nakhon Si Thammarat province, Thailand. *Energy Procedia 52* (2014), 204–215.

[110] WAGENMAKERS, E.-J., RATCLIFF, R., GOMEZ, P., AND IVERSON, G. J. Assessing model mimicry using the parametric bootstrap. *Journal of Mathematical Psychology 48*, 1 (2004), 28–50.

[111] WANG, D., TAN, D., AND LIU, L. Particle swarm optimization algorithm: an overview. *Soft Computing 22*, 2 (2018), 387–408.

[112] WANG, M.-Z., AND SHIMIZU, K. On applying Möbius transformation to cardioid random variables. *Statistical Methodology 9*, 6 (2012), 604–614.

[113] WANG, Z.-W., ZHANG, W.-M., ZHANG, Y.-F., AND LIU, Z. Circular-linear-linear probabilistic model based on vine copulas: An application to the joint distribution of wind direction, wind speed, and air temperature. *Journal of Wind Engineering and Industrial Aerodynamics 215* (2021), 104704.

[114] XU, R., VAIDA, F., AND HARRINGTON, D. P. Using profile likelihood for semiparametric model selection with application to proportional hazards mixed models. *Statistica Sinica 19*, 2 (2009), 819.

[115] ZHANG, J., CHOWDHURY, S., MESSAC, A., AND CASTILLO, L. A multivariate and multimodal wind distribution model. *Renewable Energy 51* (2013), 436–447.

[116] ZHANG, L., LI, Q., GUO, Y., YANG, Z., AND ZHANG, L. An investigation of wind direction and speed in a featured wind farm using joint probability distribution methods. *Sustainability 10*, 12 (2018), 4338.

[117] ZHANG, M. H. *Wind resource assessment and micro-siting: science and engineering*. John Wiley & Sons, 2015.

[118] ZHANG, X., AND LIANG, H. Focused information criterion and model averaging for generalized additive partial linear models. *The Annals of Statistics 39*, 1 (2011), 174–200.

[119] ZHENG, X.-W., LI, H.-N., AND LI, C. Damage probability analysis of a high-rise building against wind excitation with recorded field data and direction effect. *Journal of Wind Engineering and Industrial Aerodynamics 184* (2019), 10–22.